CLONAL ANALYSIS OF THALAMUS DEVELOPMENT AND FUNCTION

A Dissertation

Presented to the Faculty of the Weill Cornell Graduate School

of Medical Sciences

In Partial Fulfillment of the Requirements for the Degree of

Doctor of Philosophy

By

Wei Shi

December 2017

CLONAL ANALYSIS OF THALAMUS DEVELOPMENT AND FUNCTION

Wei Shi, PhD

Cornell University 2018

The thalamus, with its intricate cortical, subcortical, and cerebellar connections, is a pivotal network node in relaying and modulating sensory and motor signals to the cortex as well as supporting higher-order cognitive functions. It is composed of more than 30 cytoarchitectonically and functionally distinct nuclei, each with a different anatomical connectivity pattern. In particular, every sensory modality (with the exception of olfaction) relies on a first order (FO) thalamic nucleus that receives peripheral signals and projects to the primary cortical area, and a higher order (HO) thalamic nucleus that relays information from one cortical area to another cortical area. While the order-specific nuclear organization across different modalities provides an influential framework for understanding thalamic structure and function, very little is known about the mechanisms responsible for its establishment.

Previous studies have shown that lineage relationship plays an instructive role in guiding the structural and functional assembly of the cortex, a laminated structure reciprocally interconnected with the thalamus. However, it remains unclear whether lineage relationship influences the structural formation and functional organization of the generally non-laminated thalamus. To address this, I performed a systematic clonal analysis of mouse thalamus assembly using mosaic analysis with double markers (MADM) and Cre-dependent retroviral labeling.

I found that individual radial glial progenitors in the developing thalamus actively divide and generate a cohort of neuronal progeny that exhibits striking spatial configuration and nuclear occupation related to thalamic functionality. While the

anterior clonal clusters display relatively more tangential dispersion and contribute predominantly to nuclei with cognitive functions, the medial ventral posterior clonal clusters form prominent radial arrays and contributes mostly to nuclei with sensory/motor-related activities. Moreover, neurons occupying the FO or HO sensory/motor-related nuclei across different modalities are largely segregated clonally and exhibit distinct gene expression profiles. Notably, the spatial distribution of clones depends on the SHH signaling activity that exhibits a gradient in the developing thalamus. Together, our study reveals a previously unknown ontogenetic logic for the structural and functional assembly of the mammalian thalamus.

BIOGRAPHICAL SKETCH

Wei Shi was born and brought up in Hangzhou, China. She attended Sichuan University where she obtained her Bachelor's degree of Science in Biology in 2011. It was during her college years that she grew her interest in science. During the summer vacations of her sophomore and junior years, she got the opportunity to work in the laboratory of Dr. Jianwei Jiao at Institute of Neuroscience, Chinese Academy of Sciences, in Shanghai. There, she worked with Dr. Chenyan Ma to explore the role of metabolic stress in adult hippocampal neurogenesis and with Dr. Xingya Chang to generate functional neurons from fibroblasts via direct reprogramming. It was in the Institute of Neuroscience that she was introduced to scientific research and developed a passion for neuroscience. In the fall of 2009, her interest in brain development drove her to the laboratory of Dr. Hedong Li in Sichuan University, where she studied the function of miRNA in cortical interneuron development.

After graduating from Sichuan University in 2011, Wei enrolled in the Neuroscience graduate program at Weill Cornell Graduate School of Medical Sciences in New York City. She joined the laboratory of Dr. Song-Hai Shi in the Department of Developmental Biology at Memorial Sloan Kettering Cancer Center for her dissertation work, where she studied the structural development and functional organization of the mouse thalamus.

ACKNOWLEDGMENTS

I would like to, first and foremost, express my sincere gratitude to my advisor Dr. Song-Hai Shi for giving me the opportunity to join your lab and for your continuous support through my PhD study. You are an incredible scientist and a wonderful mentor. I have learnt a lot from working with you. You gave me the freedom to explore my interest and have always had faith in me even when I, myself, didn't. Your insightful advices and encouragement helped me through the most difficult times. I could not have imagined having a better mentor for my graduate study.

I am also grateful to all members of the Shi lab, past and present, for your help and support over the years. It is my privilege to have worked with all of you. I would especially like to thank Anjin Xianyu for your indispensable help with my experiments and data analysis. Without you, my thesis research would not have been possible. I would also like to thank Zhizhong Li for helping prepare retroviruses and for teaching me various techniques, and Dr. Siqiang Ren and Dr. Xinjun Zhang for many insightful discussions on neural physiology. A special thank you goes to Lily Erdy, Susan Lin, Cara Monaco and Sonia Das for helping with everything throughout my graduate study.

I would especially like to acknowledge my committee members: Dr. Elizabeth Ross, Dr. Alexandra Joyner and Dr. Natalia De Marco Garcia for your thoughtful advice and constant support throughout my PhD. I am extremely fortunate to have your guidance.

I would like to thank my collaborators - members of the Huang, Mao and Zhong labs, for your immense help with my thesis research. And I would like to extend my acknowledgement to members of the Joyner, Kaltschmidt and Goll labs for your technical support over the years and for creating an enjoyable work environment on the 7th floor.

I am grateful to all members of the Weill Cornell Neuroscience graduate program, especially Dr. BJ Casey for convincing me to join the program, and my fellow classmates for your friendship and support. I am also thankful to all my dear friends here in New York City. I would especially like to thank Zhaohui Yang and Dr. Qian Ma for your incredible friendship over the past six years. Thank you for always being with me in my joys and sorrows.

I would like to thank my previous mentors Dr. Jianwei Jiao and Dr. Hedong Li, for enlightening me the first glance of scientific research and introducing me to neuroscience. Thank you for inspiring me to pursue my academic goals.

Most importantly, I would like to express my deepest gratitude to my family for their unconditional love and support, especially my parents, Jianmin Shi and Yunbo Han, who have always believed in me and encouraged me to follow my dreams. Lastly, I would like to express my deepest love and thanks to my loving husband, Dr. Yang Yu, who has always been standing strong by my side and keeping me motivated in difficult times. I would not have made it here without you.

TABLE OF CONTENTS

LIST OF FIGURES

LIST OF ABBREVIATIONS

2D 2-dimensional
3D 3-dimensional
'a' ..... anterior
AAV ..... adeno-associated virus
ABA ..... Allen Brain Atlas
ACC ..... anterior cingulated cortex
AD ..... anterodorsal
AM ..... anteromedial
AV ..... anteroventral
BG ..... basal ganglion
BLBP ..... brain lipid-binding protein
BrdU ..... 5-bromo-2'-deoxyuridine
CB ..... cerebellum
CL ..... central lateral
CP ..... caudate putamen
Ctx ..... cortex
dLG ..... dorsal part of the lateral geniculate nucleus
dMG ..... dorsal part of the medial geniculate nucleus
E ..... embryonic day
EdU ..... 5-ethynyl-2'-deoxyuridine
EGFP ..... enhanced green fluorescent protein
ER ..... estrogen receptor
FO ..... first order
GABA ..... γ-aminobutyric acid
GE ..... ganglionic eminance
HO ..... higher order
HTh ..... hypothalamus
IMD ..... intermediodorsal
LD ..... lateral dorsal
LGN ..... lateral geniculate nucleus
LH ..... lateral habenular
LP ..... lateral posterior
MADM ..... mosaic analysis with double markers
MD ..... mediodorsal
'md' ..... medial dorsal
MDO ..... mid-diencephalic organizer
mGRASP ..... Mammalian GFP reconstitution across synaptic partners
MH ..... medial and lateral habenula
'mvp' ..... medial ventral posterior
NND ..... nearest neighbor distance
OB ..... olfactory bulb
OLIG3 ..... oligodendrocyte transcription factor 3
P ..... postnatal day

p1 ..... prosomere 1
p2 ..... prosomere 2
p3 ..... prosomere 3
PBS ..... phosphate-buffered saline
PCN ..... paracentral
PFA ..... paraformaldehyde
PFC ..... prefrontal cortex
PO ..... posterior
PrL ..... prelimbic cortex
PT ..... pretectum
PTh ..... prethalamus
pTH-C ..... caudal progenitor domain of the thalamus
pTH-R ..... rostral progenitor domain of the thalamus
PVT ..... paraventricular
RE ..... nucleus of reunions
RFP ..... red fluorescent protein
RGP ..... radial glial progenitor
RH ..... rhomboid
RORa ..... retinoic acid receptor-related orphan receptor a
SGN ..... suprageniculate
Smo ..... smoothened
SMT ..... submedial
SP ..... signal peptide
spG11 ..... split-GFP fragment GFP11
spG1-10 ..... split-GFP fragment GFP1-10
SPF ..... subparafascicular
tdTomato ..... tandem dimer Tomato
TM ..... tamoxifen
TRN ..... thalamic reticular nucleus
VA ..... ventral anterior
VAL ..... ventral anterior lateral
VL ..... ventral lateral
vLG ..... ventral part of the lateral geniculate nucleus
VM ..... ventral medial
vMG ..... ventral part of the medial geniculate nucleus
VP ..... ventral posterior
VPL ..... ventral posterolateral
VPM ..... ventral posteromedial
VZ ..... ventricular zone
ZI ..... zona incerta
ZLI ..... zona limitans intrathalamica

Chapter 1
Introduction to Thalamic Structure and Function

1.1 The basic organization of the thalamus

The vertebrate thalamus is a bilateral, symmetrical structure located in the dorsal part of the diencephalon **(Figure 1.1)**, and it has traditionally been thought of as a gate in the information flow from the periphery to the cortex. It receives inputs from diverse brain regions including the retina, medial lemniscus, inferior colliculus, basal ganglia, spinal cord, cerebellum, and cortex, and projects to multiple brain structures, especially the cortex [1,2]. The extensive reciprocal connections between the cortex and thalamus allow the traveling of different sensory and motor information along separate pathways, as well as effective information integration.

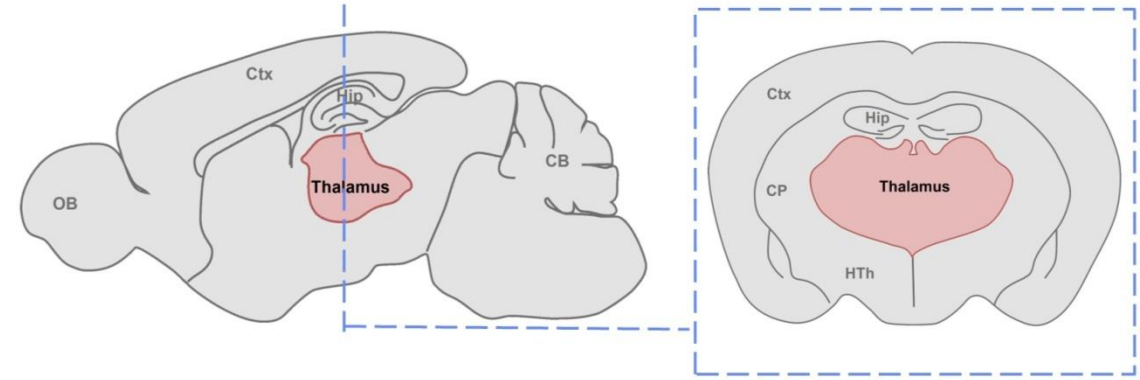

Figure 1.1: Sagittal and coronal sections of the mouse brain with the thalamus highlighted. OB, olfactory bulb; Ctx, cortex; Hip, hippocampus; CB, cerebellum; CP, caudate putamen; HTh, hypothalamus.

The thalamus is more than just a relay. With its intricate cortical, subcortical, and cerebellar connections, the thalamus actively regulates information transmitted to the cortex by modulating the response magnitude, firing mode and neuronal synchrony in a state dependent manner [1,3,4]. It also serves many other functions such as emotion regulation, motivation, learning and memory.

To process the various types of information, the thalamus has evolved to contain a highly heterogeneous neuronal population, where neurons dedicated to a particular task are clustered to form a nucleus. The basic layout of thalamic nuclei is similar across mammalian species, except a few specific nuclei with differing nuclei shapes and functional connections among species. Based on distinct axonal projection patterns and gene expression profiles, a number of thalamic nuclei have been identified [1]. Since the nomenclature of thalamic nuclei is far from standardized, in this study, our anatomic nomenclature of the adult thalamus is based on the Allen Mouse Brain Atlas (ABA, http://mouse.brain-map.org/static/atlas)

1.2 Driver input and modulatory input to the thalamus

The thalamus is composed of more than 30 cytoarchitectonically and functionally distinct nuclei, each of which has a different pattern of anatomical connectivity [1,5-7]. The names of thalamic nuclei are broadly based on their anatomical locations within the thalamus, whereas the functional identities are mostly determined by early lesion studies, or based on their sources of inputs and axonal targets [8].

Individual thalamic nuclei receive various inputs, some of which carry the main message this nucleus serves to relay (driver input), while others assist to modify how the message is going to be relayed (modulatory input)[4,9,10]. The nature of the main

message is modified to a greater or lesser extent when passed from one thalamic nucleus to its target region, driven by the modulatory inputs in a state dependent manner.

Distinguishing driver from modulator is essential in understanding the function of any thalamic nucleus. The driver input of any nucleus originates from a single source and comprises only a small proportion, usually around 5-10%, of the total inputs to the target nucleus, but is nevertheless the primary determinate of the activity being transmitted. Driver inputs are glutamatergic and have relatively thick axons and large synaptic terminals, making multiple complex contacts onto the target cells with little or no convergence. In contrast, modulatory inputs may come from glutamatergic cortical layer VI neurons, GABA (γ-aminobutyric acid)-ergic inhibitory neurons, cholinergic neurons in the parabrachial complex, histaminergic neurons in the hypothalamus and other sources. Modulatory inputs have relatively small terminals and delicate terminal arbors on more proximal parts of the dendritic segments of the target neurons. Notably, the driver input induces large EPSPs and defines the sensory receptive field properties of neurons in the corresponding nucleus, whereas the modulatory input influences the activity of thalamic neurons without directly triggering spikes. Silencing the driver input has been reported to result in the loss of receptive field properties [10,11].

Further efforts are required to examine whether this definition of driver and modulator is applicable to all thalamic nuclei across mammalian species [12]. For example, studies in primates suggest the lack of driver inputs, or subdivision heterogeneity in some nuclei [13]. Nonetheless, this framework has provided a valuable organizing principle for the study of thalamic structure and function.

1.3 Functional modalities and hierarchical orders of thalamic nuclei

Specialized portions of the thalamus allow different types of information to travel along separate pathways in the brain. These nuclei are therefore linked to different functional modalities. These principal sensory nuclei, including the dorsal lateral geniculate nucleus (dLG), ventral posterior nucleus (VP) and the ventral part of the medial geniculate nucleus (vMG), are the most distinctive thalamic nuclei, in terms of their morphology and function. Neurons in these nuclei project densely onto single cortical areas in a topographic manner: visual, somatosensory and auditory cortices respectively.

In addition, the distinct sources and properties of the driver inputs have led to the concept of first-order (FO) and higher-order (HO) thalamic nuclei linked to different sensory modalities [10,11]. Every sensory system (with the exception of olfaction) relies on a FO thalamic nucleus that receives peripheral sensory signals and sends them to the corresponding primary cortical area. In contrast, the HO nuclei receive very little, if any, sensory input. Instead, driver inputs to HO nuclei originate from layer V of the cortex, carrying already processed cortical information **(Figure1.2)**. HO nuclei thus relay information from one cortical area to another cortical area or to subcortical regions. Specifically, visual inputs from the retinal ganglion cells travel via the optic tract to the dLG, which in turn projects to the primary visual cortex. In comparison, the pulvinar (i.e. lateral posterior, LP, in rodents) nucleus relays information between the primary and higher-order visual cortical areas, or between two higher-order cortical areas. Similarly, peripheral somatosensory inputs reach the primary and higher-order somatosensory cortical areas largely via the VP and posterior (PO) thalamic nuclei, respectively. Peripheral auditory inputs reach the primary and higher-order auditory cortical areas mostly via

the ventral division (vMG) and dorsal division (dMG) of the medial geniculate nucleus in the thalamus, respectively.

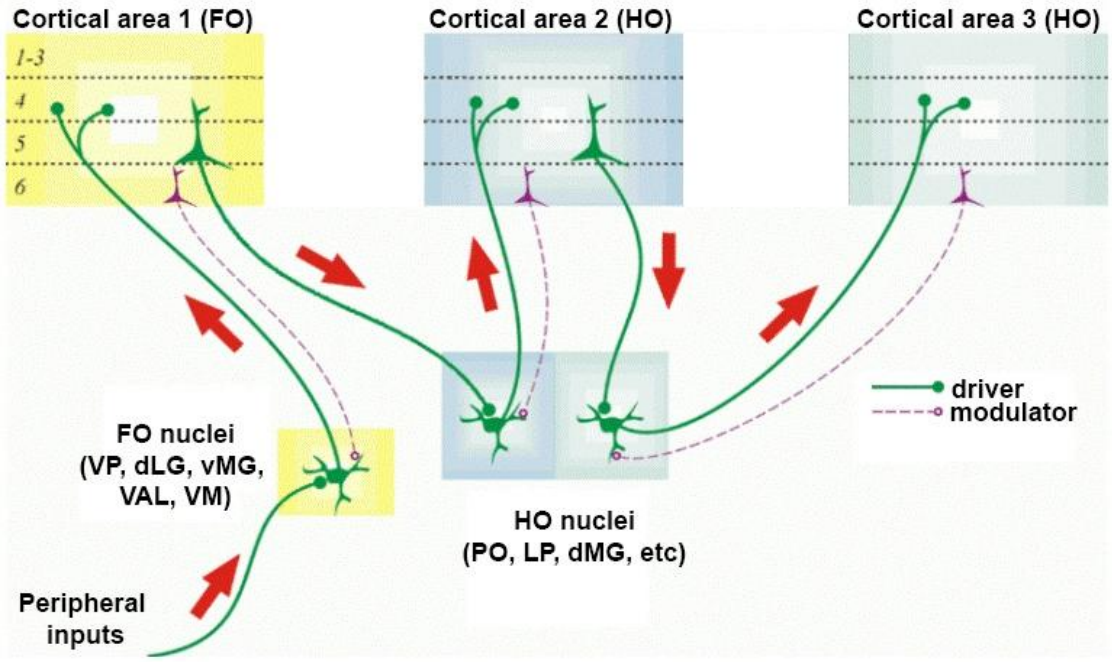

Figure 1.2 FO and HO thalamic relays. This is a simplified diagram showing the major information flow (red arrows) among periphery, thalamus and cortex. A FO thalamic relay represents the first relay of peripheral or subcortical information of a particular type to a FO or primary cortical area. A HO relay transmits information from layer V of one cortical area to another cortical area; this can be between FO and HO cortical areas or between two HO cortical areas. The difference is the driver input, which is subcortical for a FO relay and from layer V of cortex for a HO relay. Adapted from Reichova and Sherman (2004)[14] and reliawire.com/thalamus.

The framework of FO and HO thalamic nuclei for motor control is less clear from the literature[13,15-18]. Motor thalamus is located in the ventral part of the thalamus and is well conserved across mammalian species. In rodents, ventral anterior lateral (VAL) and ventral medial (VM) nuclei are well-recognized motor thalamic nuclei because of their extensive interconnections with the motor related structures, such as

motor cortex, cerebellum and basal ganglion (BG). VAL can be further divided to ventral anterior (VA) and ventral lateral (VL) nuclei in cats and more subdivisions in primates. In addition to cerebellum and BG, VAL and VM also receive extensive projections from layer V and VI of the motor cortex, superior colliculus, spinal cord and pedunculopontine nucleus. There remains debate whether cortical, cerebellar and basal ganglion projections to the motor thalamus are drivers or modulators. Cerebellar afferents to the thalamus exhibit several driver characteristics, including the large synaptic boutons onto the primary dendrites, and fast and strong responses elicited in the target thalamic neurons [8,13]. BG inputs to the motor thalamus are GABAergic, and thus can't be drivers. However, some anatomical and physiological features of BG inputs support a driver-like role [13,19,20]. To add another layer of complexity, layer V afferents from the motor cortex have been reported to match the anatomical criteria of a driver input in some studies, but not others [13,21]. Full characterization of the physiological properties of cortical layer V afferents to motor thalamus is not yet available. Despite controversy on BG and cortical layer V inputs, we were encouraged by the driver-like properties of cerebellar inputs and decided to treat VAL and VM as the FO motor nuclei in our study. Although some nuclei have been suggested to project densely onto the supplementary motor cortex (M2), such as PO, LP, PCN, central lateral (CL) and latera dorsal (LD) nuclei [6], the identity of HO motor thalamic nuclei remains unclear, due to the uncertainty of the property of layer V motor cortical inputs to the thalamus [15,18]. Therefore, we did not define any HO motor nucleus in this study.

In spite of controversial views on some nuclei, the thalamus is generally well organized in regards to order and modality. While the order-specific nuclear organization across different modalities provides an influential framework for

understanding thalamic structure and function, very little is known about the mechanisms responsible for its establishment.

1.4 Cognition related thalamic nuclei

The function of thalamus extends well beyond relaying sensory and motor activities. It also contributes to a wide variety of basic cognitive functions, including but not limited to stress regulation, learning, decision-making and perception [22]. In this study, the term ‘cognition related nuclei’ was used to describe the thalamic regions with little direct contribution to basic sensory and motor activities, but highly evolved in different aspects of cognitive behaviors. All the cognitive thalamic nuclei receive their driver inputs from the cortex and therefore are HO nuclei. They are deeply intertwined with the cognition related cortical regions, although the principles governing this interconnection remain poorly understood. In rodents, these nuclei are mostly distributed in the anterior and medial dorsal part of the thalamus, whereas the sensory/motor nuclei mostly occupy the ventral and posterior thalamus. Here, we will discuss the intricate anatomical connections and functions of the anterior nuclei group and the mediodorsal nucleus (MD) as examples of the cognitive nuclei.

Anterodorsal (AD), anteroventral (AV) and anteromedial (AM) nuclei are three major nuclei located in the anterior or rostral part of the thalamus. With their widespread limbic connections, the anterior thalamic nuclei group is a central component of ‘Papez' circuit responsible for emotion regulation, learning and memory[23-26]. In particular, cells in this region are densely connected with the retrosplenial cortex, subiculum, mammillary bodies and the hippocampus. The lateral dorsal thalamic nucleus (LD) is sometimes regarded as the fourth part of the anterior

thalamus due to its limbic association [25]. In rodents, the anterior thalamic nuclei contribute importantly to the role of hippocampus in spatial learning and memory [23,24]. Head direction cells are found in several cortical and subcortical regions, including the anterior thalamic nuclei. These cells discharge as a function of the animal's directional heading, independent of the animal's location or ongoing behavior [27]. Lesion studies in rodents support the role of anterior thalamus as part of a hierarchically organized circuit for the propagation of head directional signals and spatial navigation [23,28].

The mediodorsal nucleus of the thalamus (MD) is well recognized because of its extensive connection to the prefrontal cortex (PFC) and its contribution to working memory, associative learning and decision-making [29]. Based on different cell morphologies, the rodent MD can be divided into at least three subdivisions interconnected to distinct regions of PFC and other regions [23,30,31]. Lesions to the whole MD in monkeys and rats cause similar cognitive deficits in executive functions as seen in monkeys and rats with PFC damage, suggesting the essential role of MD in supporting PFC function [32,33]. Moreover, selective lesions to different MD subdivisions result in dissociable cognitive deficits in both rodents and humans [34,35]. These studies suggest that individual MD subdivisions with varying connectivity patterns function across interdependent neural circuits related to multiple aspects of cognition.

The cognitive function of the thalamus has received increasing attentions in recent years [36-39]. Technical advances in viral-based neuronal tracing, optogenetics, chemogenetics as well as functional imaging have brought unprecedented insights into our understanding of the cognition contribution of the thalamus. Future research that combines different behavioral, cognitive and systems neuroscience techniques in

humans and in animal models will further advance our understanding of the key roles that thalamus plays in cognitive behaviors.

1.5 Inhibitory interneurons in the thalamus

GABAergic inhibition is a key component of modulatory inputs to thalamic excitatory neurons, and enables thalamic circuits to differentially process information according to ongoing behavioral needs [40]. So the central question is: how does the heterogeneity of inhibition arise in the thalamus? Within the thalamus, there are at least two types of GABAergic inhibitory neurons: local interneurons that inhibit excitatory neurons within the same nucleus, and interneurons from dedicated inhibitory nuclei which harbor exclusively GABAergic interneurons including the thalamic reticular nucleus (TRN), ventral lateral geniculate nucleus (vLG) and zona incerta (ZI). Since TRN and vLG are ventral to other thalamic nuclei, they are referred to as 'prethalamus' or 'ventral thalamus' by some researchers. The rest of thalamus is generally referred to as the dorsal thalamus. TRN neurons provide inhibitory control over the entire dorsal thalamus, whereas vLG neurons mostly contribute to visual activity and visuomotor integration [41]. ZI provides GABAergic inputs to both cortex and thalamus, predominantly the HO thalamic nuclei [42], and it is sometimes included in the prethalamus. In this study, ZI was considered a hypothalamic nucleus, based on Allen Mouse Brain Atlas. Here we focus on (1) local interneurons in dLG as an example of the local inhibition and (2) TRN neurons as an example of long distance inhibition.

1.5.1 Local interneurons

The amount of local interneurons highly varies across mammalian species [43]. The primary visual nucleus, dLG, is the only thalamic nucleus that contains local interneurons in all species. The presence and number of local interneurons in other nuclei progressively increase in species with more complex behaviors. For example, most mouse and rat thalamic nuclei, other than dLG, are composed exclusively of excitatory neurons. In rabbit, local interneurons are found in both dLG and VP, representing 25% and 18% of the total number of neurons in dLG and VP respectively. In humans, local interneurons are present in all thalamic nuclei and account for 40% of the total neuronal population in the FO sensory nuclei.

Studies of dLG interneurons in cats revealed an interesting feature of local interneurons: they send their inhibitory outputs via both axons and dendrites [44,45]. While the axonal terminals predominantly synapse onto proximal dendrites of the target excitatory neuron, the dendritic terminals are frequently observed in a complex synaptic arrangement known as triads, where three synapses are involved. In addition, cable modeling suggests the possibility that inputs to the dendritic terminals of these interneurons might be isolated from the soma and thus their dendritic outputs function independently of the axonal outputs [46]. If such modeling is reliable, this would allow each local interneuron to provide multiple independent influences to the target cells. The uneven distribution of local interneurons in the thalamus likely contributes to the heterogeneity of inhibition in different thalamic regions. Further efforts to study dLG local interneurons in rodents would provide valuable insights into our understanding of how thalamus functions in human.

1.5.2 Thalamic reticular nucleus

TRN is a sheath-like structure, composed exclusively of GABAergic neurons, that surrounds the thalamus [40,47]. It receives inputs from collaterals of both thalamocortical and corticothalamic neurons, thus in a unique position to provide both feedback and feedforward inhibition to all other thalamic nuclei **(Figure 1.3)**[48]. The anatomical connections imply its crucial role in modulating information transmitted along the thalamo-cortico-thalamic circuit.

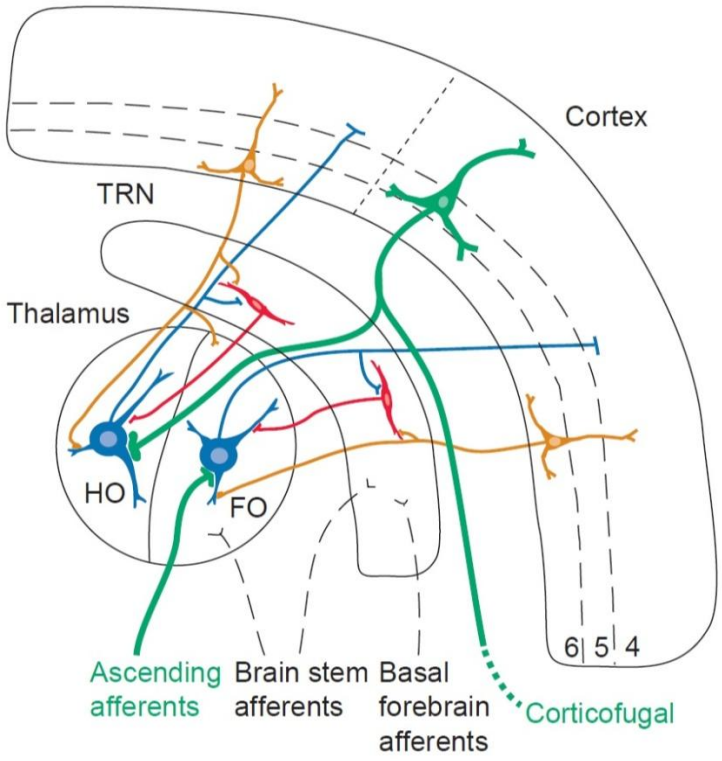

Figure 1.3: The major connections between thalamus (blue), TRN (red) and the cerebral cortex (orange). Both FO and HO nuclei receive modulatory afferents from layer VI of the cortex, and that these corticothalamic cells (orange) as well as the thalamocortical cells (blue) send branches to TRN, whereas the primary afferents (green) whether coming from cortical layer V or from ascending pathways send no branches to TRN. Adapted from Guillery et al., (1998)[48].

TRN neurons are not a homogeneous population. Increasing evidences suggest subdivisions within TRN, each interconnected topographically with thalamic and cortical regions related to different functions [48,49]. Previous anatomical and electrophysiological studies have demonstrated the existence of at least five TRN sectors, associated with the animal's somatosensation[50-53], vision[54], hearing[55,56], movement[57] and the limbic system[58]. Moreover, recent studies revealed 'functional subnetworks' within TRN by combining TRN ensemble recordings and connectivity-based optogenetic manipulations[59]. The authors found that the activity of visual-related TRN is suppressed by attentional states, likely enabling the engagement of their target thalamic regions in visual processing. In contrast, the activity of limbic-associated TRN is positively correlated with attentional states, indicating the involvement of limbic thalamus in offline processing during quiescent states. These findings demonstrate that TRN activity in gating thalamo-cortical interactions is matched to the animal's behavioral state[59]. Moreover, the engagement of TRN subnetworks in modulating thalamic activities is likely influenced by dynamic extrinsic inputs from the cortex. For example, the prefrontal cortex exerts top-down control over TRN subnetworks to modulate thalamic sensory gain [60]. In addition to extrinsic inputs, TRN neurons develop connections among themselves that can potentially alter the scale of their action. TRN neurons can be electrically coupled by gap junctions, and thereby exhibit coordinated firing patterns [61,62]. Furthermore, electrical synapses between TRN neurons display activity-dependent plasticity [63]. The activation of Group I and Group II metabotropic glutamate receptors induces long-term depression and long-term potentiation of electrical synapses respectively, which contributes to the inhibitory dynamics of TRN cells [64,65]. Although gap junctions have only been reported among adjacent TRN neurons, some electrically coupled neurons extend their axons to more than one thalamic nucleus [66]. Notably, anatomical and

physiological studies demonstrated morphological, neurochemical and physiological diversities of TRN neurons, and suggest multiple TRN subtypes within each TRN sector [67]. The functional role of different TRN subtypes on information processing requires further investigation.

In summary, inhibitory interneurons exert spatially and temporally dynamic influences on the thalamus, enabling variable scales of inhibitory modulation to thalamic activity to accommodate the animal's behavioral demands.

1.6. Thalamus development

The structural and functional complexity of the mature thalamus greatly depends on a precise control of the cellular and molecular activities in the developing thalamus. The thalamus originates from the embryonic diencephalon along the third ventricle. In the prosomere model, the pretectum, thalamus and prethalamus are derived from prosomere 1 (p1), prosomere 2 (p2) and prosomere 3 (p3) respectively **(Figure 1.4a,b)** [68,69]. The thalamic progenitor domain is marked by the expression of oligodendrocyte transcription factor 3 (*Olig3*), and it can be further divided to two distinct domains based on differential gene expressions, the caudal progenitor domain of the thalamus (pTH-C) and the rostral progenitor domain of the thalamus (pTH-R) **(Figure 1.4c,d)** [70]. The excitatory and inhibitory neurons in the thalamus have distinct distribution patterns as well as progenitor origins. Previous genetic mapping studies in mice have demonstrated that the pTH-C generates all thalamic excitatory neurons, whereas pTH-R and prethalamus (PTh) produce GABAergic interneurons in dLG, vLG and TRN [70,71].

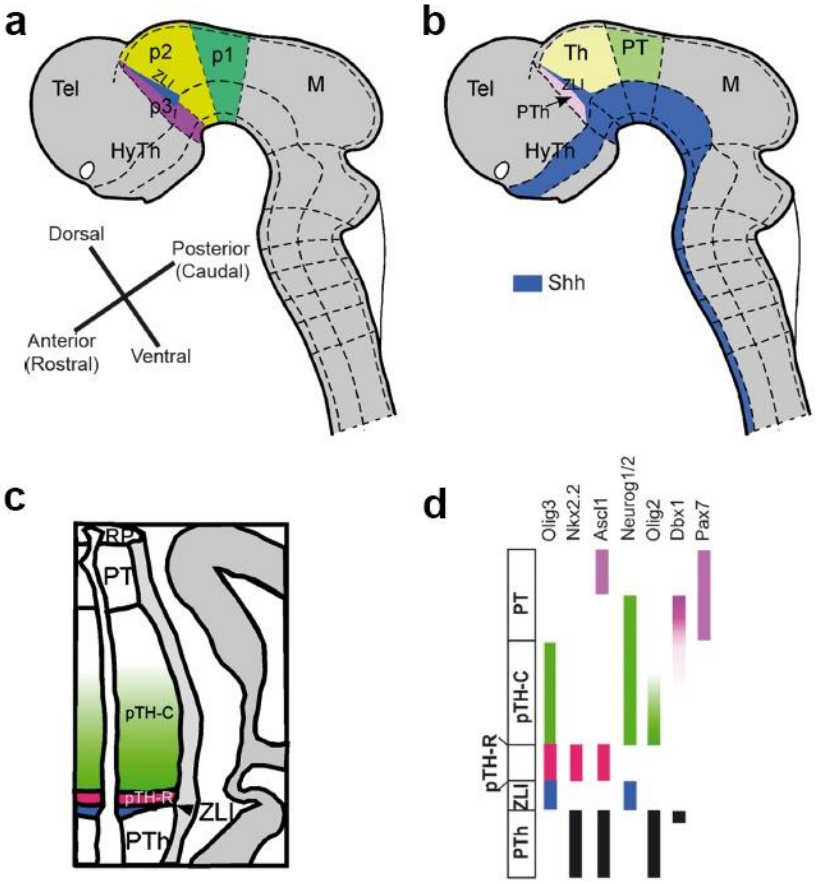

Figure 1.4: Progenitor domains of the developing diencephalon. (a) Lateral view of embryonic mouse forebrain. The diencephalon is subdivided into transverse domains p1, p2 and p3, from posterior to anterior. AP and DV axes around the thalamus are also shown. **(b)** The pretectum (PT), thalamus (Th) and prethalamus (PTh) are located in the alar plate of p1, p2 and p3, respectively. The zona limitans intrathalamica (ZLI) forms a transverse boundary in the alar plate between the thalamus and the prethalamus. **(c)** Horizontal section of the embryonic diencephalon. (d) Differential expression of transcription factors in discrete progenitor domains. Adapted from Nakagawa and Shimogori (2012) [68].

1.6.1 Progenitor domains of the developing diencephalon

Studies on gene expression and function identify the molecular heterogeneity of thalamic progenitors, which likely contributes to the formation and specification of

thalamic nuclei. OLIG2 and DBX1 show opposite expression patterns in the pTH-C **(Figure 1.4d)**. Analysis of *Olig2-EGFP* and *Dbx1-LacZ* animals suggest that anatomical positions of progenitors provide a broad map for their descendent neurons, and other mechanisms may underlie the specification and assembly of thalamic nuclei [70]. Fates of the pTH-R progenitors were studied using *Olig3-EGFP*, *Ascl1-EGFP* and *Tal1-CreER* animals, which collectively showed that the pTH-R progenitors generate part of the vLG population [70,72]. The remaining vLG cells are originated from PTh progenitors expressing *Dlx2* and *Dlx5/6*, indicating the multiple progenitor origins of vLG [72]. However, the functional difference between these two vLG populations remains to be explored. pTh consists of various progenitors, generating neuronal progenies populating several thalamic and hypothalamic nuclei, such as vLG, TRN and ZI [70,73]. Remarkably, dLG local interneurons in rodents have also been suggested to derive from a small PTh progenitor pool expressing *Otx2* [74]. Newborn cells first reach the vLG between E12.5 and E15.5, among which a subset of neurons migrate to and distribute within the dLG after birth. The migration and synaptic differentiation of these local interneurons show activity-dependent plasticity during the critical period from P0 to P12.

As discussed in Chapter 1.5.1, although local inhibitory interneurons are only found in dLG in rodents, their presence and density increases dramatically in animals performing more complicated behaviors, such as primates. Local interneurons in most mammalian species are locally derived from the diencephalon. In humans, however, histological studies and organotypic slice culture of human forebrain provide evidence of the migration of ganglionic eminence (GE) derived interneurons to the diencephalon [75,76]. This migration stream is absent in macaque monkey or any other

mammalian species, and might serve to specifically increase the interneuron population in HO nuclei of human thalamus.

1.6.2 Molecular pathways controlling thalamic patterning

Similar to other neural tube regions, dorsal and ventral signals in the developing diencephalon codify positional information to specify dorsal-ventral regional patterning. WNT, fibroblast growth factor 8 (FGF8), bone morphogenetic proteins (BMPs) and retinoic acid signals act upon the diencephalic epithelium to arrange the dorsal structure, while sonic hedgehog (SHH) directs ventral regionalization [77]. After the formation of neural tube, zona limitans intrathalamica (ZLI) is formed around E8.5 in mice and separates the developing thalamus to pTH-C and pTH-R. ZLI provides additional positional information to its surrounding tissues by releasing signaling molecules such as SHH, WNT and FGF, and is therefore termed the mid-diecephalic organizer (MDO) [78,79].

Before discussing the details, it should be noted that, due to the substantial expansion of cell population and neuronal migration during development, the thalamus shape changes significantly with some ventral regions bending towards dorsal and posterior. Therefore, subdivisions within the embryonic thalamus based on the anterior-posterior or dorsal-ventral axes may not correspond very well to those in the mature thalamus.

WNT/β-Catenin and SHH signaling pathways function in parallel to induce the differential expression of several transcription factors, which lead to the differentiation of glutamatergic excitatory neurons from progenitors in pTH-C and PT, and GABAergic inhibitory neurons from the progenitors in pTH-R and pTh [80,81]. These

two signaling pathways are active in partially complementary patterns within the thalamus [82]. WNT is secreted first from the dorsal roof plate, then through the MDO as development proceeds **(Figure 1.5 a)**, whereas SHH is expressed first in the basal plate and then extended dorsally through MDO (**Figure 1.5 b)**. In general, the lack of SHH signaling in the developing diencephalon leads to the loss of pTH-R and its interneuron progeny, reduced pTH-C markers and increased PT markers. Increasing SHH activity causes the expansion of the total thalamus especially the interneuron population, mixing of excitatory and inhibitory neurons at the pTH-C and pTH-R boarder, as well as a significantly reduced PT [81]. On the other hand, blocking WNT/β-Catenin activity by deleting β-Catenin gene (*Ctnnb1*) induces ectopic expression of pTH-R markers at the expense of pTH-C progenitors and their progenies. And the ectopic expression of pTH-R markers occurs throughout pTH-C, unlike the restricted pattern in animals with increased SHH level [80]. To dissect the interaction between these two signaling pathways, experiments were performed using animals in which both signals were reduced. It has been shown that different transcription factors expressed in the same thalamic progenitor domain have different requirements for β-Catenin and SHH signaling. For example, expression of NKX2.2 in pTH-R relies entirely on high SHH level, whereas HELT and ASCL1 expression in the same region is independent of direct SHH activity but requires the absence of β-Catenin[80].

FGF8 functions independently of SHH and WNT in specifying pTH-R identity[81,83]. It is first expressed in the dorsal roof plate and then extended to the dorsal tip of MDO (**Figure 1.5 c)**. Although both thalamus and prethalamus are exposed to FGF signaling, only the thalamic progenitor domain is affected by FGF8 manipulation[83]. Similar to the other two pathways, FGF8 controls pTH-C and pTH-R

in a complementary manner. Further studies are required to understand the crosstalk and collaboration among these three signaling pathways.

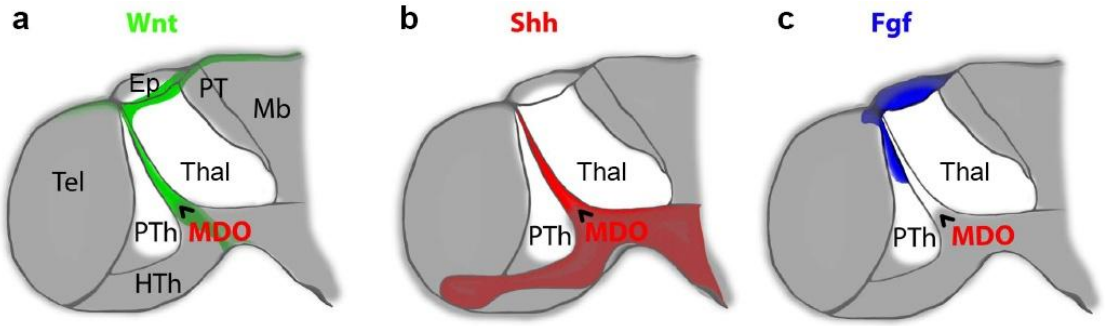

Figure 1.5: Partially overlapped expression of three morphogen signaling families in the embryonic diencephalon. These three families of signaling molecules encircle the developing thalamus from dorsal (WNT and FGF), ventral (SHH) and rostral (WNT, SHH, and FGF). Th, thalamus; PTh, prethalamus; Ep, epithalamus; Tel, Telencephalon; PT, pretectum; Mb, midbrain; MDO, mid-diencephalic organizer. Adapted from Hagemann and Scholpp (2012) [79].

The functional importance of the thalamus warrants a better understanding of its development. While the progenitor domains and major signaling pathways in the developing thalamus have been largely delineated, the principles underlying complex nuclear formation and organization of the mammalian thalamus remain largely elusive.

Chapter 2
Overview of Experimental Approach

2.1 Introduction to clonal analysis using MADM

Previous studies have demonstrated that lineage relationships play an instructive role in guiding the structural and functional assembly of the cortex [84-88], a laminated structure intimately associated with and reciprocally interconnected with the thalamus [10,89,90]. Lineage history not only contributes to the spatial/structural organization, but also influences the functional development of the neocortex as excitatory cells derived from the same progenitor cell exhibit preferential (both electrical and chemical synapse-based) connectivity and similar physiological properties amongst each other in comparison to nearby non-lineage related cells.

It has previously been suggested that cell lineages in the chick diencephalon exhibit diverse migration routes in general [91,92]. However, it remains largely unclear whether lineage relationships influence the complex nuclear formation and organization of the generally non-laminated thalamus. To address this, we performed a systematic clonal analysis of the progenitor behavior and progeny organization in the developing mouse thalamus using mosaic analysis with double markers (MADM) [93-95], as well as Cre recombinase-dependent retroviral labeling [96].

MADM is a powerful approach to investigate progenitor behavior and lineage progression with single cell resolution. It was developed by Luo and colleagues to allow simultaneous labeling and gene knockout in clones of somatic cells in mice. The first generation of MADM was reported in 2005 and contained MADM cassettes on chromosome 6 (MADM-6) [93]. The labeling was achieved by recombination-induced reconstitution of chimeric fluorescent proteins, GFP and Dsred2. The frequency of Cre-loxP-mediated recombination is generally low, and it varies depending on the

chromosomal location of the MADM cassettes and the strength of Cre activity. Extension of MADM to chromosome 11 (MADM-11) was reported in 2010 [95], which offered several advantages for genetic labeling and lineage tracing over the original MADM-6. DsRed2 in the original chimeric MADM cassettes was replaced by tdTomato, which allowed for more prominent labeling of axonal processes and direct visualization of the red fluorescence marker in live animals. More importantly, the inter-chromosomal recombination rate in MADM-11 was markedly increased compared to MADM-6, and it enabled temporally-controlled clone induction in many brain regions, including the thalamus.

2.2 MADM analysis of thalamic neurogenesis*

To label individual neural progenitors lining the third ventricle in the developing mouse thalamus, we introduced the *Nestin-CreER^{T2}* transgene [97], in which a tamoxifen (TM)-inducible Cre recombinase was selectively expressed in neural progenitors, including OLIG3 [70] and brain lipid-binding protein (BLBP)-positive thalamic radial glial progenitors (RGPs) **(Figure 2.1a)**, into the *MADM11* system [95]. In MADM, Cre recombinase-mediated inter-chromosomal recombination in dividing progenitors followed by X-segregation (G_2-X) restores one fluorescent marker, enhanced green fluorescent protein (EGFP, green) or tandem dimer Tomato (tdTomato, red), in each of the two daughter cells [93] **(Figure 2.1b)**. This results in permanent labeling of the two daughter cells and all their descendent lineages in two distinct colors. In addition, upon G_2-Z recombination and segregation, or $G_{1/0}$

* Shi W, Xianyu A, Han Z, Tang X, Li Z, Zhong H, Mao T, Huang K, and Shi SH. Ontogenetic establishment of order-specific nuclear organization in the mammalian thalamus. *Nature Neuroscience* **20**, 516–528 (2017).

recombination events, both EGFP and tdTomato are restored simultaneously in the same daughter cell, resulting in double-labeled (yellow) lineages.

We induced Cre recombinase activity to trigger recombination and labeling via a single dose of TM administered to timed pregnant female mice at one of the following embryonic (E) stages: E9, E10, E11, or E12, and analyzed the brains at the embryonic stages or postnatal (P) days 21-24 **(Figure 2.1c)**. We found no labeling in the absence of TM treatment (n=3 mice). We sometimes observed labeled cells in the other brain regions (data not shown). Notably, OLIG3 was specifically expressed in thalamic progenitors in the developing forebrain, and thalamic progenitors produced neurons exclusively located in the thalamus (**Figure 2.1d)**, as previously shown[70]. Also, there was no evidence of cells generated in other regions migrating into the rodent thalamus during development. Therefore, *Nestin-CreER*$^{T2+/-}$*/MADM-11* animals allowed us to examine thalamic neurogenesis. To recover all labeled cells in the thalamus, we performed serial sectioning, immunostaining, and three-dimensional (3D) reconstruction of individual thalami.

Figure 2.1: Experimental paradigm of MADM-based clonal analysis of thalamus development. (a) Confocal images of an E12 *Nestin-CreERT2;Ai9-tdTomato* brain treated with TM at E10 and stained for BLBP (green), a radial glial progenitor-specific marker, tdTomato (red), and OLIG3 (white), and with DAPI (blue). A schematic of brain structures is shown at the top. Note that BLBP-expressing radial glial progenitors in the developing thalamus marked by OLIG3 expression are labeled by tdTomato upon TM treatment, indicating that $CreER^{T2}$ is expressed in thalamic radial glial progenitors in the *Nestin-CreER*^{T2} mouse line. Scale bar: 100 μm. (b) Schematic of MADM labeling (Adapted from Fig. S1A, Gao et al., 2014 [94]). (c) Experimental paradigm of MADM-based clonal analysis. (d) Confocal image of a P21 *Olig3-Cre;Ai9-tdTomato* brain stained for tdTomato (red) and with DAPI (blue). Note the specific expression of tdTomato in the thalamus and thalamocortical projections. Scale bar: 500 μm. TC, thalamocortical.

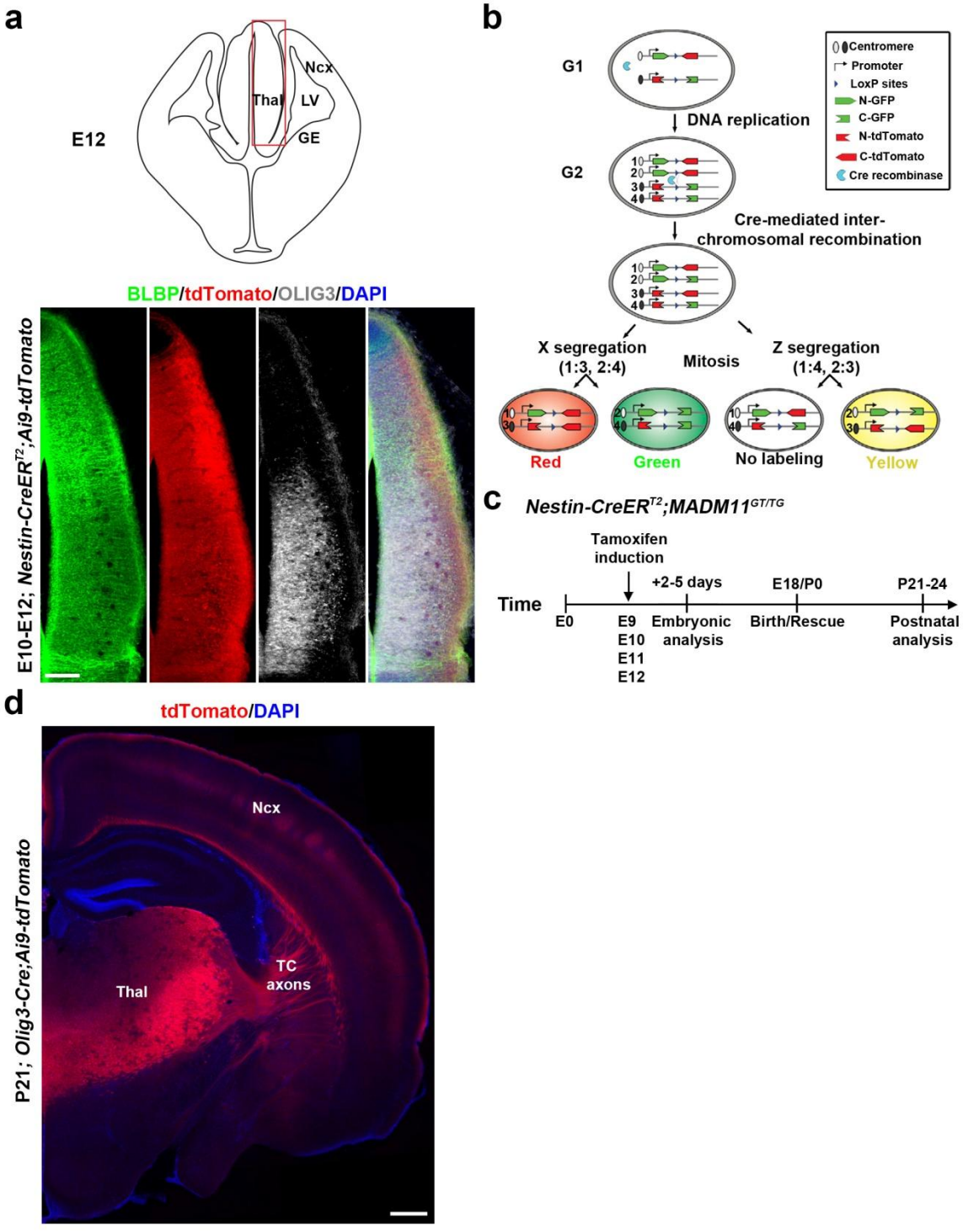
a
E12
Ncx
Thal
LV
GE
BLBP/tdTomato/OLIG3/DAPI
E10-E12; Nestin-CreER^{T2};Ai9-tdTomato
b
G1
DNA replication
G2
Cre-mediated inter-chromosomal recombination
X segregation (1:3, 2:4)
Mitosis
Z segregation (1:4, 2:3)
Red
Green
No labeling
Yellow
Centromere
Promoter
LoxP sites
N-GFP
C-GFP
N-tdTomato
C-tdTomato
Cre recombinase
c
Nestin-CreER^{T2};MADM11$^{GT/TG}$
Tamoxifen induction
Time
E0
E9
E10
E11
E12
+2-5 days
Embryonic analysis
E18/P0
Birth/Rescue
P21-24
Postnatal analysis
d
tdTomato/DAPI
P21; Olig3-Cre;Ai9-tdTomato
Ncx
Thal
TC axons

We observed individual clusters of cells in green and red **(Figure 2.2a-c)**, or yellow **(Figure 2.3a)** fluorescence in the embryonic thalamus. These clusters were radially (i.e. mediolaterally) organized and contained bipolar RGPs with the defining morphological characteristics including a cell body in the ventricular zone (VZ) (arrows), a short process reaching the VZ surface with a large end-foot (asterisks), and a long fine radial glial fiber pointing towards the pial surface (open arrowheads), as well as a number of cells with short processes arrayed along the long radial glial fiber(s) (arrowheads) **(Figure 2.2c)**. To ensure unequivocal clonal analysis, we titrated the TM dose to achieve very sparse labeling, i.e. on average 1-2 progenitors (i.e. clones) per thalamic hemisphere (n=120 from 60 embryonic brains) **(Figure 2.2d)**. There were no scattered fluorescent cells or mixed clusters of green or red fluorescent cells with yellow fluorescent cells **(Figure 2.2)**.

Figure 2.2: Labeling of thalamic clones using MADM. (a) Confocal image of a MADM-labeled E12 clone labeled by TM treatment at E10 and stained for EGFP (green), tdTomato (red), and OLIG3 (white), a transcription factor selectively expressed in developing thalamic progenitors, and with 4',6-Diamidino-2-phenylindole (DAPI, blue). Scale bars: 100 μm. **(b)** 3D reconstructed image of the hemisphere in a. Blue lines indicate the contours of brain structures, white lines indicate the OLIG3-positive thalamic domain, and colored dots represent the cell bodies of labeled neurons. A, anterior; P, posterior; D, dorsal; V, ventral; M, medial; L, lateral. Scale bar: 100 μm. **(c)** High magnification confocal images of the clone in a. Arrows indicate the bipolar RGPs and arrowheads indicate the progeny that are arrayed along the radial glial fibers (open arrowheads). Broken lines indicate the surface of the VZ. Zoomed-in images of RGPs (area 1) and a progeny located near the pia with numerous branches (area 2) are shown to the right. The asterisks indicate the ventricular endfeet of RGPs. Ep, epithalamus; Thal, thalamus; PTh, prethalamus; Ncx, neocortex; Hip, hippocampus; GE, ganglionic eminence; LV, lateral ventricle; 3rd V, 3rd ventricle. Scale bars: 20 μm, 10 μm and 10 μm. **(d)** Percentage of the thalamic hemispheres with 0, 1, 2, 3, or 4 green/red clone or yellow clones.

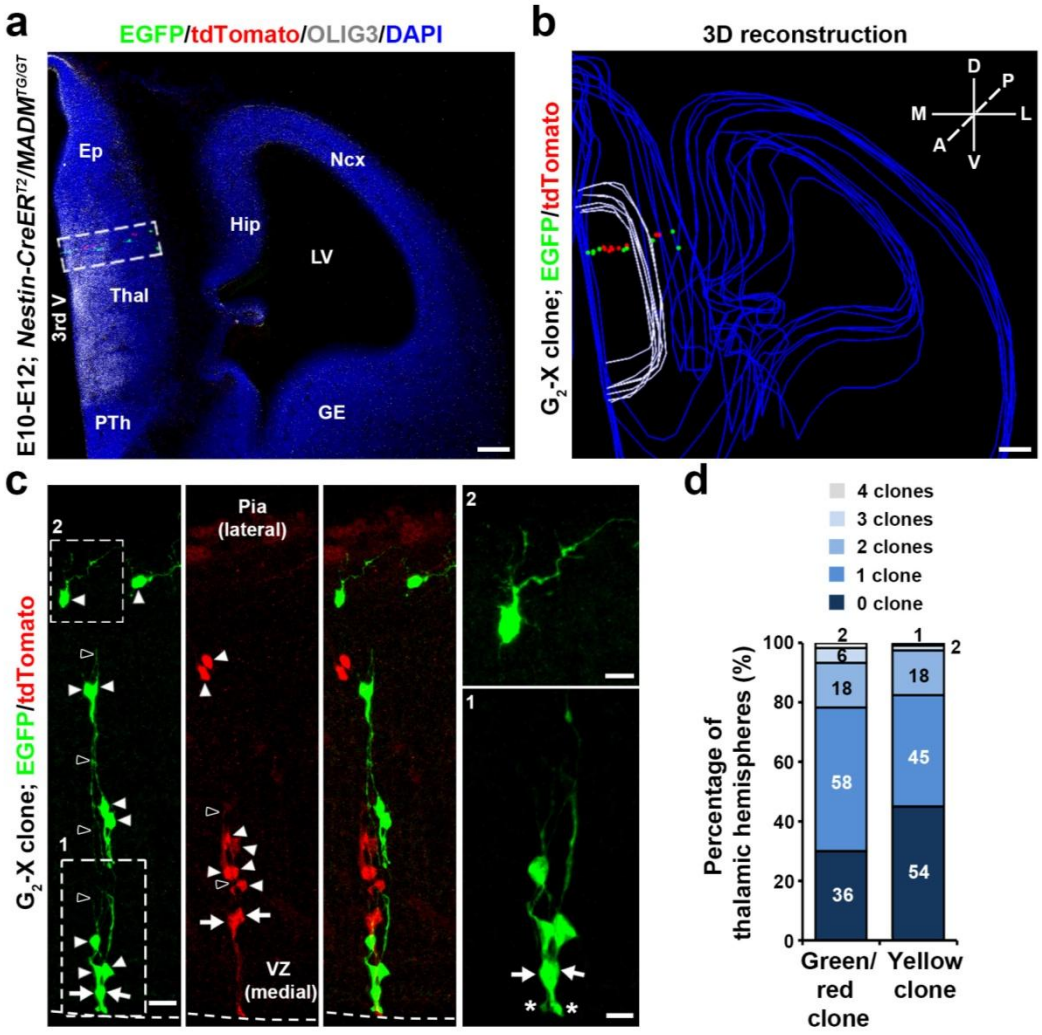
a
EGFP/tdTomato/OLIG3/DAPI
E10-E12; Nestin-CreER^{T2}/MADM$^{TG/GT}$
Ep
Ncx
Hip
LV
Thal
3rd V
PTh
GE
b
3D reconstruction
G$_2$-X clone; EGFP/tdTomato
D
P
M
L
A
V
c
G$_2$-X clone; EGFP/tdTomato
2
1
Pia
(lateral)
VZ
(medial)
d
4 clones
3 clones
2 clones
1 clone
0 clone
Percentage of thalamic hemispheres (%)
100
80
60
40
20
0
2
6
18
58
36
1
2
18
45
54
Green/ red clone
Yellow clone

Notably, similar discrete radial clusters in the embryonic thalamus were also reliably labeled by *in utero* intraventricular injection of low titer Cre recombinase-dependent retroviruses expressing EGFP into the *Olig3-Cre* [81] mouse embryos **(Figure 2.3b)**, which selectively infected individual OLIG3-expressing thalamic progenitors dividing at the VZ surface and thereby labeled their progeny. The consistent observation of radial clusters with two distinct clonal labeling methods confirmed the clonal nature of individual radial clusters in the developing thalamus.

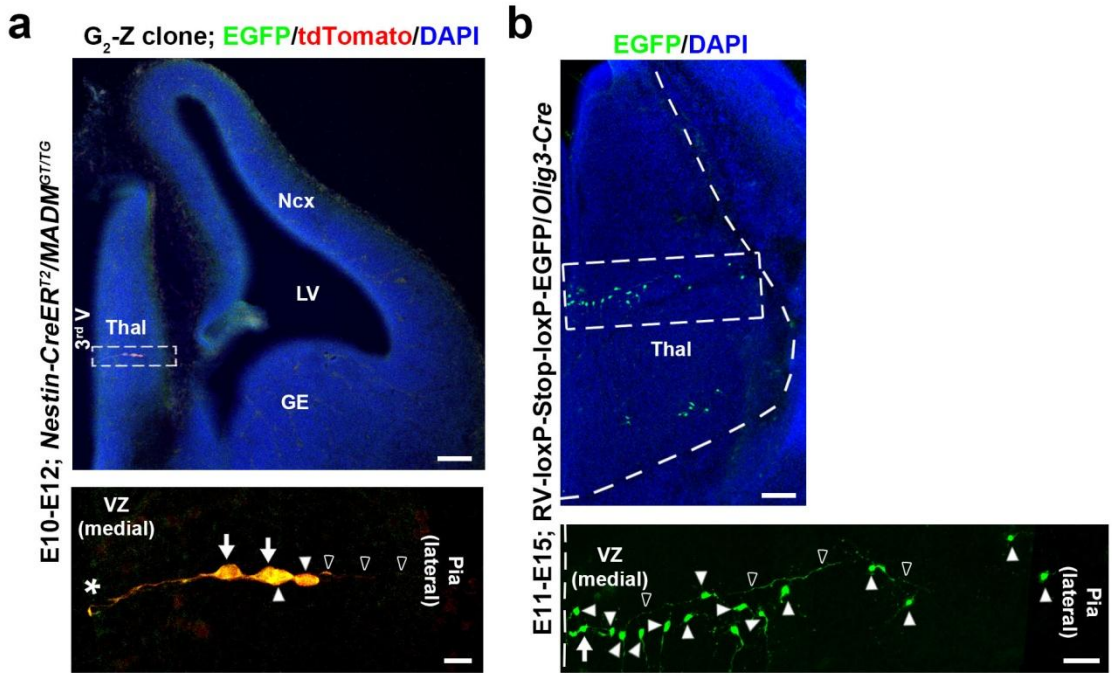

Figure 2.3: Cre recombinase-dependent retroviral labeling of thalamic clones. (a) Confocal images of an E12 brain treated with TM at E10 and stained for EGFP (green) and tdTomato (red), and with DAPI (blue). High magnification image of a G_2-Z yellow clone in the thalamus (boxed area) is shown to the right. Arrows indicate bipolar radial glial progenitors, arrowheads indicate the progeny, open arrowheads indicate the radial glial fibers, and the asterisk indicates the ventricular endfoot. Scale bars: 100 μm and 20 μm. **(b)** Confocal image of an E15 *Olig3-Cre* brain injected with low titer Cre recombinase-dependent retrovirus expressing EGFP at E11 and stained for EGFP (green) and with DAPI (blue). Note two radial clonal clusters in the developing thalamus (broken line). High magnification image of a clone (boxed area) is shown at the bottom. The arrow indicates the bipolar radial glial progenitor and arrowheads indicate the progeny that are radially arrayed along the radial glial fiber (open arrowheads). Another labeled clonal cluster is located ventrally. Scale bars: 200 μm and 50 μm.

Chapter 3
Production of Thalamic Clones

3.1 Cellular composition of embryonic thalamic clones*

In the *Nestin-CreER$^{T2+/-}$/MADM-11* animals, thalamic clones were labeled along the third ventricle by TM treatment at one of the following stages: E9, E10, E11, or E12. The clones were analyzed two days after TM treatment. We assessed the identity of cells in individual radial clonal clusters and found that the bipolar RGPs were positive for the neural progenitor cell marker NESTIN **(Figure 3.1a)** and the proliferation marker Ki-67 **(Figure 3.1b)**. We also observed cells with short-processes outside of the ventricular zone that were positive for Ki-67 **(Figure 3.1b)**, suggesting the existence of intermediate progenitors (i.e. basal progenitors) in the developing thalamus, as previously suggested [98]. Besides RGPs and intermediate progenitors, individual radial clonal clusters also contained cells located further away from the ventricular zone that grew relatively long processes with numerous branches and expressed the neuron-specific marker TUJ1 **(Figure 3.1c)**. Together, these results suggest that individual RGPs in the ventricular zone of the developing thalamus actively divide to produce intermediate progenitors and post-mitotic neurons that are spatially organized along the mother radial glial fiber into radial clusters.

---

* Shi W, Xianyu A, Han Z, Tang X, Li Z, Zhong H, Mao T, Huang K, and Shi SH. Ontogenetic establishment of order-specific nuclear organization in the mammalian thalamus. *Nature Neuroscience* **20**, 516–528 (2017).

Figure 3.1: Cellular composition of MADM-labeled embryonic thalamic clones. (a) Confocal image of an E12 G_2-X clone labeled at E10 and stained for EGFP (green), tdTomato (red), and NESTIN (white), a neural progenitor marker. The arrow indicates the RGP and arrowheads indicate the progeny. High magnification images (areas 1 and 2) are shown in the middle and cross-section images are shown to the right. Broken lines indicate the cell bodies. Scale bars: 20 μm, 10 μm, and 10 μm. (b) Confocal image of an E12 G_2-X clone labeled at E10 and stained for EGFP (green), tdTomato (red), and Ki-67 (white), a proliferation marker. Arrows indicate the bipolar RGPs and arrowheads indicate the progeny. High magnification images (areas 1-3) are shown in the middle and cross-section images are shown to the right. Broken lines indicate the cell bodies. Scale bars: 20 μm, 10 μm, and 10 μm. (c) Confocal image of an E12 G_2-X clone labeled at E10 and stained for EGFP (green), tdTomato (red), and TUJ1 (white), a neuronal marker. The arrow indicates the RGP and arrowheads indicate the progeny. High magnification images (areas 1-3) are shown in the middle and cross-section images are shown to the right. Broken lines indicate the cell bodies. Scale bars: 20 μm, 10 μm, and 10 μm.

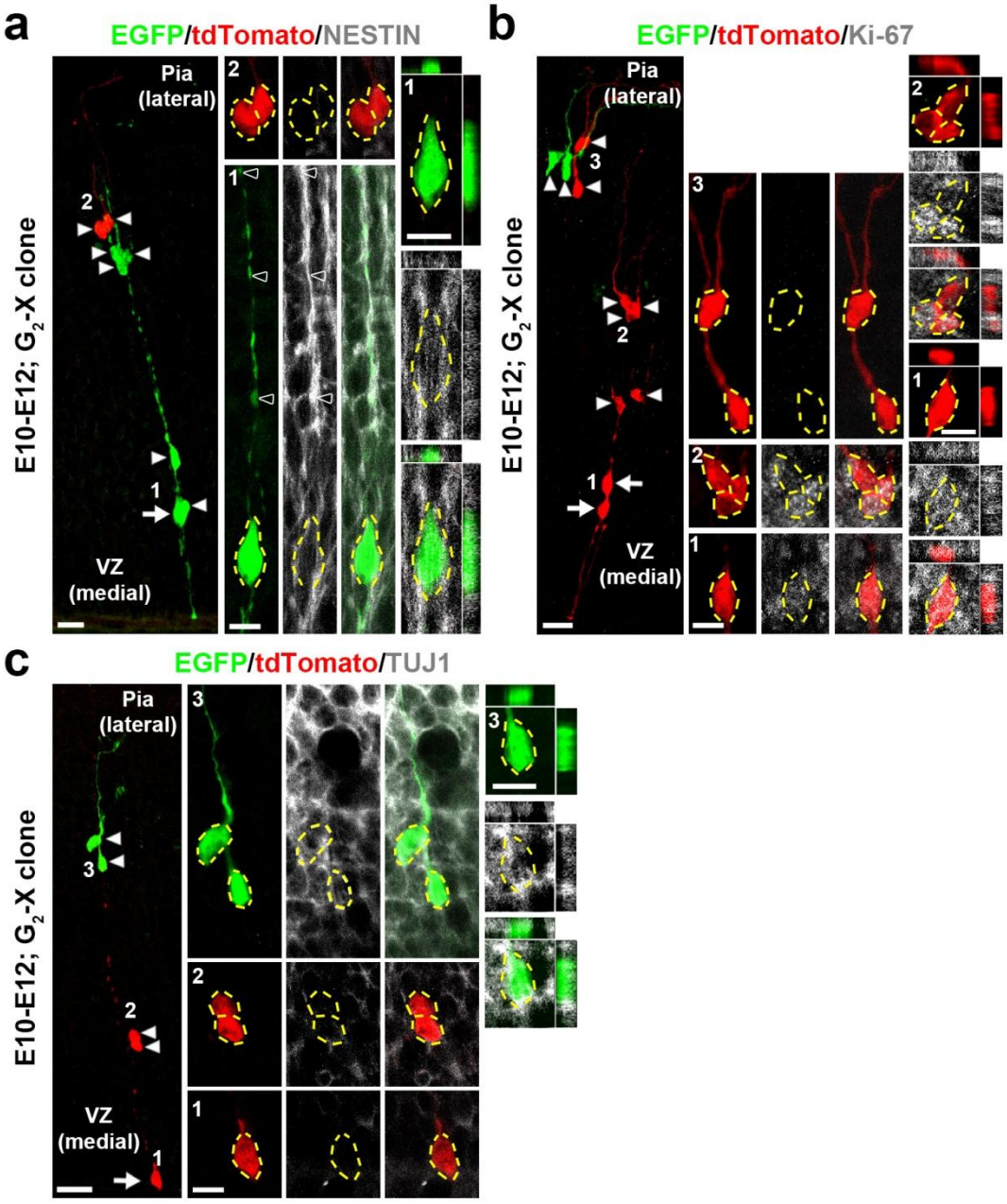
a
EGFP/tdTomato/NESTIN
E10-E12; G2-X clone
Pia (lateral)
VZ (medial)
b
EGFP/tdTomato/Ki-67
E10-E12; G2-X clone
Pia (lateral)
VZ (medial)
c
EGFP/tdTomato/TUJ1
E10-E12; G2-X clone
Pia (lateral)
VZ (medial)

3.2 Symmetric and asymmetric divisions of thalamic neural progenitors*

RGPs divide either symmetrically to generate two RGPs or asymmetrically to give rise to a RGP and a differentiating progeny such as an intermediate progenitor or a post-mitotic neuron. Consistent with this, we observed two types of G_2-X green and red fluorescent clones. One type contained both green and red fluorescent RGPs as well as a cohort of green and red fluorescent progeny distributed radially along the radial glial fibers **(Figure 2.2a-c)**, representing the symmetrically dividing RGP clones. In contrast, the other type contained a 'majority' population including RGP(s) in one color and a 'minority' population in the other color that did not include RGPs **(Figure 3.1)**. The scarcity of the minority population indicates that the original daughter cell, from which the minority population arises, is either a neuron or an intermediate progenitor capable of undergoing limited (e.g. 1-2) rounds of division, whereas the majority population originates from a self-renewing RGP that undergoes multiple rounds of division consecutively. Therefore, these clones represent the asymmetrically dividing RGP clone. We found that as development proceeded, the frequency of observing symmetric clones decreased, while the frequency of observing asymmetric clones concurrently increased **(Figure 3.2a)**, indicating that RGPs progressively lose their proliferative potential in the embryonic thalamus. Related to this, we observed a progressive decrease in the average number of neurons in clones labeled between E10-E12 **(Figure 3.2b)**. Clones also contained glia cells, which will be discussed in Chapter 4.2.

---

* Shi W, Xianyu A, Han Z, Tang X, Li Z, Zhong H, Mao T, Huang K, and Shi SH. Ontogenetic establishment of order-specific nuclear organization in the mammalian thalamus. *Nature Neuroscience* **20**, 516–528 (2017).

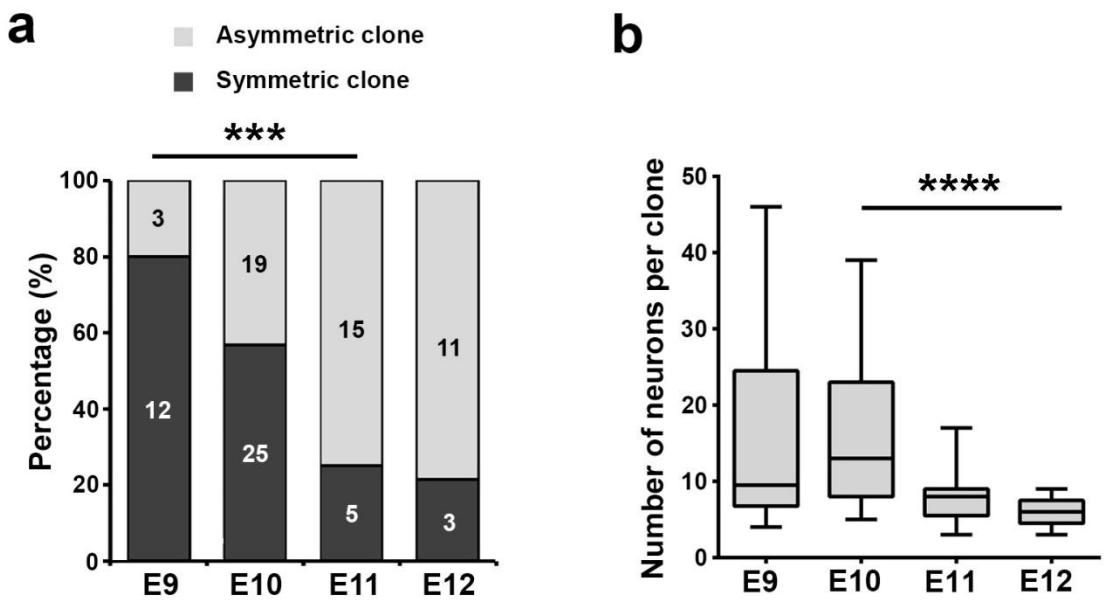

Figure 3.2: Division modes of thalamic neural progenitor. (a) Percentage of symmetric (Sym.) vs. asymmetric (Asym.) thalamic clones labeled at different embryonic stages and examined two days later (E9, n=15 clones; E10, n=44 clones; E11, n=20 clones; E12, n=14 clones). ***, p=0.0006 (chi-square test for linear trend). **(b)** Quantification of the average number of neurons in individual green/red G_2-X clones labeled at different embryonic stages and examined at P21-24 (E9, n=10 clones; E10, n=23 clones; E11, n=13 clones; E12, n=9 clones). Data are presented as median with interquartile range, and whiskers are the minimum and maximum. ****, p=2.5e-05 (linear regression analysis).

There was a small but significant decrease in the average number of neurons in clones labeled at E10 and examined at E15 and P21-24 **(Figure 3.3a)**, indicating that some neurons are pruned away during development. We also occasionally observed small local clusters without RGPs in animals with TM treatment at E12 and analyzed at E14 **(Figure 3.3b)**, likely representing dividing intermediate progenitor-derived clones.

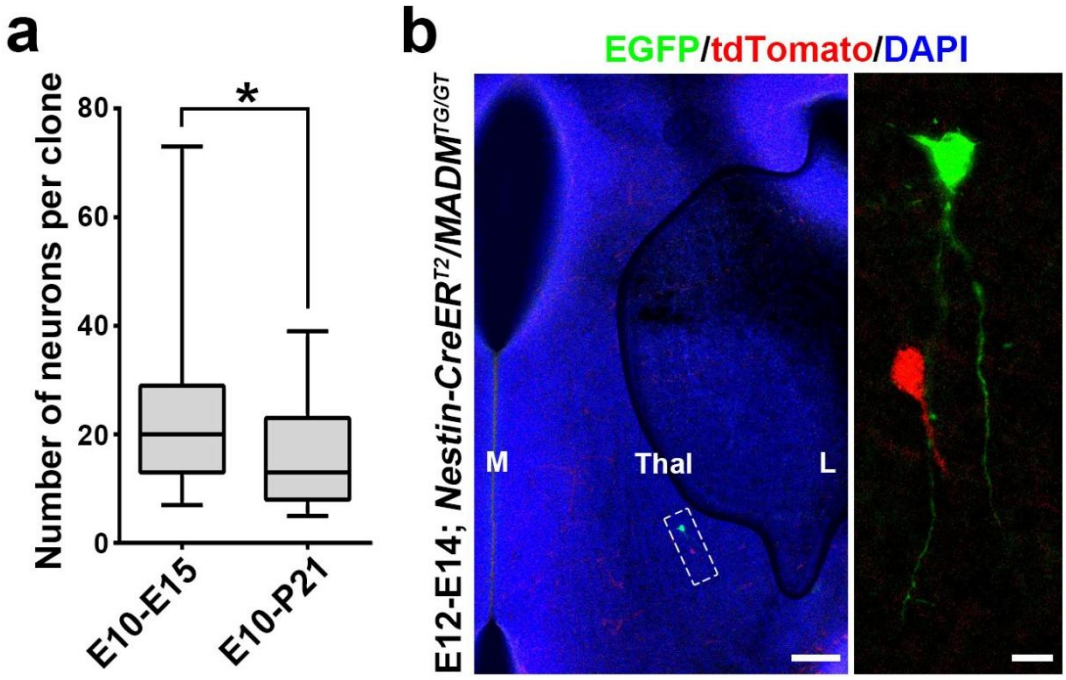

Figure 3.3: Small but significant cell death in the developing thalamus (a) Quantification of the average number of neurons in clones labeled at E10 and examined at E15 or P21 (E10-15, n=23; E10-P21, n=23). Data are presented as median with interquartile range and whiskers are the minimum and maximum. *, $p<0.05$ (Mann Whitney test). **(b)** Confocal images of an E14 MADM-labeled thalamus treated with TM at E12 and stained for EGFP (green) and tdTomato (red), and with DAPI (blue). A two-cell local cluster without any radial glial progenitors (boxed area) is labeled in the developing thalamus. High magnification image is shown to the right. M, medial; L, lateral. Scale bars: 100 μm and 10 μm.

3.3 Birth date-dependent outside-in migration of thalamic neurons

Notably, the minority population in asymmetric clones labeled at E12 and analyzed at E14 typically resided furthest in the mantle region (i.e. laterally) relative to the majority population and was positive for the neuronal marker TUJ1 **(Figure 3.1)**, suggesting that these cells represent the earliest born neurons in the labeled lineage. Moreover, these results indicate that thalamic neurons migrate outward in a birth date-

dependent outside-in pattern at the clonal level, consistent with the previous classic population birthdating analyses [99-101].

To further explore neuronal migration in the developing thalamus, we performed sequential pulse-chase birth dating experiments using EdU (5-ethynyl-2'-deoxyuridine) and BrdU (5-bromo-2'-deoxyuridine), and found that the early born neurons were indeed located more laterally than the late born neurons **(Figure 3.4a)**. Moreover, as implicated previously [99], neurons in the posterolateral region appeared to be born earlier than those in the anteromedial region **(Figure 3.4b)**, reflecting a birth date-dependent outside-in migration as well as the growth and reshaping of the thalamus (i.e. a swirling shift of the ventrolateral region towards the dorsoposterior). Together, these results suggest that, while clonally related neurons in both the cortex and thalamus form radial clusters at the embryonic stages, they exhibit drastic differences in migration. Thalamic neurons migrate radially in a birth date-dependent outside-in manner, whereas cortical neurons migrate radially in a birth date-dependent inside-out manner[84].

Figure 3.4: Birth date-dependent outside-in migration of thalamic neurons. (a) Confocal images of an E13 thalamus subjected to sequential pulse-chase labelling with EdU (red) and BrdU (green) at E12 separated by 6 hours, and stained for Ki67 (white), a proliferation marker, and with DAPI (blue). The labelling protocol is shown at the top. The solid line indicates the midline (M) while the left and right broken lines indicate the front lines of Ki67+ progenitor domain and BrdU-labelled cells towards the lateral (L), respectively. Note that the early born EdU-labelled cells are more laterally located than the late born BrdU-labelled cells, indicating a birth date-dependent outside-in migration pattern of thalamic neurons. D, dorsal; V, ventral. Scale bar: 100 μm. **(b)** Confocal images of a P0 thalamus subjected to sequential pulse-chase labelling with EdU (red) and BrdU (green) at E11 and E12, respectively, and stained for SOX2 (blue), a transcription factor selectively expressed in the developing thalamus. The labelling protocol is shown at the top. The anterior, medial, and posterior sections are shown in the top, middle, and bottom panels, respectively. The white broken lines indicate the thalamus and the yellow broken lines indicate the boundary of EdU and BrdU labelled neurons in the medioposterior part of the thalamus. Note that the early born EdU labelled neurons are located more laterally (L) than the late born BrdU labelled neurons. In addition, the ventral thalamus is bent towards the dorsal (D) surface. V, ventral; M, medial. Scale bars: 200 μm, 200 μm, and 200 μm.

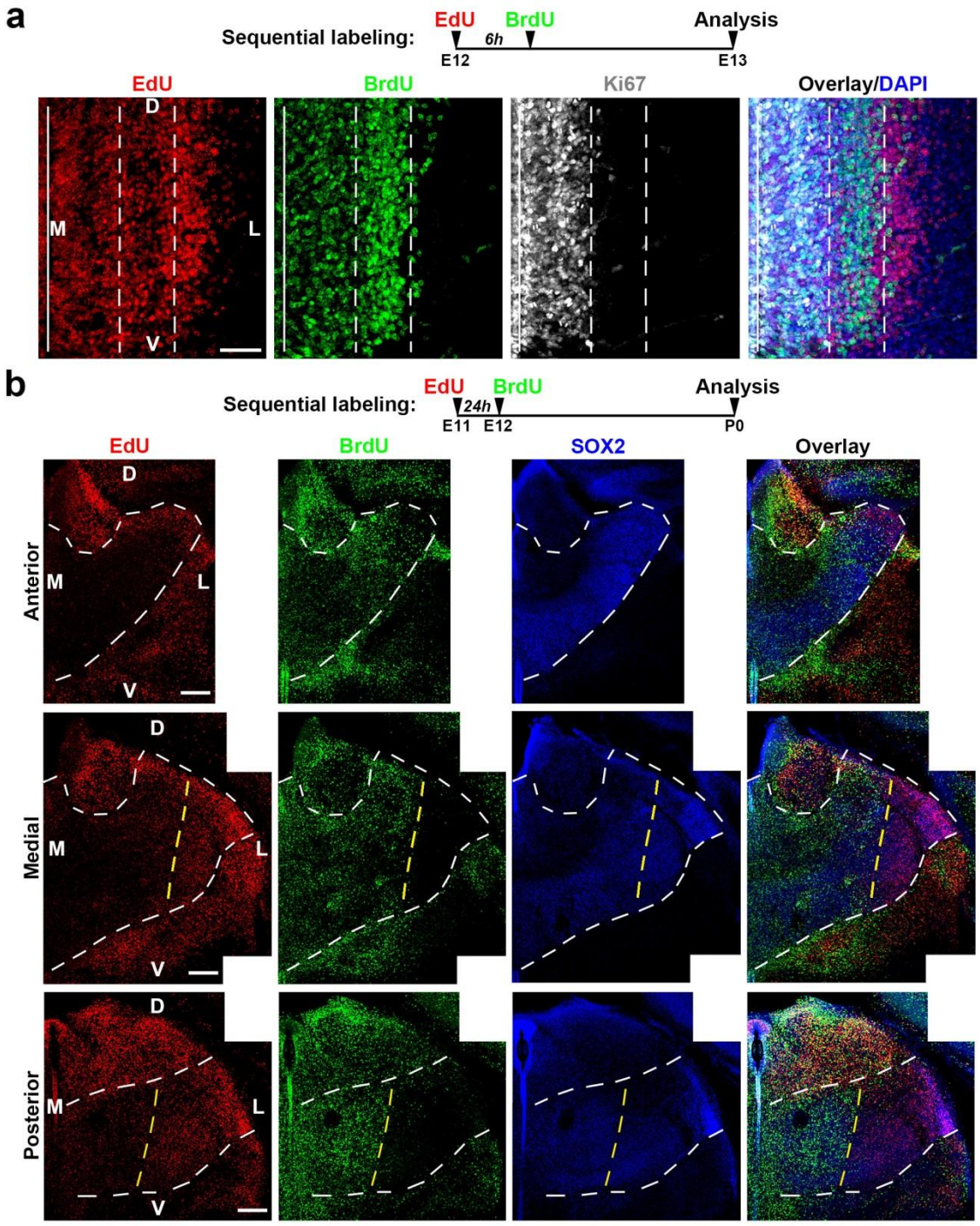
a
Sequential labeling:
EdU
BrdU
6h
Analysis
E12
E13
EdU
BrdU
Ki67
Overlay/DAPI
D
M
L
V
b
Sequential labeling:
EdU
BrdU
24h
Analysis
E11
E12
P0
EdU
BrdU
SOX2
Overlay
Anterior
Medial
Posterior
D
M
L
V

Chapter 4
Spatial clustering of Thalamic Clones at the mature stage *

4.1 Spatial clustering of clonally-related thalamic neurons

The diverse functions of the thalamus are carried out by a large number of nuclei [1,4]. To test whether the progenitor origin and lineage relationships of cells influence nuclear formation and organization in the thalamus, we systematically examined the spatial distribution of individual E9, E10, E11, and E12-labeled thalamic clones at P21-24, when the nuclei are formed and functional connections are largely established. The vast majority of clones spanned several consecutive sections and consisted of NEUN-positive neurons with the characteristic morphological features of thalamic excitatory neurons, including tufted or spherically radiating dendrites **(Figure 4.1a)** as shown previously [102]. Moreover, within individual sections, neurons in individual clones were not broadly distributed, but restricted to a defined (e.g. dorsal or ventral) region, as revealed by confocal imaging and 3D reconstruction **(Figure 4.1a,b)**.

* Shi W, Xianyu A, Han Z, Tang X, Li Z, Zhong H, Mao T, Huang K, and Shi SH. Ontogenetic establishment of order-specific nuclear organization in the mammalian thalamus. *Nature Neuroscience* **20**, 516–528 (2017).

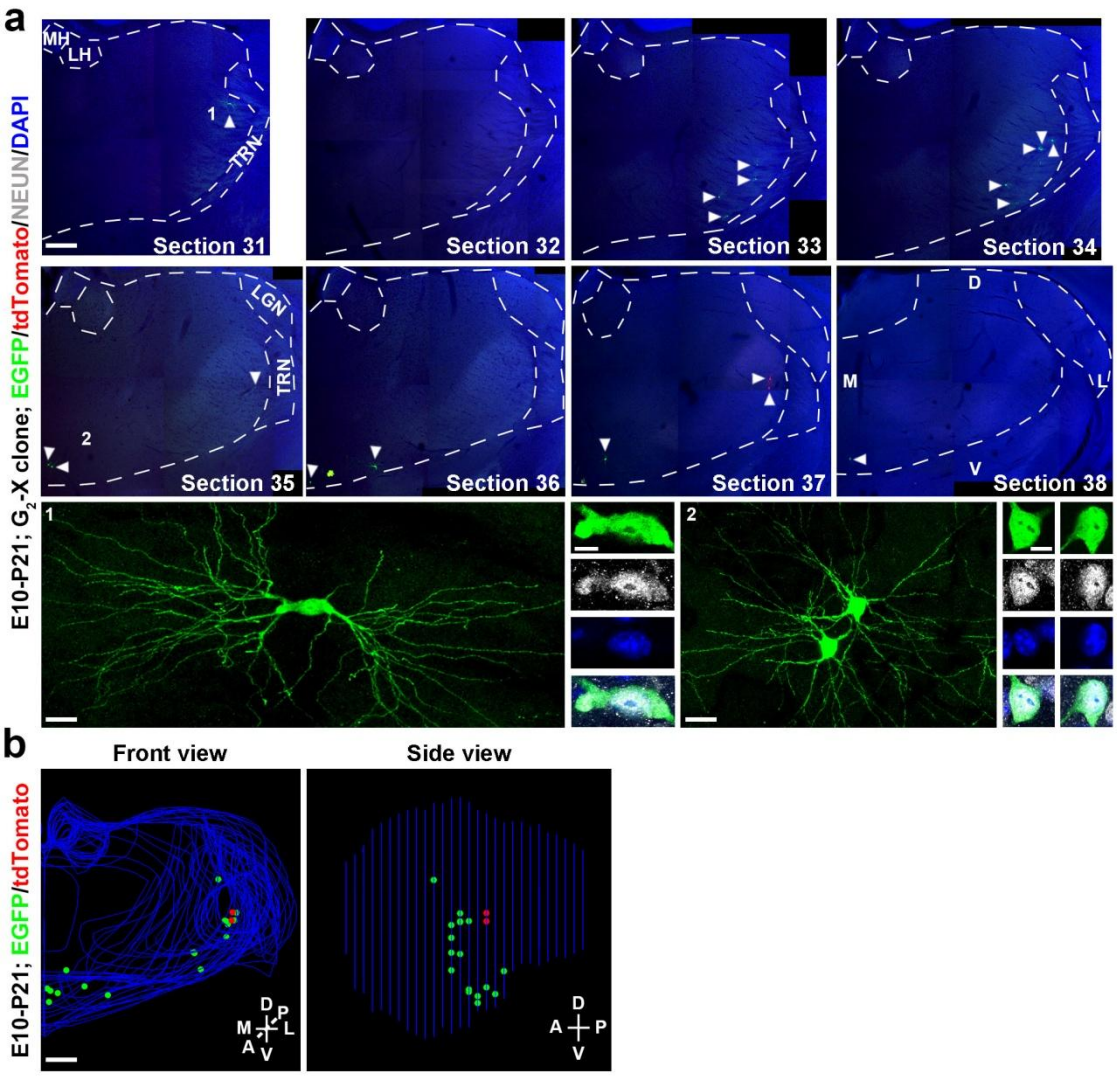

Figure 4.1: 3D reconstruction of thalamic clones at the mature stage. (a) Confocal images of a green/red G_2-X clone in a P21 brain treated with TM at E10. Consecutive sections were stained for EGFP (green) and tdTomato (red), and with DAPI (blue). Broken lines indicate the contours of the thalamus and landmark nuclei including the medial and lateral habenula (MH, LH), lateral geniculate nucleus (LGN), and the thalamic reticular nucleus (TRN). Arrowheads indicate the labeled neurons. High magnification images of representative labeled neurons positive for neuronal marker NEUN (white) (areas 1 and 2) are shown at the bottom. Scale bars: 500 μm, 20 μm, 10μm, 20 μm, and 10μm. **(b)** 3D reconstructed images of the thalamic hemisphere containing the clone shown in a (Front view, left; Side view, right). Blue lines indicate the contours of the thalamus and landmark nuclei and colored dots represent the cell bodies of labeled neurons. M, medial; L, lateral; D, dorsal; V, ventral; A, anterior; P, posterior. Similar display is used in subsequent 3D reconstructed images. Scale bar: 500 μm.

Notably, the overall spatial localization of progenitors labeled at different embryonic stages correlated well with the overall regional localization of clones observed at P21-24 **(Figure 4.2)**, suggesting that clones located in different regions of the mature thalamus are most probably derived from progenitors located in the corresponding regions of the embryonic thalamus. This is consistent with the previous genetic fate mapping studies showing that progenitors in the rostral (pTH-R) and caudal (pTH-C) subdomains of the developing thalamus contribute to distinct thalamic nuclei [70,81].

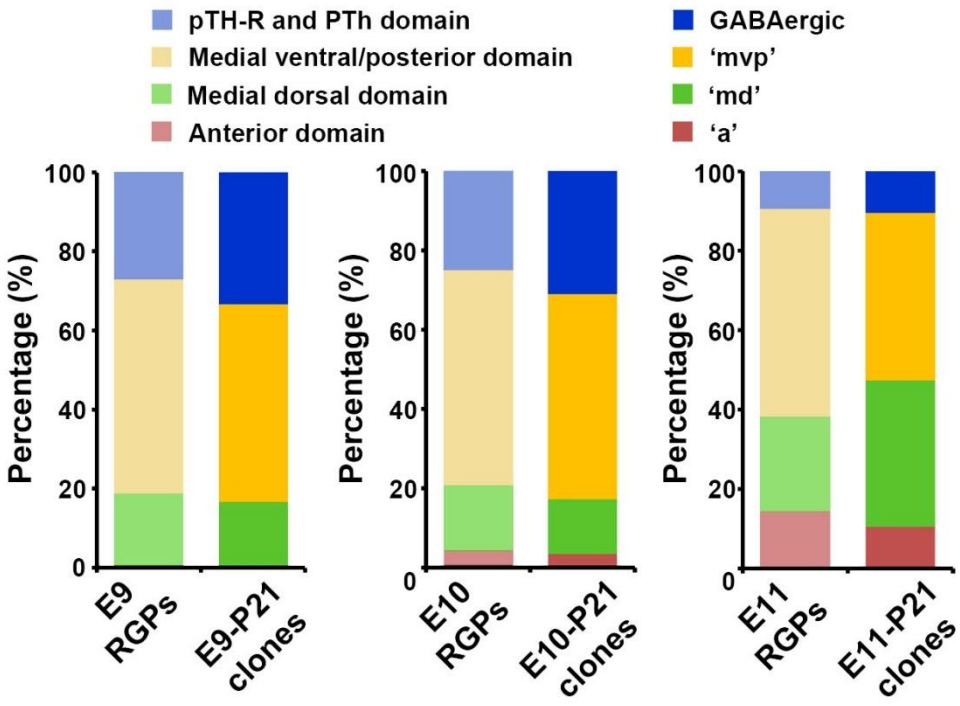

Figure 4.2: Correlated localization of MADM-labeled RGPs at the indicated embryonic stage and clones at a more mature stage. Note a clear correlation between the localizations of labeled progenitor cells and labeled clones at different embryonic stages. pTH-R: rostral progenitor domain of the thalamus; PTh: prethalamus.

To quantitatively assess the spatial distribution and clonal relationship of labeled neurons, we applied nearest neighbor distance (NND) analysis to all the 3D reconstructed P21-24 thalamic datasets labeled at E9-E12 (n=77 in total from over 45 mice; E9, n=18; E10, n=29; E11, n=19; and E12, n=11), which calculates the cumulative frequency distribution of the NND for the data points and thereby reports the spacing patterns of the dataset [94,103-105]. Compared with spatially random simulated datasets containing the same number of data points within the same volume (i.e. the thalamus) repeated 100 times (gray), the experimental datasets of thalamic clones (red) labeled at different embryonic stages exhibited similar and much shorter (i.e. left-shifted) NNDs **(Figure 4.3a-c)**. Moreover, in the datasets containing both green/red and yellow fluorescent clones, the green/red fluorescent neurons (blue) or the yellow fluorescent neurons (yellow) (i.e. intra-clonal NNDs) exhibited similar and significantly shorter NNDs than the green/red and yellow fluorescent neurons (magenta, i.e. inter-clonal NNDs) **(Figure 4.3d,e)**. Together, these results demonstrate that clonally related neurons originating from sparsely-labeled progenitors do not randomly mix, but form spatially segregated regional clusters in the thalamus. Thereby, each regional neuronal cluster represents a clone that arises from a single dividing thalamic progenitor.

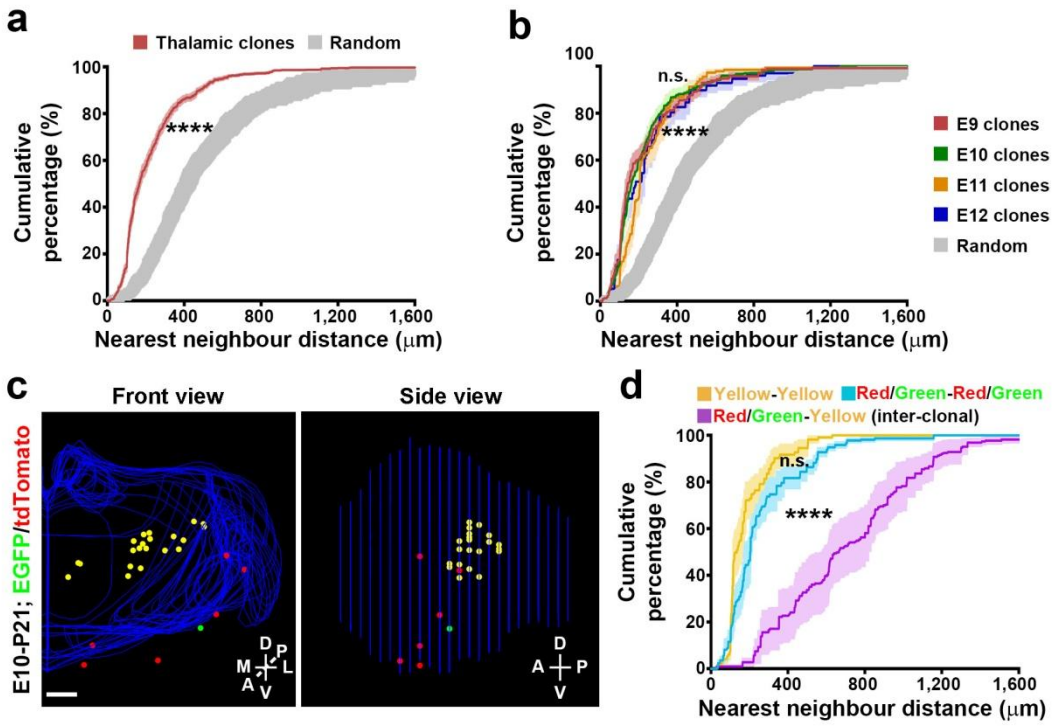

Figure 4.3: Spatial clustering of clonally related neurons in the thalamus at the mature stage. (a) Nearest neighbor distance (NND) analysis of MADM-labeled neuronal clones (n=77) in the P21-24 thalamus. Data are presented as mean±s.e.m. ****, p=1e-15 (unpaired t-test with Welch's correction). **(b)** NND analysis of clones labeled at different embryonic stages. Note that the cumulative frequency of NND of clones labeled at E9 (red, n=18), E10 (green, n=28), E11 (orange, n=19), and E12 (blue, n=11) is similar and significantly left-shifted than that of random simulated dataset (gray). Data are presented as mean±s.e.m. n.s., not significant; ****, p<0.0001 (unpaired t test with Welch's correction). **(c)** 3D reconstructed images of a thalamic hemisphere containing both a green/red G_2-X clone and a yellow clone. Scale bar: 500 μm. **(d)** NND analysis of MADM-labeled green/red and yellow neuronal clones in the same thalamic hemisphere. Note that the cumulative frequency of NND of green/red (blue, n=11) or yellow (yellow, n=11) fluorescent neurons (i.e. intra-clonal) is similar and significantly left-shifted than that of green/red and yellow (magenta, n=11) fluorescent neurons (i.e. inter-clonal). Data are presented as mean±s.e.m. ****, p=1e-15 (unpaired t-test with Welch's correction).

4.2 Spatial clustering of clonally-related glial cells in the mature thalamus

Notably, we also observed NEUN-negative cells with a small soma/nucleus and short neurite processes in nearly half (34 out of 77) of the clones labeled at E9-E12 **(Figure 4.4)**.

Additional immunohistochemsitry analyses revealed that cells with a small soma/nucleus and short bushy neurites typically expressed S100, an astrocyte marker, and that cells with a small soma/nucleus and short parallel neurites characteristically expressed OLIG2, an oligodendrocyte maker **(Figure 4.5)**. These results suggest that the NEUN-negative cells are glial cells. Notably, the morphological features of these glial cells are consistent with the previous observation in the rat thalamus [106]. The labeled glial cells were typically located in close proximity to the labeled neurons **(Figure 4.4, 4.5)**.

Figure 4.4: Shared progenitor origin of neurons and glial cells in the thalamus. (a, b) Scanned images of a yellow G_2-Z clone in a P21 brain treated with TM at E9. Consecutive sections were stained for EGFP (green) and tdTomato (red), and with DAPI (blue). Open arrowheads indicated the labeled NEUN-negative cells and arrowheads indicate the labeled neurons. High magnification images of the representative labeled neuron positive for NEUN (white) (area 1) and glial cells (areas 2 and 3) negative for NEUN are shown in b. Scale bars: 500 μm, 20 μm, 10μm, 20 μm, and 10 μm. **(c)** 3D reconstructed images of the thalamic hemisphere containing the clone shown in a (Front view, left; Side view, right). Scale bar: 500 μm. **(d)** Quantification of the fraction of P21-24 clones labeled at E9-12 containing neuron only (N) or neuron and glia (N+G).

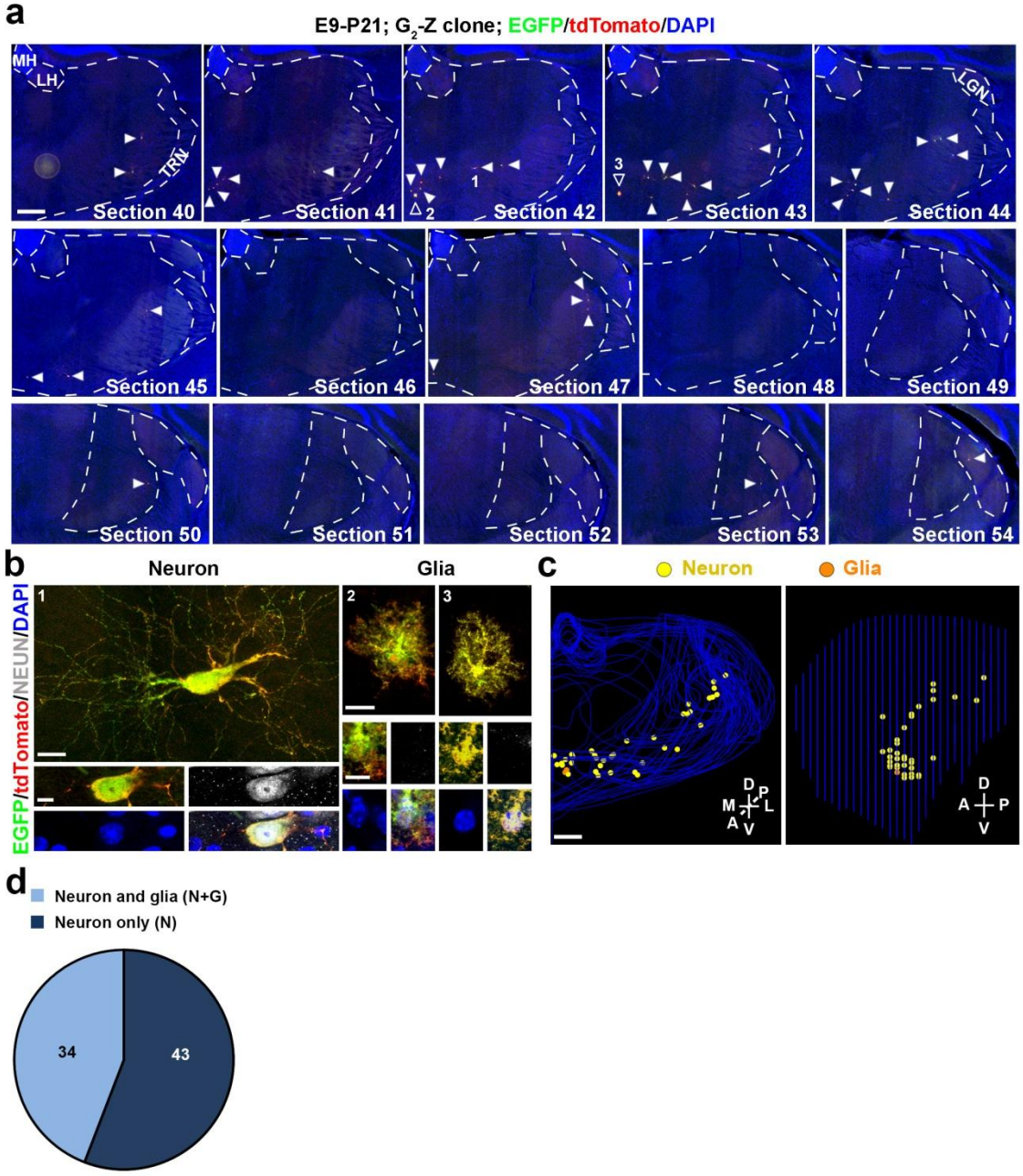
a
E9-P21; G2-Z clone; EGFP/tdTomato/DAPI
MH
LH
TRN
LGN
Section 40
Section 41
Section 42
Section 43
Section 44
Section 45
Section 46
Section 47
Section 48
Section 49
Section 50
Section 51
Section 52
Section 53
Section 54
b
Neuron
Glia
EGFP/tdTomato/NEUN/DAPI
c
Neuron
Glia
d
Neuron and glia (N+G)
Neuron only (N)
34
43

Figure 4.5: Distinct morphological features of excitatory neurons, astrocytes, and oligodendrocytes in the thalamus. (a, b) Representative 3D projection (a) and confocal (b) images of a G_2-X clone (green and red) in the thalamus labeled at E9, and immunostained for neuronal marker NEUN (white) and counterstained with DAPI (blue) at P21. High magnification images of the somas of four cells are shown to the right in b. Broken line circles indicate the nuclei. Scale bars: 20 μm and 20 μm. **(c, d)** Representative 3D projection (c) and confocal (d) images of a G_2-X thalamic clone (green and red) occupying TRN (contoured in yellow lines) and ZI labeled at E9, and immunostained for astrocyte marker S100 (white), and counterstained with DAPI (blue) at P21. High magnification images of the soma of the astrocyte are shown to the right in d. The broken line circle indicates the nucleus. Scale bars: 20 μm and 20 μm. **(e, f)** Representative 3D projection (e) and confocal (f) images of a G_2-Z thalamic clone (yellow) occupying TRN (contoured in yellow lines) and ZI labeled at E9, and immunostained for oligodendrocyte marker OLIG2 (white), and counterstained with DAPI (blue) at P21. High magnification images of the somas of two oligodendrocytes (arrows) are shown to the right in e. Broken line circles indicate the nuclei. Note the labeled oligodendrocytes possess characteristic short parallel neurites. Scale bars: 20 μm and 20 μm. **(g)** Quantification of the fraction of labeled cells with a large soma/nucleus and long neurites or a small soma/nucleus and short bushy or parallel neurites that are positive for NEUN, S100, or OLIG2, respectively.

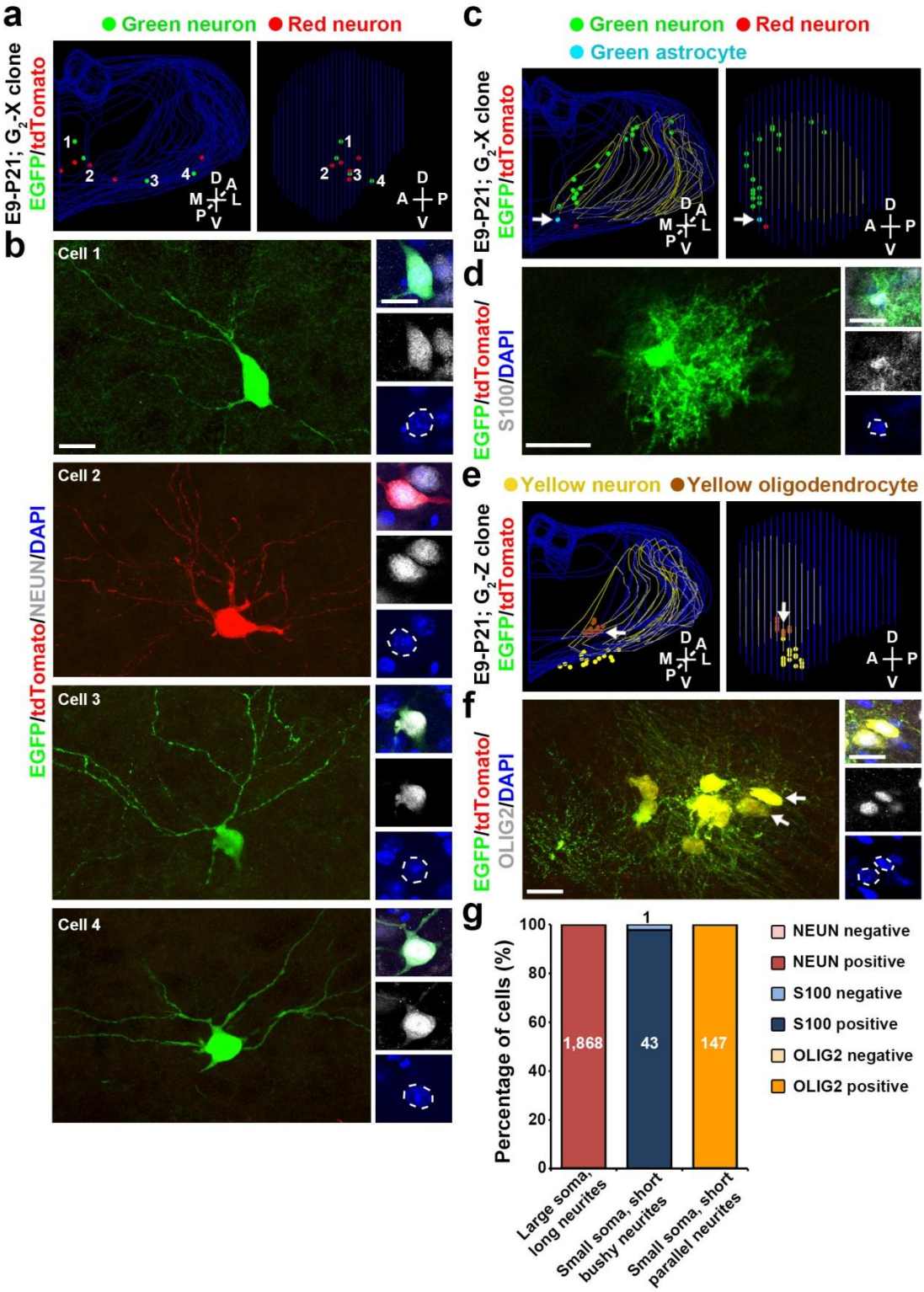
a
Green neuron
Red neuron
E9-P21; G2-X clone
EGFP/tdTomato
b
Cell 1
Cell 2
Cell 3
Cell 4
EGFP/tdTomato/NEUN/DAPI
c
Green neuron
Red neuron
Green astrocyte
E9-P21; G2-X clone
EGFP/tdTomato
d
EGFP/tdTomato/
S100/DAPI
e
Yellow neuron
Yellow oligodendrocyte
E9-P21; G2-Z clone
EGFP/tdTomato
f
EGFP/tdTomato/
OLIG2/DAPI
g
Percentage of cells (%)
1,868
43
147
1
Large soma, long neurites
Small soma, short bushy neurites
Small soma, short parallel neurites
NEUN negative
NEUN positive
S100 negative
S100 positive
OLIG2 negative
OLIG2 positive

There was no obvious correlation between the number of glial cells and the number of neurons at the clonal level **(Figure 4.6a)**. Similar to clonally related neurons, clonally related glial cells exhibited a clear clustering feature in spatial distribution, as reflected by the NND analysis **(Figure 4.6b)**. We observed only one glia-only clone with no neuron among all MADM-labeled brains at E9-E12. Interestingly, the fraction of glia-containing clones exhibited a progressive decrease between E9 and E11 **(Figure 4.6c)**. This likely reflects the progressive decrease in the number of RGPs in individual clones as a result of the temporal switch of symmetric proliferative to asymmetric neurogenic division of individual labeled RGPs **(Figure 3.2a)**. The fraction of glia-containing clones became largely stable (i.e. ~32-36%) at E11 and E12, when RGPs largely divide asymmetrically. These results suggest that a defined fraction of asymmetric neurogenic RGPs are capable of generating glia, likely at the completion of neurogenesis.

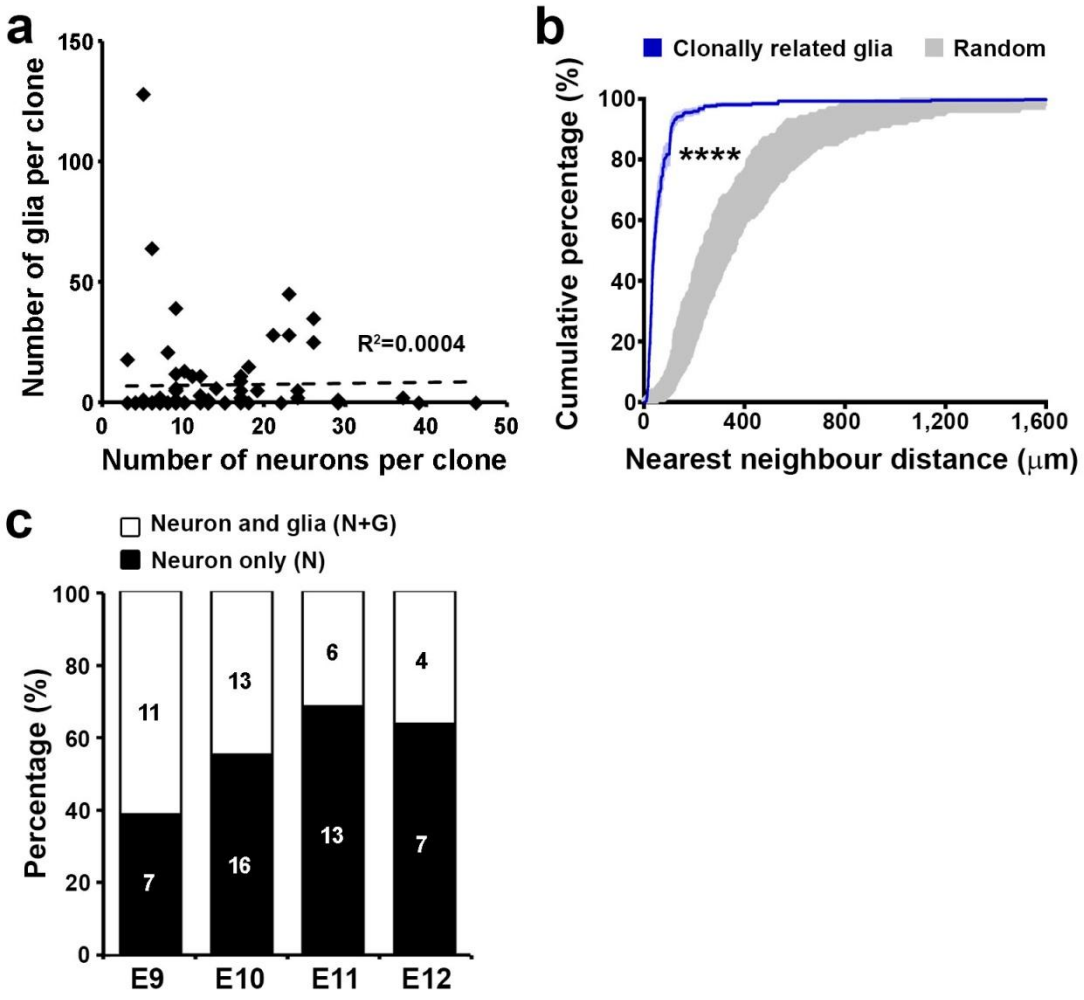

Figure 4.6: Spatial clustering of clonally related glial cells in the thalamus at the mature stage. (a) No correlation between the number of neurons and the number of glia at the clonal level (n=77 clones). The broken line indicates the linear regression of the data. **(b)** NND analysis of MADM-labeled glial clones (n=25) in the P21-24 thalamus. Note that compared to random datasets simulated 100 times (gray), the cumulative frequency of NND of thalamic glial clones (blue) is significantly left-shifted towards shorter distances, indicating a spatial clustering. Data are presented as mean±s.e.m. ****, p=1e-15 (unpaired t-test with Welch's correction). **(c)** Quantification of the fraction of clones containing neurons only (N) or neurons and glia (N+G) at different embryonic stages.

Chapter 5
Spatial and Functional Organization of Thalamic Clones *

5.1 Progenitor origin of thalamic nuclei

While a few nuclei (e.g. VP) are discernible based on nuclear counterstaining or ctyochrome oxidase staining, a majority of nuclei and their boundaries defy an easy identification [107]. To reveal the specific nuclear occupation of neurons in individual clones, we systematically aligned individual experimental 3D datasets to the reference thalamus with a defined nuclear boundary based on the Allen Brain Atlas (ABA) by adopting a previously established method [6] **(Figure 5.1a)**. After normalization and alignment, individual experimental thalami were found to be highly similar to each other, as well as to the reference thalamus in both two-dimensional (2D) border location **(Figure 5.1b-d)** and 3D volume **(Figure 5.1e,f)**, indicating that the alignment and inference of individual nuclear identity are reliable. Notably, the labeled clones as a whole covered a vast majority of thalamic nuclei representing over 98% of the total volume. Moreover, consistent with a regional restriction in spatial distribution, individual clones generally occupied a few nuclei (~4.2±0.3 out of a total of 34 nuclei) in the thalamus. Similar observation of individual clones occupying more than one nucleus has also been reported in the developing chick diencephalon [91]. Notably, it has also been previously suggested that neurons in the principle sensory nuclei are born relatively early, whereas neurons in the nuclei close to the midline are born relatively late [68]. The regional occupation of individual clones raised an intriguing possibility that different nuclei may have distinct progenitor origins.

---

* Shi W, Xianyu A, Han Z, Tang X, Li Z, Zhong H, Mao T, Huang K, and Shi SH. Ontogenetic establishment of order-specific nuclear organization in the mammalian thalamus. *Nature Neuroscience* **20**, 516–528 (2017).

Figure 5.1: Alignment of the experimental thalamus with the ABA reference thalamus. (a) Flowchart of the alignment process. **(b)** Aligned single coronal sections from 34 experimental brains (gray outlines) in the position corresponding to ABA section 69. Red lines indicate 6 line profiles used to calculate thalamus edge (i.e. border) variability. D, dorsal; V, ventral. **(c)** Thalamus border variability for the section in *B* (n=45). **(d)** Average border variability for 5 sections along the anterior to posterior axis (n=45). **(e)** Aligned 3D reference ABA thalamus after normalization (red) with the average experimental thalamus (blue). **(f)** Percentage of volume overlap between reference ABA thalamus and individual experimental thalami (n=45). Data in **c**, **d** and **f** are presented as median with interquartile range, whiskers are the minimum and maximum.

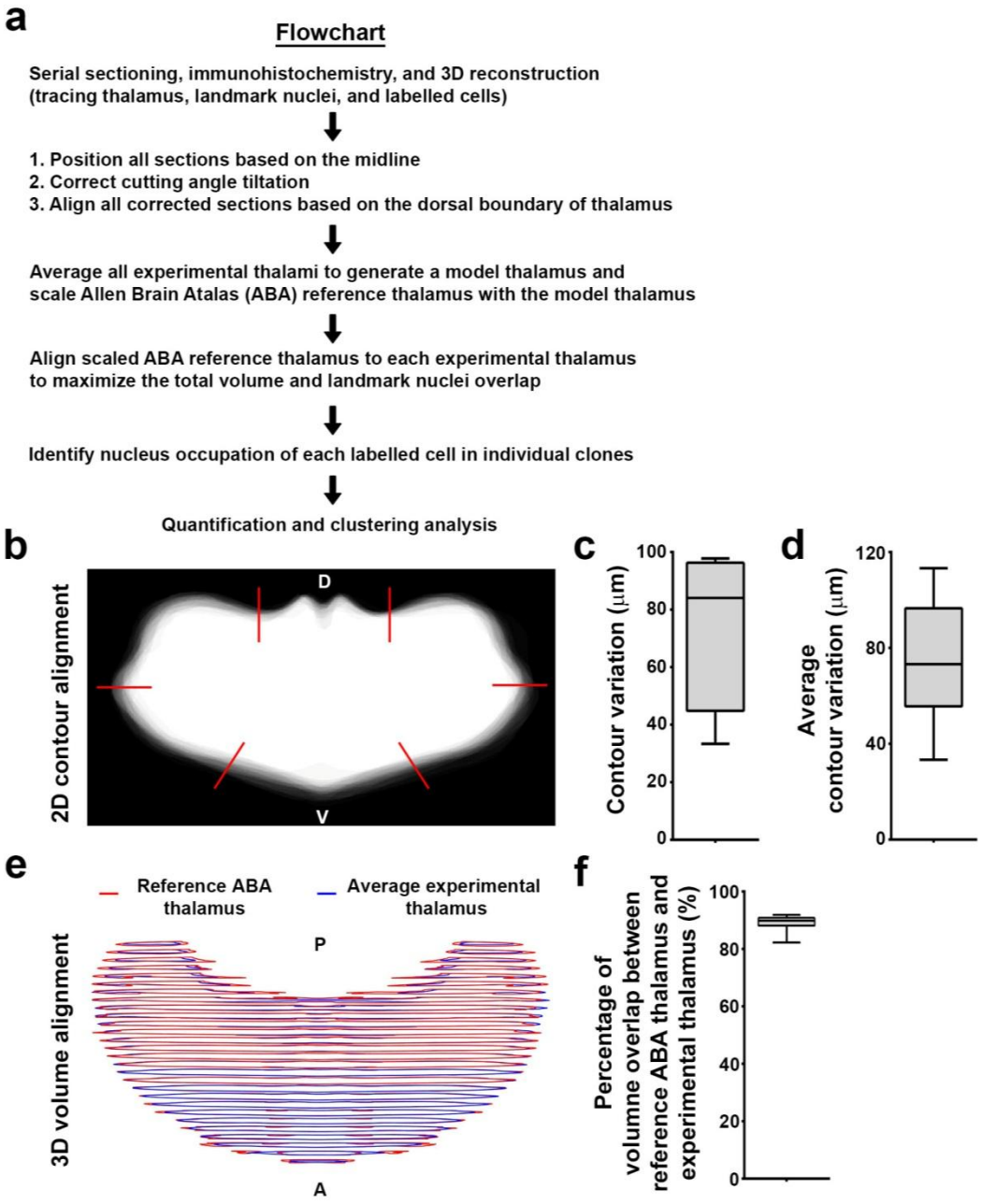
a
Flowchart
Serial sectioning, immunohistochemistry, and 3D reconstruction
(tracing thalamus, landmark nuclei, and labelled cells)
1. Position all sections based on the midline
2. Correct cutting angle tiltation
3. Align all corrected sections based on the dorsal boundary of thalamus
Average all experimental thalami to generate a model thalamus and
scale Allen Brain Atalas (ABA) reference thalamus with the model thalamus
Align scaled ABA reference thalamus to each experimental thalamus
to maximize the total volume and landmark nuclei overlap
Identify nucleus occupation of each labelled cell in individual clones
Quantification and clustering analysis
b
2D contour alignment
D
V
c
Contour variation (μm)
100
80
60
40
20
0
d
Average
contour variation (μm)
120
80
40
0
e
Reference ABA
thalamus
Average experimental
thalamus
3D volume alignment
P
A
f
Percentage of
volumne overlap between
reference ABA thalamus and
experimental thalamus (%)
100
80
60
40
20
0

To systematically characterize the nuclear occupation of each clone and reveal the progenitor origin of thalamic nuclei, we performed an unsupervised agglomerative hierarchical clustering analysis of all neurons in individual RGP clones labeled at E9-E12 (n=77 clones) on the basis of their distribution in different nuclei **(Figure 5.2a)**. Remarkably, we observed two major clonal clusters (i.e. the farthest dendrogram branches) corresponding to excitatory neuron clones and inhibitory interneuron clones, respectively **(left dendrogram, Figure 5.2a)**. Clones occupying the TRN and ZI were exclusively GABAergic inhibitory interneurons **(Figure 5.3a,b)** and segregated from the clones located in all other thalamic nuclei except the LGN **(Figure 5.2a)**, the only other rodent thalamic nucleus besides the TRN that contains inhibitory interneurons [71,74], suggesting a clear lineage separation of excitatory and inhibitory neurons in the thalamus at the clonal level. This lineage separation is consistent with the previous genetic mapping studies [70,71] and strongly supports the reliability of our clonal labeling and clustering analysis.

The remaining excitatory neuron clones fell into three main subclusters validated by both the within and between cluster variation (i.e. elbow) analysis and the Silhouette coefficient evaluation **(Figure 5.3c)**. They were located predominantly in the anterior (a), medial dorsal (md), or medial ventral posterior (mvp) regions, respectively. We thus termed them the ‘a’, ‘md’, and ‘mvp’ clonal clusters. Similar analysis of glial cells in individual clones did not yield any obvious clustering.

We then quantitatively analyzed the fraction of individual neuronal clones in these four clonal clusters located in different thalamic nuclei **(Figure 5.2b)**. As expected, the GABAergic neuron clonal cluster was exclusively located in the TRN and LGN, as well as the ZI **(blue, Figure 5.2b)**. The three excitatory neuron clonal clusters occupied largely non-overlapping nuclei, as reflected by the top 6-7 dominant nuclei that harbored over 80% of neurons in each clonal cluster **(Figure 5.2b)**.

Specifically, the ‘md’ clonal cluster largely occupied the mediodorsal (MD), posterior (PO), lateral posterior (LP), central medial (CM), paracentral (PCN), and intermediodorsal (IMD) nuclei **(green, Figure 5.2b)**. The ‘mvp’ clonal cluster mostly occupied the ventral posteromedial (VPM), ventral posterolateral (VPL), ventral anterior lateral (VAL), dLG, ventral medial geniculate (vMG), ventral medial (VM), reunions (RE) nuclei **(yellow, Figure 5.2b)**. The ‘a’ clonal cluster predominantly occupied the anteromedial (AM), RE, anteroventral (AV), rhomboid (RH), paraventricular (PVT), VM, and LD nuclei **(red, Figure 5.2b)**. These results suggest that individual progenitors produce neurons preferentially located to distinct sets of nuclei in the thalamus.

Figure 5.2: Nuclear localization of thalamic clones. (a) The heat map of the distribution of individual clones labeled at E9-E12 in different thalamic nuclei based on an unsupervised agglomerative hierarchical clustering analysis. The dendrogram is shown to the left. Each row represents an RGP-derived thalamic clone (n=77 in total). dLG-i, interneurons in dLG. Note that there are two major clonal clusters corresponding to excitatory neuron clones and inhibitory interneuron clones (blue, n=17), respectively. Within the excitatory neuron clones, there are three main subclusters largely corresponding to the 'md' (green, n=33), 'mvp' (yellow, n=9), and 'a' (red, n=18), clones. **(b)** Quantification of the distribution of the four clonal clusters in different nuclei. Color shades highlight the top 6-7 dominant nuclei harboring over 80% of labeled neurons in the respective clonal clusters. Data are presented as mean±s.e.m. AD, anterodorsal; AM, anteromedial; AV, anteroventral; CL, central lateral; CM, central medial; IAD, interanterodorsal; IAM, interanteromedial; IMD, intermediodorsal; LD, lateral dorsal; dLG, dorsal lateral geniculate; vLG, ventral lateral geniculate; LP, lateral posterior; MD, mediodorsal; MG, medial genicualte; PCN, paracentral; PF, parafascicular; PO, posterior; POL, posterior limiting; PP, peripenduncular; PT, paratenial; PVT, paraventricular; RE, nucleus of reunions; RH, rhomboid; SGN, suprageniculate; SMT, submedial; SPF, subparafascicular; VAL, ventral anterior lateral; VM, ventral medial; VPL, ventral posterolateral; VPM, ventral posteromedial.

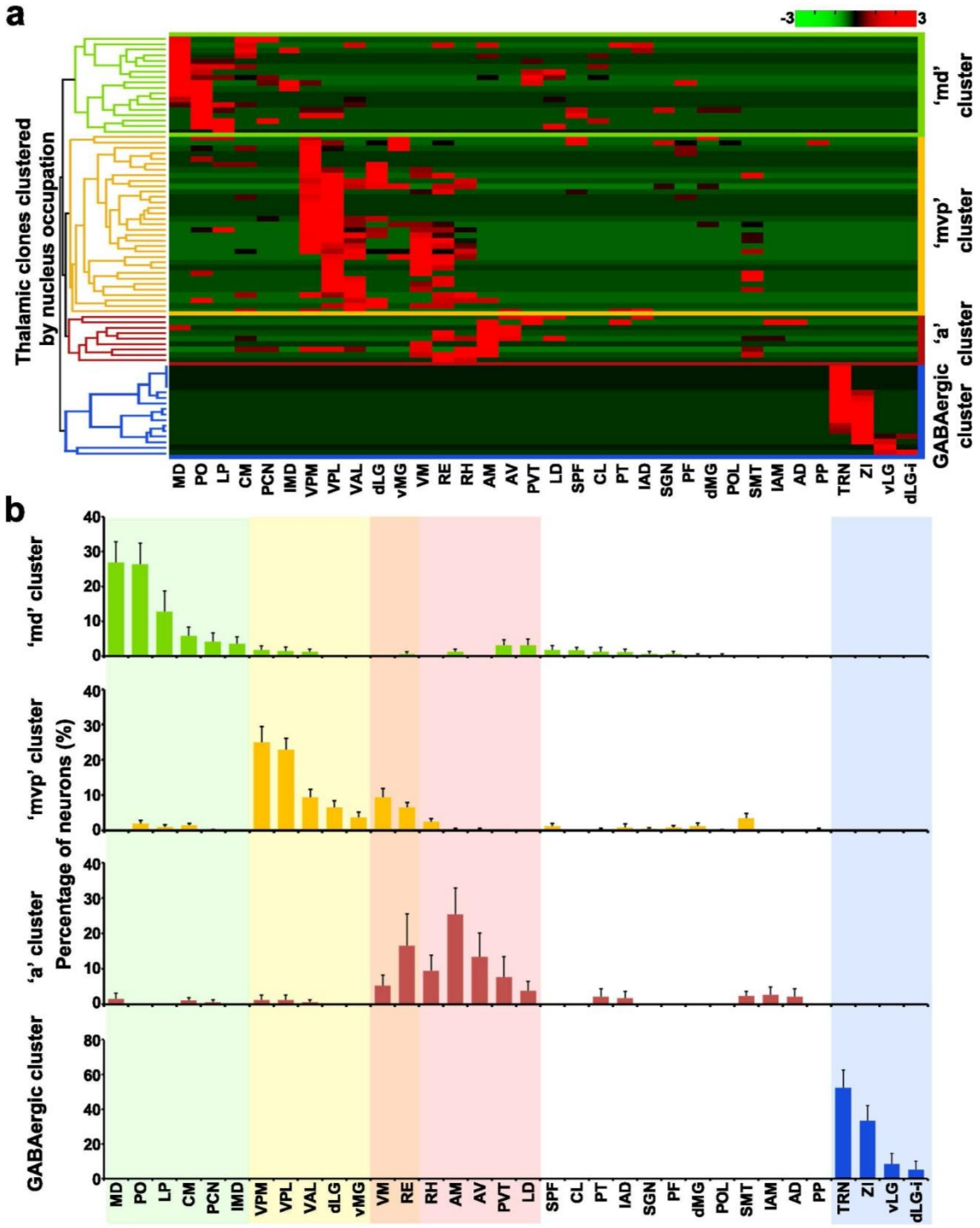
a
-3
3
Thalamic clones clustered by nucleus occupation
'md' cluster
'mvp' cluster
'a' cluster
GABAergic cluster
MD PO LP CM PCN IMD VPM VPL VAL dLG vMG VM RE RH AM AV PVT LD SPF CL PT IAD SGN PF dMG POL SMT IAM AD PP TRN ZI vLG dLG-i
b
'md' cluster
'mvp' cluster
'a' cluster
GABAergic cluster
Percentage of neurons (%)
0 10 20 30 40
0 20 40 60 80
MD PO LP CM PCN IMD VPM VPL VAL dLG vMG VM RE RH AM AV PVT LD SPF CL PT IAD SGN PF dMG POL SMT IAM AD PP TRN ZI vLG dLG-i

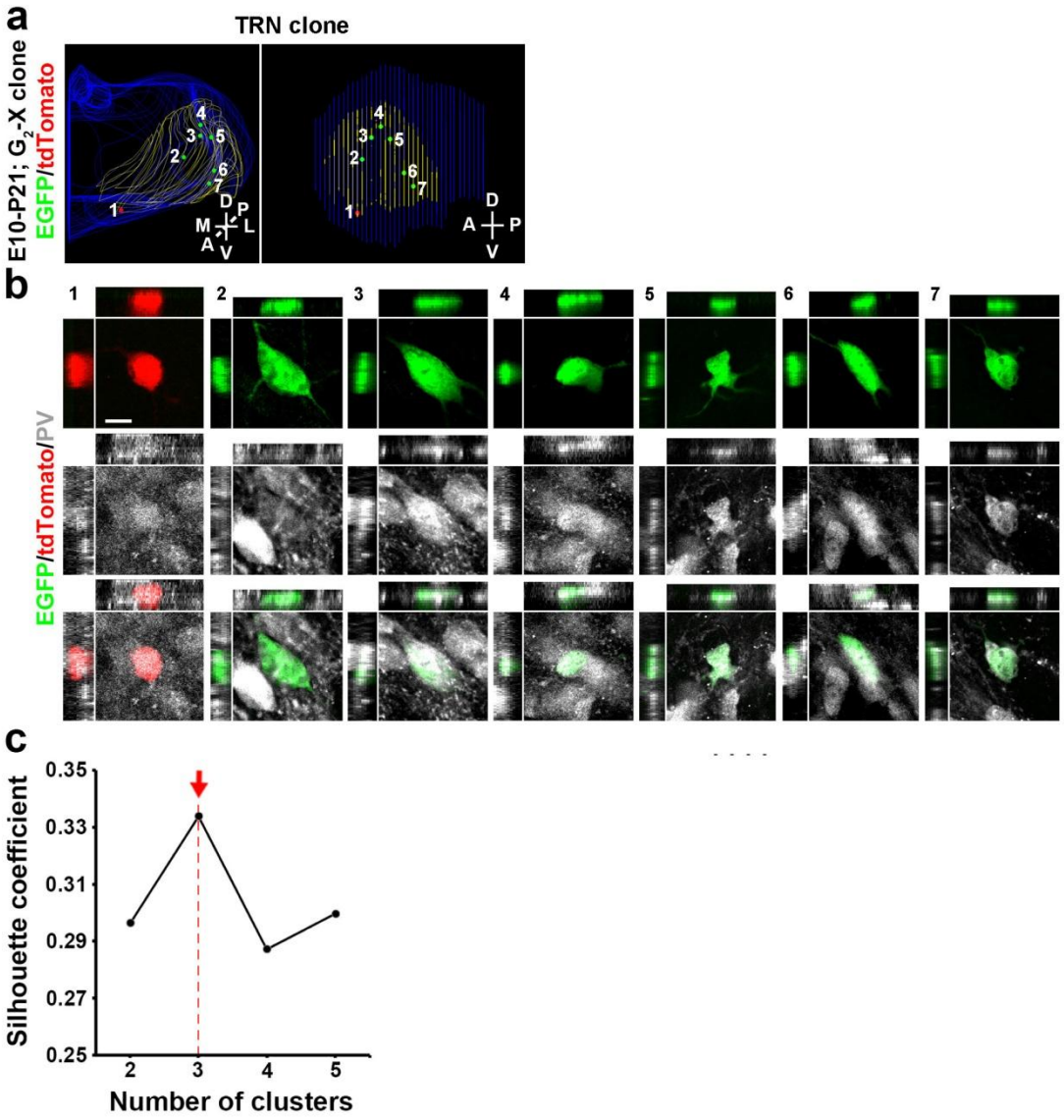

Figure 5.3: Inhibitory interneuron clones in TRN (a) 3D reconstructed images of a G_2-X clone containing 7 labeled neurons in the TRN contoured by yellow lines. **(b)** High magnification cross-section confocal images of the 7 labeled neurons stained for parvalbumin (PV, white), a GABAergic interneuron-specific marker. Note that all 7 neurons are positive for PV, indicating their interneuron identity. Scale bar: 10 μm. **(c)** Quantification of the Silhouette coefficients with regard to the number of clusters. The red arrow indicates the highest Silhouette coefficient at three clusters.

Notably, the nuclei occupied by the ‘mvp’ clonal cluster largely overlap with the nuclei harboring the excitatory neuron progeny of OLIG2-positive progenitors in the pTH-C subdomain of the developing thalamus **(Figure 5.4)**, indicating a lineal correlation between the ‘mvp’ clones and OLIG2-positive thalamic progenitors. The four sets of a total of 20 dominant nuclei (not including ZI) account for more than 80% of the entire thalamic volume. Moreover, clonally labeled neurons occupied all 34 nuclei, including those non-dominant nuclei that are generally small **(Figure 5.2)**. These results suggest that our clonal labeling and clustering analysis effectively covers the vast majority, if not all, of the thalamus and that the small non-dominant nuclei are likely marginally formed by the three excitatory neuron clonal clusters.

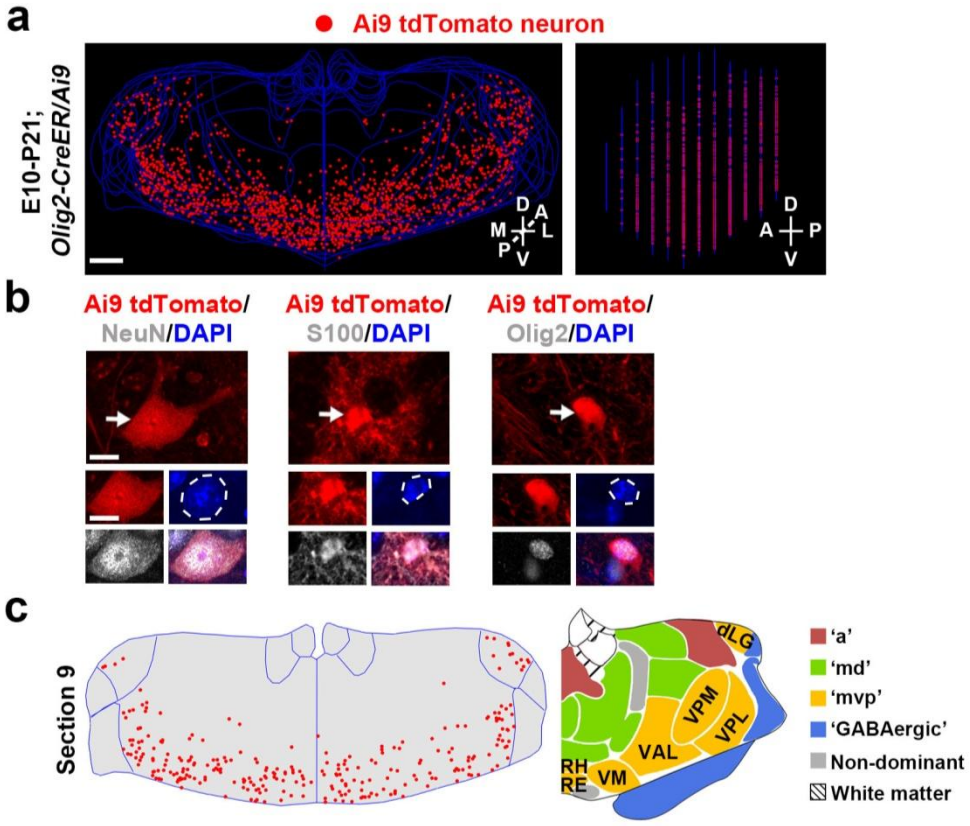

Figure 5.4: Overlap between the nuclei occupied by the 'mvp' clonal cluster and the nuclei harboring excitatory neuron progeny of OLIG2-positive progenitors in the developing thalamus. (a) Representative 3D projection images of tdTomato-expressing excitatory neuron progeny (red filled circles) generated by OLIG2-positive progenitors in the thalamus. Note that the inhibitory interneurons located in the vLG and TRN, likely derived from OLIG2-positive progenitors in the prethalamus, were not traced. Scale bar: 500 μm. **(b)** Representative confocal images of tdTomato-expressing excitatory neuron (left), astrocyte (middle), and oligodendrocyte (right) progeny generated by OLIG2-positive thalamic progenitors. High magnification images of the somas (arrows) are shown at the bottom. Broken line circles indicate the nuclei. Scale bars: 10 μm and 10 μm. **(c)** Representative nuclear occupation of tdTomato-expressing excitatory neuron progeny (red filled circles) generated by OLIG2-positive progenitors.

5.2 Lineage distinction between cognitive and sensory/motor-related nuclei

The observation of three largely non-overlapping sets of excitatory neuron nuclei with distinct clonal relationships prompted us to postulate that the ontogenetic origin influences the structural and functional organization of the thalamus. The average number of neurons in the ‘a’ and ‘md’ clonal clusters was comparable, but less than that of the ‘mvp’ clonal cluster **(Figure 5.5a)**; yet, the average number of nuclei that these three clonal clusters occupied was comparable **(Figure 5.5b)**. Among the major nuclei occupied by excitatory neuron clones, VM and RE were partially occupied by both the ‘mvp’ and ‘a’ clonal clusters, raising the question as to whether the labeled neurons between these two clonal clusters in these two overlapping nuclei were the same or different populations. Interestingly, we found that neurons labeled in the ‘a’ clonal cluster were predominantly located in the anterior half of VM and RE, as well as RH, whereas neurons labeled in the ‘mvp’ clonal cluster were mostly located in the posterior half of these three nuclei **(Figure 5.6a)**, suggesting a lineage-based segregation of the anterior and posterior parts of VM, RE, and RH.

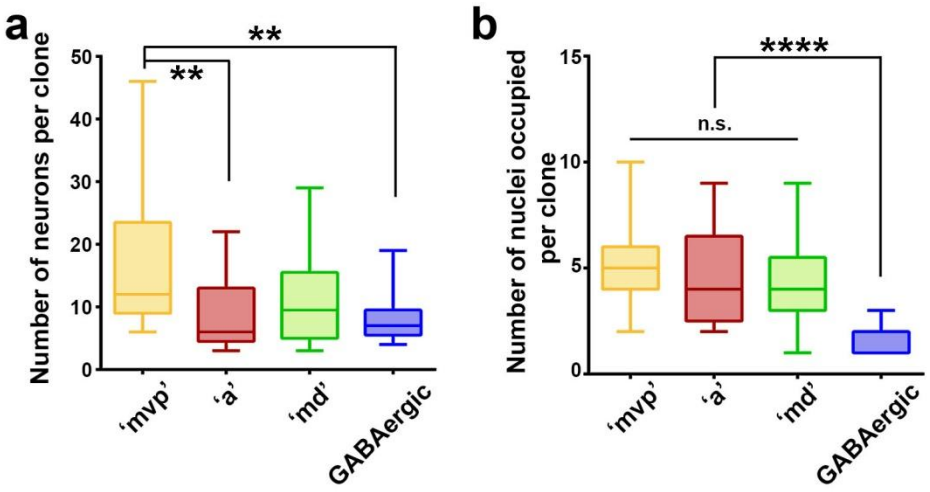

Figure 5.5: Average size of thalamic clones in four clusters (a) Quantification of the average number of neurons in the four clonal clusters ('mvp', n=33; 'a', n=9; 'md', n=18; 'GABAergic', n=17). Data are presented as median with interquartile range, and whiskers are the minimum and maximum. **, p=0.005; **, p=0.001 (Mann Whitney test). **(b)** Quantification of the average number of nuclei that the four clonal clusters occupy. Data are presented as median with interquartile range, and whiskers are the minimum and maximum. n.s., not significant; ****, p<0.0001 (Mann Whitney test).

Interestingly, our further analysis of Hunnicutt, B. J. et al's thalamocortical axonal tracing experiments using focal injections of adeno-associated viruses (AAVs) expressing fluorescent proteins [6] showed that the anterior parts of VM, RE, and RH predominantly projected to cognition-related HO areas of the cortex such as the anterior cingulated cortex (ACC) and prelimbic cortex (PrL) **(asterisks, Figure 5.6b)**. In contrast, the posterior parts of VM, RE, and RH mostly projected to the sensory and motor areas of the cortex, consistent with the notion that they are involved in multimodal sensory processing and motor activity [108,109]. Moreover, the remaining cells in the respective clones (n=18) were located in regions sharing a similar cognition-related HO versus sensory/motor-related cortical projection pattern **(Figure 5.6b)**, indicating a clonal but not nuclear level of correlation in functionality. Together, these results suggest that lineage relationship influences the organization of thalamic structures associated with distinct functionality, even at a resolution beyond the conventional individual nucleus level.

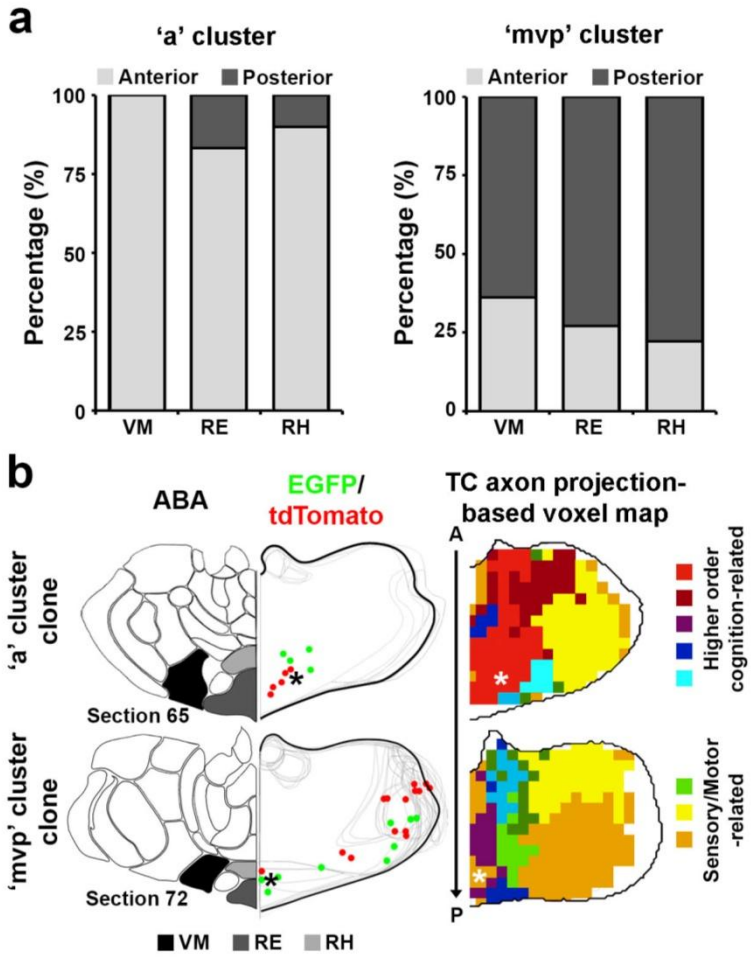

Figure 5.6: Distinct localization and functionality of labeled neurons in VM, RE, and RH between the 'a' and 'mvp' clonal clusters. (a) Percentage of labeled neurons in the 'a' (left) and 'mvp' (right) clonal clusters that are located in the anterior or posterior half of VM, RE and RH. Note that labeled neurons in the 'a' clonal cluster are predominantly located in the anterior part, whereas those in the 'mvp' cluster are mostly located in the posterior part. **(b)** Distinct functionality of labeled neurons in the 'a' (top) and 'mvp' (bottom) clonal clusters located in VM, RE, and RH. Representative 'a' and 'mvp' cluster clones with corresponding ABA sections with nuclear boundaries are shown to the left. Asterisks indicate labeled neurons located in VM (black area), RE (dark gray area) and RH (light gray area). Gray lines indicate the contours of the thalamic sections where the labeled clones are located and black lines indicate the sections where labeled VM/RE/RH neurons are located. The corresponding cortical projection-based voxel maps of the same regions are shown to the right. Note that the anterior parts of VM, RE, and RH predominantly contribute to higher order cognitive functions, whereas the posterior part of VM, RE, and RH mostly contribute to sensory/motor-related activities. TC, thalamocortical.

To further test this, we systematically analyzed the properties of individual clones in the ‘mvp’ and ‘a’ clonal clusters with regard to their spatial configuration and nuclear occupation. Interestingly, we found that clones in the ‘mvp’ cluster were prominently arrayed radially along the mediolateral axis with a dorsoposterior bend **(Figure 5.7a left and 5.7b)**. In contrast, clones in the ‘a’ cluster were relatively more tangentially dispersed **(Figure 5.7a right and 5.7b)**. This distinction in clonal configuration appeared to be an intrinsic feature of the respective lineages, as we observed similar differences in clonal organization at the embryonic stage **(Figure 5.7c,d)**. That is, clonally related neurons in the anterodorsal region were not tightly associated with the mother radial glial fiber but more tangentially dispersed, whereas those in the medial ventral posterior region were closely aligned along the mother radial glial fiber. Notably, radial and tangential migration of clonally related cells has previously been suggested in the developing chick diencephalon [92].

Remarkably, we also found that there was a tight association between the ‘mvp’ and ‘a’ clonal clusters and distinct functionalities. The ‘a’ clonal cluster mostly occupied the nuclei associated with cognition-related HO functions (e.g. AM, AV, anterior RE/RH/VM, IAM) **(Figure 5.7a,e,f right)**, whereas the ‘mvp’ clonal cluster predominantly occupied the nuclei associated with sensory/motor-related activities (e.g. VPL, VPM, VAL, dLG, vMG, posterior RE/RH/VM) **(Figure 5.7a,e,f left)**. Together, these results suggest that the HO cognitive nuclei and sensory/motor-related nuclei in the thalamus are ontogenetically segregated with distinct progenitor origins.

Figure 5.7: Distinct spatial configuration and functionality of the clonal clusters. **(a)** 3D rendered images of a representative 'mvp' (left) or 'a' (right) cluster clone that predominantly occupies sensory/motor-related nuclei and cognition-related higher order nuclei, respectively. Broken lines indicate the radial (white) versus tangential (black) dispersion of the clone. Scale bar: 500 μm. **(b)** Quantification of the average ratio of the radial versus tangential dispersion normalized to the total number of neurons in individual clones at P21-24 ('mvp', n=33; 'a', n=9). Data are presented as median with interquartile range, and whiskers are the minimum and maximum. **, p=0.008 (Mann-Whitney test). **(c)** Confocal images of a representative E15 medial ventral/posterior (top) or anterior dorsal (bottom) clone labeled at E10. Broken lines indicate the contours of the thalamus. High magnification images of the clone are shown to the right. Arrows indicate the radial glial progenitors with a long radial glial fiber (open arrowheads) and arrowheads indicate the progeny. Scale bars: 200 μm and 50 μm. **(d)** Quantification of the average ratio of the radial versus tangential dispersion normalized to the total number of neurons in individual clones at E15-16 ('mvp', n=20; 'a', n=5). Data are presented as median with interquartile range, and whiskers are the minimum and maximum. *, p=0.012 (Mann-Whitney test). **(e)** Quantification of the percentage of individual 'mvp' and 'a' cluster clones located in sensory/motor-related, cognition-related, or unclear function nuclei. Each bar represents a clone. **(f)** Quantification of the percentage of all 'mvp' or 'a' cluster clones located in sensory/motor-related, cognition-related, or unclear function nuclei ('mvp': sensory/motor-related, 83.7±3.6%; cognition-related, 11.9±3.3%; unclear function, 4.4±1.6%; 'a': sensory/motor-related, 16.3±11.1.0%; cognition-related, 80.7±11.4%; unclear function, 3.0±1.7%). Data are presented as mean±s.e.m. ****, p=5e-05; ****, p=2.5e-05 (Mann-Whitney test).

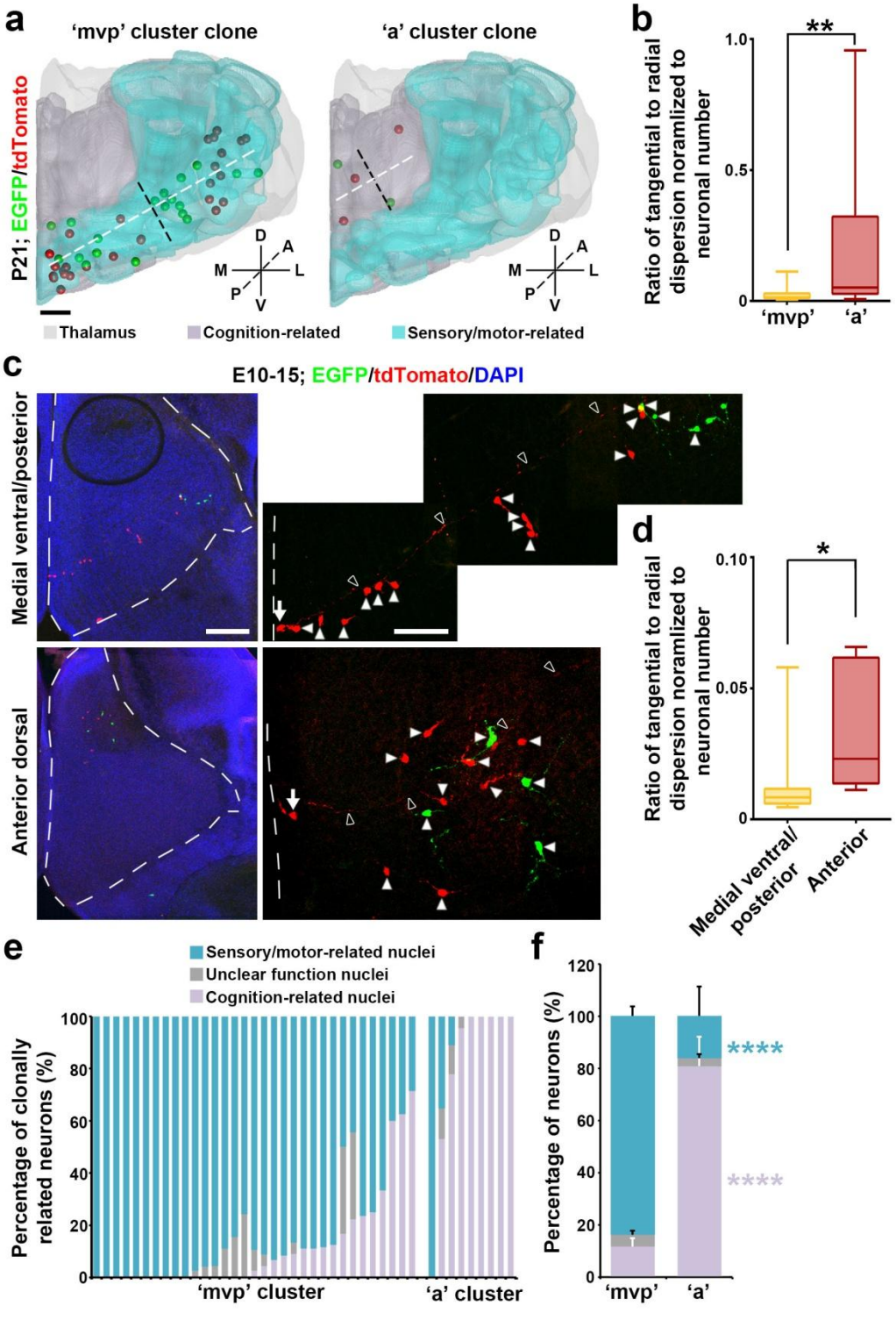
a
'mvp' cluster clone
'a' cluster clone
P21; EGFP/tdTomato
D
A
M
L
P
V
Thalamus
Cognition-related
Sensory/motor-related
b
**
Ratio of tangential to radial dispersion noramlized to neuronal number
1.0
0.5
0
'mvp'
'a'
c
E10-15; EGFP/tdTomato/DAPI
Medial ventral/posterior
Anterior dorsal
d
*
Ratio of tangential to radial dispersion noramlized to neuronal number
0.10
0.05
0
Medial ventral/ posterior
Anterior
e
Sensory/motor-related nuclei
Unclear function nuclei
Cognition-related nuclei
Percentage of clonally related neurons (%)
100
80
60
40
20
0
'mvp' cluster
'a' cluster
f
Percentage of neurons (%)
120
100
80
60
40
20
0
****
****
'mvp'
'a'

5.3 Lineage distinction between FO and HO sensory nuclei

Clones in the 'md' clonal cluster appeared to be associated with either sensory/motor (e.g. PO and LP) or cognition-related (e.g. MD, CM, PCN, and IMD) activities **(Figure 5.8a,b)**. Interestingly, the sensory/motor activities mediated by the 'md' clonal cluster were fundamentally different from those mediated by the 'mvp' clonal cluster **(Figure 5.8c,d)**. Based on the input and output connectivity and properties, the sensory-related nuclei in the thalamus have been classified as FO or HO [10,110]. Specifically, the VP (VPL and VPM) and PO nuclei, the dLG and LP nuclei, and the vMG and dMG nuclei are the corresponding FO and HO nuclei for somatosensation, vision, and audition, respectively [10,111]. In addition, the VAL and VM nuclei relay the cerebellar and basal ganglia inputs to the primary motor and pre-motor cortical areas [108,112]. Therefore, the sensory/motor-related thalamic nuclei are well organized in a modality and hierarchy-based manner. Interestingly, we found that the clones occupying the sensory/motor-related FO and HO nuclei were largely segregated **(Figure 5.8c,d)**. The 'mvp' clonal cluster predominantly contributed to the FO sensory/motor-related nuclei such as VPL, VPM, VAL, dLG, vMG as well as a small fraction in pRE/pRH/SMT, whereas the 'md' clonal cluster mainly contributed to the HO sensory/motor-related nuclei such as PO and LP **(Figure 5.8d,f)**. These results suggest a strong lineage-related separation of the sensory/motor-related nuclei in hierarchy (i.e. order). On the other hand, individual clones were frequently found to occupy the FO or HO nuclei across different modalities **(Figure 5.8e,f)**. Notably, given that the thalamus development entails both a lateral growth and a dorsoposterior bend, the FO/HO segregation is not purely a dorsal/ventral segregation, especially in the lateral region. Together, these results support a progenitor origin of a cross-modal hierarchical framework of sensory/motor pathways in the thalamus.

Figure 5.8: Clonal segregation of the FO and HO thalamic nuclei. (a) Quantification of the percentage of individual 'md' cluster clones located in sensory/motor-related, cognition-related, or unclear function nuclei. Each bar represents a clone (n=18 in total). **(b)** Quantification of the percentage of all 'md' cluster clones located in sensory/motor-related, cognition-related, or unclear function nuclei (sensory/motor-related, 46.3±8.7%; cognition-related, 46.8±8.7%; unclear function, 6.8±2.8%). Data are presented as mean±s.e.m. **(c)** 3D rendered images of a representative 'mvp' (left) or 'md' (right) cluster clone that predominantly occupies the FO and HO nuclei, respectively. Scale bar: 500 μm. **(d)** Quantification of the percentage of clonally related neurons in sensory/motor-related nuclei that are in the FO or HO nuclei. Each bar represents a clone. **(e)** Quantification of the percentage of clonally related neurons in sensory/motor-related nuclei related to different modalities. **(f)** Quantification of the percentage of all clonally related neurons in sensory/motor-related nuclei according to the order (FO vs. HO) or modality (i.e. somatosensory, visual, auditory, or motor). ****, p=00019; ****, p=2e-06(chi-square test).

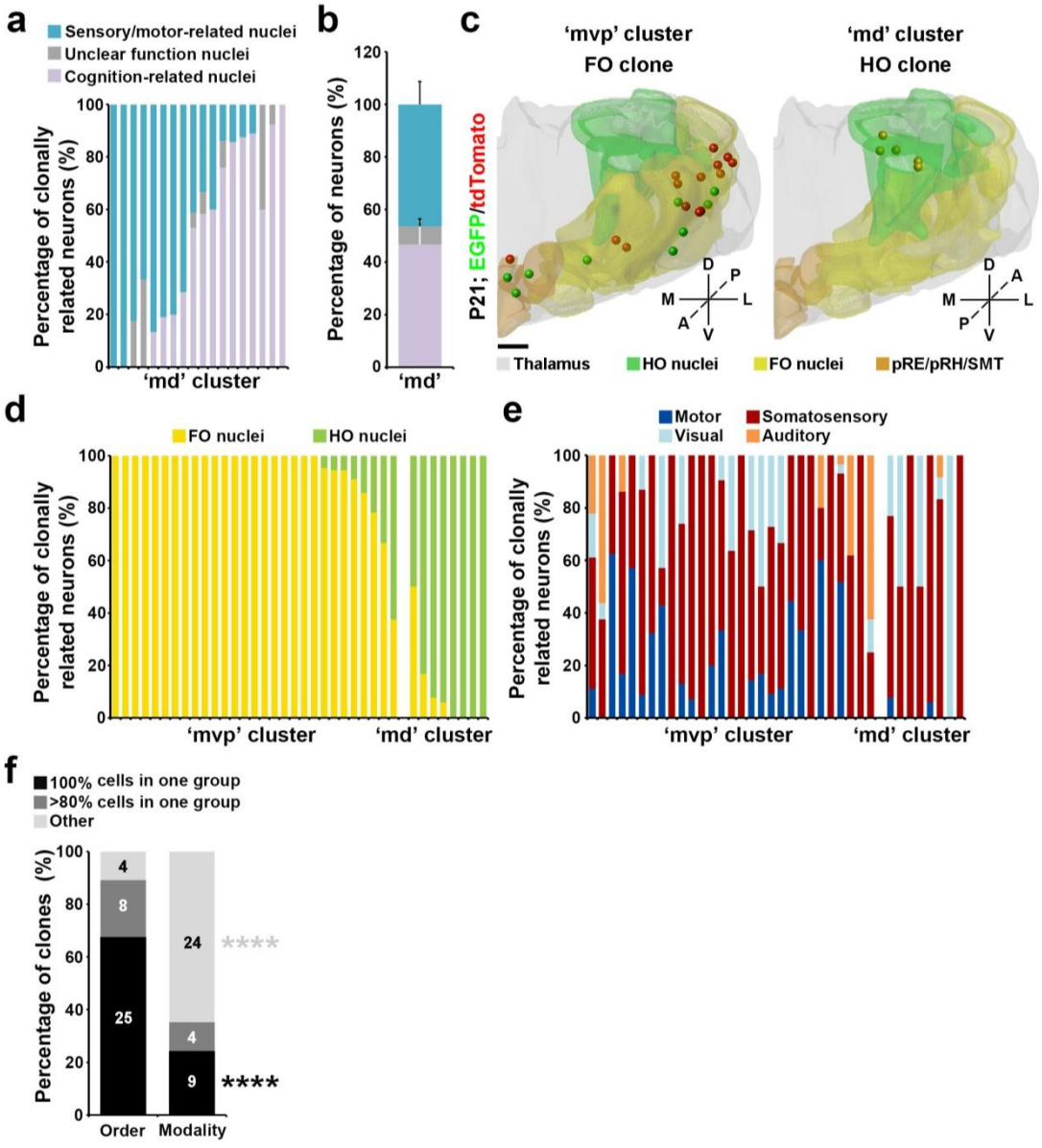
a
Sensory/motor-related nuclei
Unclear function nuclei
Cognition-related nuclei
Percentage of clonally related neurons (%)
'md' cluster
b
Percentage of neurons (%)
'md'
c
'mvp' cluster
FO clone
'md' cluster
HO clone
P21; EGFP/tdTomato
Thalamus
HO nuclei
FO nuclei
pRE/pRH/SMT
d
FO nuclei
HO nuclei
Percentage of clonally related neurons (%)
'mvp' cluster
'md' cluster
e
Motor
Somatosensory
Visual
Auditory
Percentage of clonally related neurons (%)
'mvp' cluster
'md' cluster
f
100% cells in one group
>80% cells in one group
Other
Percentage of clones (%)
4
8
25
24
4
9
****
****
Order
Modality

5.4 SHH signaling influences spatial organization of thalamic clones

Previous studies suggested that SHH signaling regulates thalamic progenitor identity and nuclear specification [81,113]. To explore the influence of SHH signaling on the development and organization of thalamic clones, we examined the size and spatial distribution of clones with a higher level of SHH signaling than normal. To achieve this, we performed MADM analysis in the *Rosa26*$^{flox\text{-}STOP\text{-}flox\text{-}SmoM2\text{-}EYFP}$ (*R26*$^{SmoM2\text{-}EYFP/+}$) mice [114]. The *SmoM2-EYFP* allele carries a constitutively active missense (Trp539Leu) mutation in the *Smoothened (Smo)* gene fused to enhance yellow fluorescent protein (EYFP) and its expression leads to a constitutive activation of SHH signaling independent of ligand binding [115]. As the *R26*$^{SmoM2\text{-}EYFP}$ and *MADM-11* transgenes are located in different chromosomes, it prevents a genetic link between EGFP or tdTomato expression and SmoM2-EYFP expression for a strict mosaic analysis. Nonetheless, in the *Nestin-CreER*^{T2}*/MADM11/R26*$^{SmoM2\text{-}EYFP/+}$ animals, a single dose of TM treatment would trigger both MADM labeling upon inter-chromosomal recombination as well as the expression of SmoM2 upon intra-chromosomal recombination, which was confirmed by the expression of SmoM2-EYFP in tdTomato-labeled RGPs **(Figure 5.9, arrows)**. We observed MADM clones at different regions of the thalamus in the P21 animals that received TM treatment at E10, E11, and E12. The rate of intra-chromosomal recombination is typically much higher than that of inter-chromosomal recombination [93,95]. Consistent with this, we observed additional non-MADM-labeled cells expressing SmoM2-EYFP **(Figure 5.9, arrowheads)**.

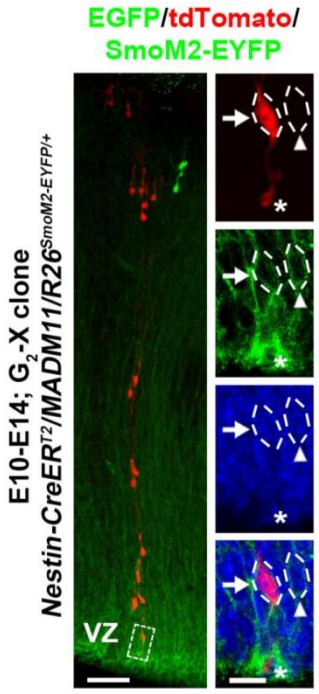

Figure 5.9: Expression of SmoM2-EYFP in MADM-labeled thalamic clones. Representative confocal images of a G_2-X clone labeled at E10, and immunostained for EYFP (green) and tdTomato (red), and counterstained with DAPI (blue) at E14. High magnification images of a tdTomato-expressing RGP in the VZ (broken lines) are shown to the right. Note the membrane expression of SmoM2-EYFP in the tdTomato-expressing RGP (arrows) with an apical endfoot (asterisks), suggesting the successful recombination of both *SmoM2-EYFP* and *MADM11* alleles in the clone. Arrowheads indicate the expression of SmoM2-EYFP in a nearby non-MADM-labeled cell, indicating a higher frequency of intra-chromosomal (i.e. *SmoM2-EYFP* allele) recombination than that of inter-chromosomal (i.e. *MADM11* allele) recombination. Broken line circles indicate the somas. Scale bars: 20 μm and 10 μm.

Within the diencephalon, SHH is expressed in the basal plate and ZLI that are ventral to the developing thalamus [81,116,117]. As a result, the embryonic thalamus is exposed to a graded SHH activity. Coinciding with this SHH signaling gradient, the clones in the anterior and medial dorsal regions were more tangentially distributed than the clones in the medial ventral/posterior region **(Figure 5.7a-d)**, indicating that a high SHH signaling suppresses tangential distribution of clonally related neurons. Interestingly, consistent with this notion, the clone located in the anterior region of the

SmoM2 thalamus became less tangentially and more radially distributed than the wild type control clone **(Figure 5.10a,c)**, whereas the clone located in the medial ventral/posterior region did not exhibit any significant change in spatial distribution **(Figure 5.10b,c)**. In addition, we observed an expansion of the expression of retinoic acid receptor-related orphan receptor α (*RORα*), a marker gene predominantly expressed in VP and dLG [118], to the anterior region as well as dorsally at P4 **(Figure 5.10d)**, indicating a change in nuclear boundary and functional organization of the thalamus, as previously shown [81]. Notably, this change prevented a reliable assessment of nuclear identity of individual clones based on ABA.

Figure 5.10: SHH signaling regulates the spatial distribution of thalamic clones depending on the localization. (a) Representative 3D reconstructed images of the thalamic hemispheres containing a MADM-labeled clone in the anterior region of the wildtype control (top) and *SmoM2* (bottom) mice. Scale bars: 500 μm and 500 μm. **(b)** Representative 3D reconstructed images of the thalamic hemispheres containing a MADM-labeled clone in the medial ventral/posterior region of the wild type control (top) and *SmoM2* (bottom) mice. Note that the clone in the *SmoM2* mouse is similarly dispersed radially to that in the control mouse. Scale bar: 500 μm. **(c)** Quantification of the average ratio of the radial versus tangential dispersion normalized to the total number of neurons in individual P21-24 clones in the anterior and medial ventral/posterior region of the control and *SmoM2* mouse (anterior: control, n=9 clones; *SmoM2*, n=4 clones; p=0.02; medial ventral/posterior: control, n=33 clones; *SmoM2*, n=20 clones; n.s., not significant, p=0.2; Mann-Whitney test). Data are presented as median with interquartile range, and whiskers are the minimum and maximum. **(d)** Representative in situ hybridization images of the anterior (top) and medial (bottom) section of the control (left) and *SmoM2* (right) thalami at P4 for *ROR*α. Note the expansion of *ROR*α expression to the anterior region, as well as dorsally, in the *SmoM2* thalamus compared to the control. Scale bar: 200 μm.

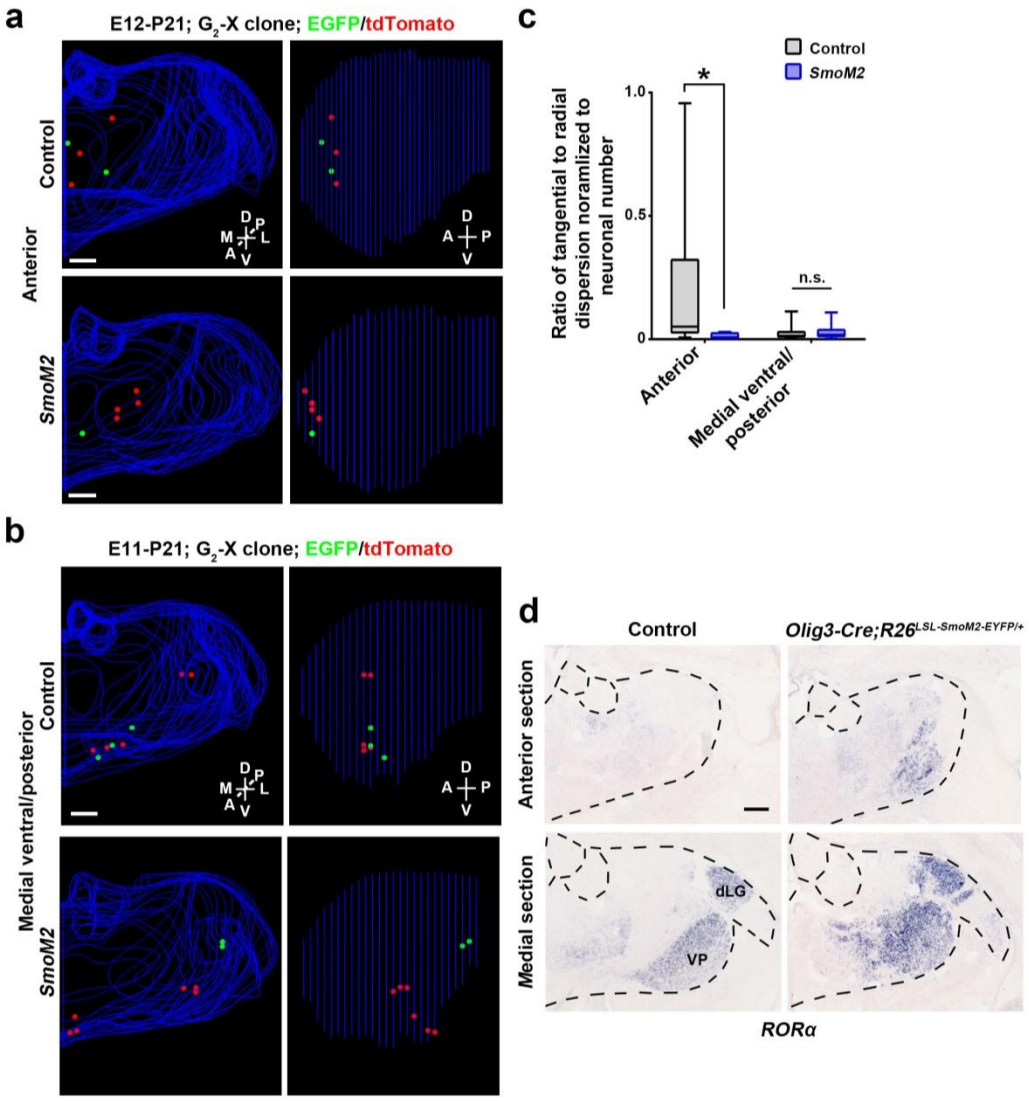
a
E12-P21; G2-X clone; EGFP/tdTomato
Control
SmoM2
Anterior
D
P
M
L
A
V
b
E11-P21; G2-X clone; EGFP/tdTomato
Medial ventral/posterior
c
Control
SmoM2
Ratio of tangential to radial dispersion noramlized to neuronal number
1.0
0.5
0
*
n.s.
Anterior
Medial ventral/ posterior
d
Control
Olig3-Cre;R26LSL-SmoM2-EYFP/+
Anterior section
Medial section
dLG
VP
RORα

5.5 SHH signaling promotes gliogenesis in the thalamus

We did not observe any significant changes in the average number of neurons in individual clones between the wild type and *SmoM2* thalami **(Figure 5.11a,b)**. However, while the average number of glial cells in individual clones was not significantly different between the wild type and *SmoM2* thalami **(Figure 5.11c)**, there was a substantial increase in the fraction of clones with glial cells in the *SmoM2* thalamus **(Figure 5.11d)**, indicating that SHH signaling promotes gliogenesis in the developing thalamus. The overall distribution of clonally related neurons and glial cells remained spatially clustered in the *SmoM2* thalamus, as reflected by the NND analysis **(Figure 5.11e,f)**. Together, these results suggest that SHH signaling influences the spatial organization of thalamic neurons at the clonal level, which likely contributes to distinct nuclear configuration and organization in the thalamus.

Figure 5.11: SHH signaling affects gliogenesis in the thalamus. (a) Quantification of the average number of neurons in clones located in the anterior (control, n=9; *SmoM2*, n=5), medial dorsal (control, n=18; *SmoM2*, n=6), and medial ventral/posterior (control, n=33; *SmoM2*, n=21) regions of the P4 control and *SmoM2* mice. Data are presented as median with interquartile range, and whiskers are the minimum and maximum. n.s., not significant. **(b)** Quantification of the average number of neurons in green/red G_2-X clones labeled at E10 (control, n=23; *SmoM2*, n=11), E11 (control, n=13; *SmoM2*, n=10), and E12 (control, n=9; *SmoM2*, n=3) between the control and *SmoM2* mice. Data are presented as median with interquartile range, and whiskers are the minimum and maximum. n.s., not significant. **(c)** Quantification of the average number of glial cells in individual clones in the control (left) and *SmoM2* (right) thalami (control, n=34; *SmoM2*, n=24). Data are presented as median with interquartile range, and whiskers are the minimum and maximum. n.s., not significant (Mann Whitney test). **(d)** Quantification of the number of clones containing neurons only (N) or neurons and glia (N+G) in the wild type control (left) and *SmoM2* (right) thalami. Note the increase in the fraction of clones containing glial cells in the *SmoM2* thalamus compared to the control. **, p=0.003 (chi-square test). **(e)** NND analysis of MADM-labeled neuronal clones in the *SmoM2* thalamus. Note that compared to random datasets simulated 100 times (gray), the cumulative frequency of NND of thalamic neuronal clones (red, n=31) is significantly left-shifted towards shorter distances, indicating a spatial clustering. Data are presented as mean±s.e.m. ****, p<0.0001 (unpaired t test with Welch's correction). **(f)** NND analysis of MADM-labeled glial clones in the *SmoM2* thalamus. Note that compared to random datasets simulated 100 times (gray), the cumulative frequency of NND of thalamic glial clones (blue, n=14) is significantly left-shifted towards shorter distances, indicating a spatial clustering. Data are presented as mean±s.e.m. ****, p<0.0001 (unpaired t test with Welch's correction).

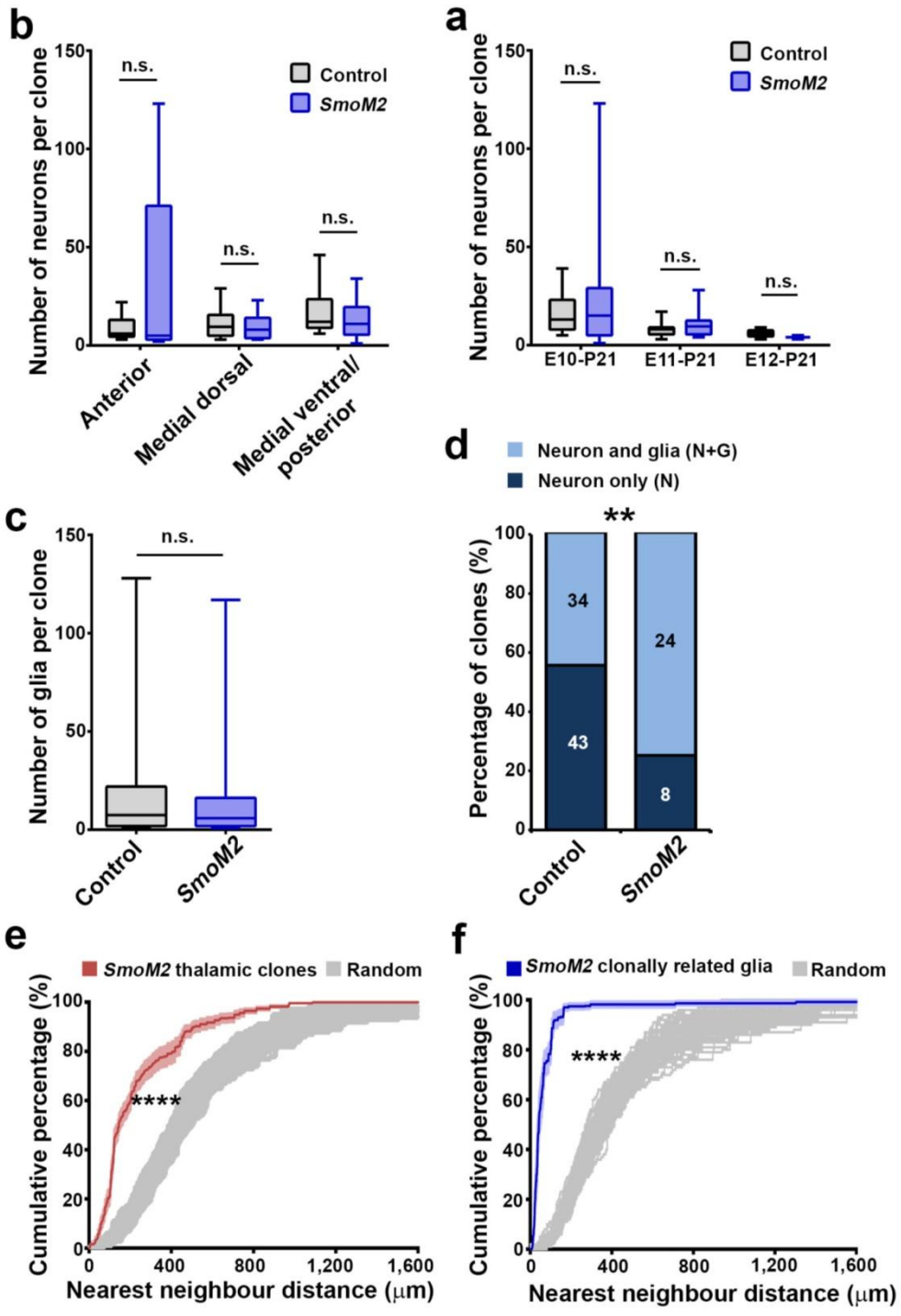
b
Number of neurons per clone
150
100
50
0
n.s.
n.s.
n.s.
Control
SmoM2
Anterior
Medial dorsal
Medial ventral/
posterior
a
Number of neurons per clone
150
100
50
0
n.s.
n.s.
n.s.
Control
SmoM2
E10-P21
E11-P21
E12-P21
c
Number of glia per clone
150
100
50
0
n.s.
Control
SmoM2
d
Neuron and glia (N+G)
Neuron only (N)
Percentage of clones (%)
100
80
60
40
20
0
**
34
43
24
8
Control
SmoM2
e
SmoM2 thalamic clones
Random
Cumulative percentage (%)
100
80
60
40
20
0
****
0
400
800
1,200
1,600
Nearest neighbour distance (μm)
f
SmoM2 clonally related glia
Random
Cumulative percentage (%)
100
80
60
40
20
0
****
0
400
800
1,200
1,600
Nearest neighbour distance (μm)

Chapter 6
Transcriptome Analysis of Thalamic Nuclei

6.1 Conserved circuit organization across different sensory modalities

Despite their functional specialization, different sensory pathways exhibit highly conserved circuit organization **(Figure 1.1)**. Peripheral inputs always reach the FO thalamic nuclei first, which project to the corresponding FO cortical regions. The sensory information is then relayed to the corresponding HO thalamic nuclei and HO cortical regions. Notably, previous studies have shown that thalamic nuclei of the same order across different modalities are composed of neurons with extremely similar axonal arborization architectures [102]. Specifically, neurons in the FO nuclei (e.g. VP, dLG, and vMG) exhibit highly topographic focal axonal projections to the cortex. In contrast, neurons in the HO nuclei (e.g. PO, LP, and dMG) possess broad and tangentially spread axonal projections to the cortex. Moreover, neurons in the FO and HO nuclei receive distinct modulatory inputs (Bokor et al., 2005; Sherman and Guillery, 1998), and respond differently to muscarinic and serotonergic activation (Varela and Sherman, 2007, 2009). Consistent with the anatomical connectivity difference, the FO and HO nuclei also exhibit distinct properties in information processing [119,120].

Our observation of the lineage segregation between FO and HO nuclei prompted us to investigate whether nuclei sharing a close progenitor origin, *i.e.* nuclei within the same order, also share a similar genetic program at early developmental stage, which might contribute to the assembly of a conserved circuit organization across modalities.

6.2 Order-specific transcriptome clustering of sensory nuclei across modalities

To assess the lineage-dependent hierarchical framework across different sensory modalities, we performed next generation RNA sequencing (RNA-seq) analysis of the transcriptome of VP and PO, the FO and HO nuclei of somatosensation, and dLG and LP, the FO and HO nuclei of vision, as well as the medial and lateral habenula (MH/LH) at P4, when the nuclei are largely formed. MH/LH serves as a control, as they have a separate progenitor origin from the thalamic nuclei [121].

We identified these nuclei based on the retrograde dye tracing from the primary somatosensory and visual cortical areas, and anatomical boundaries **(Figure 6.1a)**, extracted the tissues, and generated RNA-seq libraries as previously described [122]. To infer the developmental relationship between these nuclei, we compared their gene transcription similarity by performing unsupervised agglomerative hierarchical clustering analysis on the basis of the differentially expressed genes **(Figure 6.1b)**. As expected, the transcriptional variability between the replicates of the same nucleus was relatively small, and the same nuclei from different animals formed local clusters, indicating that our experimental preparation and analysis are reliable. Interestingly, besides the same nuclear clusters, LP and PO, and VP and dLG formed clusters, suggesting that nuclei of the same order share similar gene transcriptional profiles.

Consistent with the clustering analysis, the principal component analysis (PCA) identified three segregated clusters consisting of MH/LH, LP and PO, and VP and dLG, respectively **(Figure 6.1c)**. To quantitatively compare the transcriptional similarity between different nuclei, we calculated the cross-correlation of individual nuclei and found that LP and PO, and VP and dLG were more correlated than VP and PO, or dLG and LP **(Figure 6.1d)**.

Figure 6.1: Distinguishable transcriptomes between the FO and HO nuclei across different modalities. (a) Retrograde labeling of the FO and HO thalamic nuclei associated with the S1 and V1. Schematic of retrograde labeling is shown to the left. **(b)** Heatmap of the 2,367 most differentially expressed genes in MH/LH, VP, dLG, PO, and LP (n=3 for each nucleus), and hierarchical clustering of these nuclei. Note the similar gene expression profiles between the HO nuclei PO and LP, and the FO nuclei dLG and VP, and the corresponding clustering. **(c)** Principal Component Analysis (PCA) of different nuclei based on differential gene expression. **(d)** Pair-wise pearson correlation map of different nuclei based on differential gene expression.

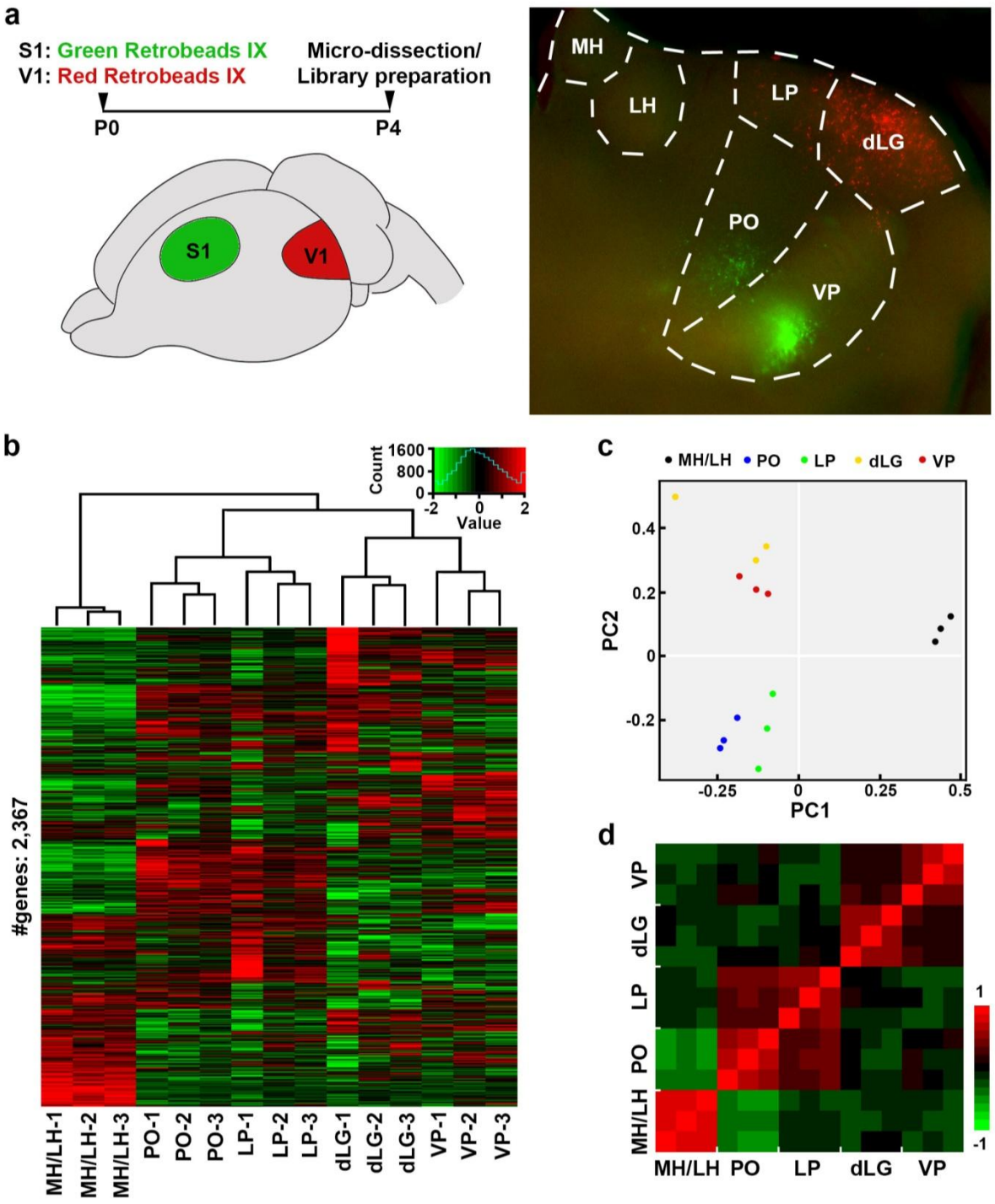
a
S1: Green Retrobeads IX
V1: Red Retrobeads IX
Micro-dissection/
Library preparation
P0
P4
S1
V1
MH
LH
LP
dLG
PO
VP
b
Count
1600
800
0
-2
0
2
Value
#genes: 2,367
MH/LH-1
MH/LH-2
MH/LH-3
PO-1
PO-2
PO-3
LP-1
LP-2
LP-3
dLG-1
dLG-2
dLG-3
VP-1
VP-2
VP-3
c
MH/LH
PO
LP
dLG
VP
0.4
0.2
0
-0.2
PC2
-0.25
0
0.25
0.5
PC1
d
VP
dLG
LP
PO
MH/LH
1
-1
MH/LH
PO
LP
dLG
VP

We confirmed this order-specific transcriptome clustering by performing *in situ* hybridization or analyzing the ABA *in situ* hybridization brain dataset for a number of candidate genes revealed by the transcriptome analysis **(Figure 6.2)**. Indeed, these genes showed either FO (i.e. VP and dLG) or HO (i.e. LP and PO) enriched expression at P4. Taken together, these results suggest that the FO or HO sensory nuclei across different modalities share more similar gene transcriptional profiles at the neonatal stage, likely reflecting a common progenitor origin of order but not modality specific nuclei. This is consistent with a recent study suggesting a cross-modal genetic framework for the development of sensory pathways in the thalamus[123].

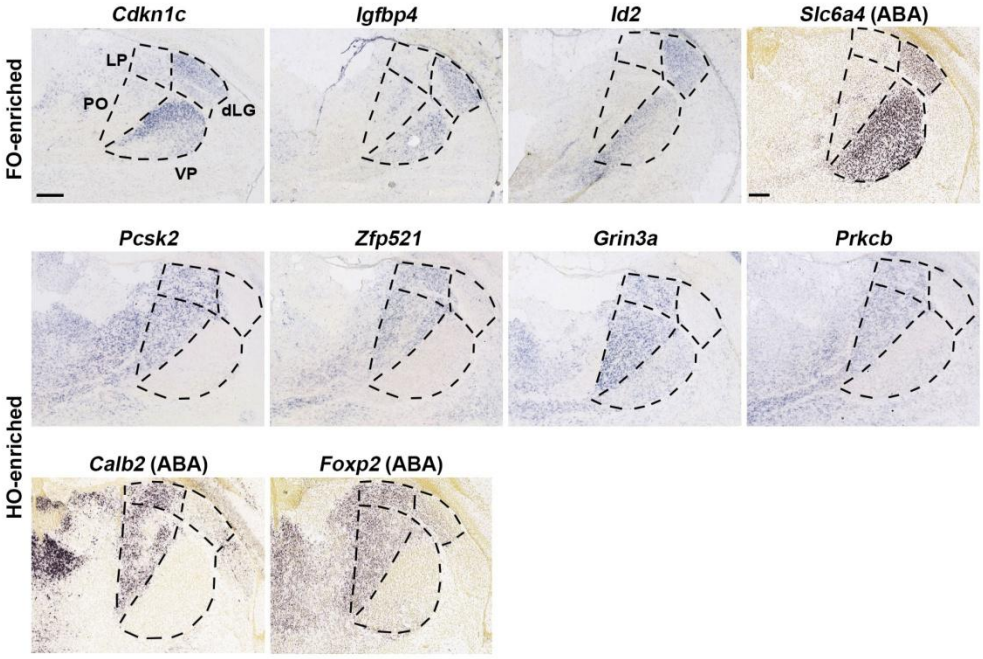

Figure 6.2: Enriched gene expression in either FO or HO sensory nuclei across modalities. RNA *in situ* hybridization images of the identified candidate genes on P4 coronal sections. Note the enriched expression of the candidate genes in either FO or HO nuclei across modalities. *Slc6a4*, *Calb2* and *Foxp2* images are from ABA dataset. Scale bars: 200 μm and 200 μm.

Chapter 7
Discussion and Future Directions

7.1 Ontogenetic establishment of order-specific nuclear organization in the thalamus *

Our systematic clonal analysis reveals a previously unknown ontogenetic logic for structural development and functional organization of the mammalian thalamus **(Figure 7.1)**. The thalamus is the largest brain structure deriving from the embryonic diencephalon. RGPs in the ventricular zone of the developing thalamus actively divide to produce a cohort of neuronal progeny either directly or indirectly via intermediate progenitors. At the early embryonic stage, individual RGPs and their progeny are similarly organized radially along a mediolateral axis **(Figure 7.2 left)**. As development proceeds, while clones in the medial ventral posterior region remain tightly arrayed radially along the radial glial fiber with the early born cells progressively moving outward (i.e. laterally) and dorsoposteriorly, contributing mostly to the FO sensory/motor-related nuclei, clones located in the anterior and medial dorsal regions become more tangentially dispersed, occupying predominantly the HO cognitive and HO sensory/motor-related nuclei **(Figure 7.2 middle and right)**.

---

* Shi W, Xianyu A, Han Z, Tang X, Li Z, Zhong H, Mao T, Huang K, and Shi SH. Ontogenetic establishment of order-specific nuclear organization in the mammalian thalamus. *Nature Neuroscience* **20**, 516–528 (2017).

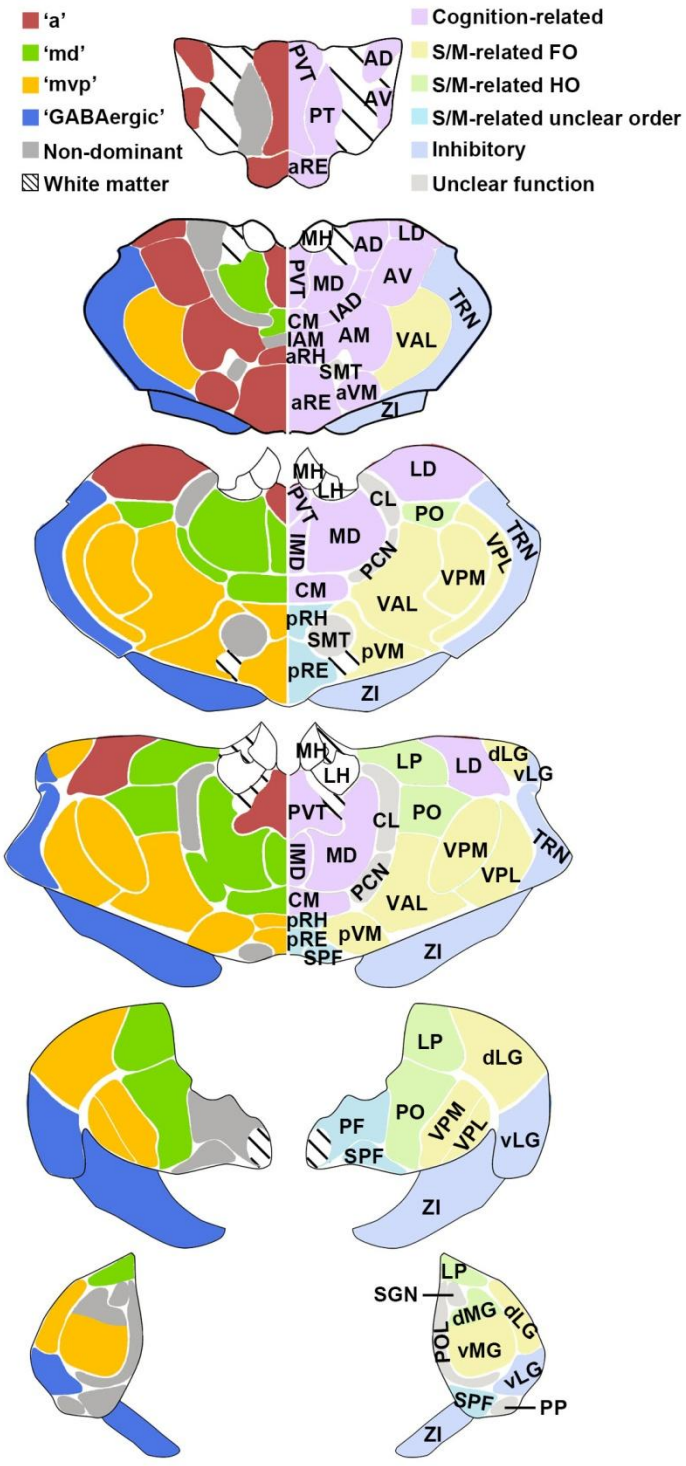

Figure 7.1: Schematic representation of lineage-related nuclear formation and functional organization in the thalamus. S/M, sensory/motor.

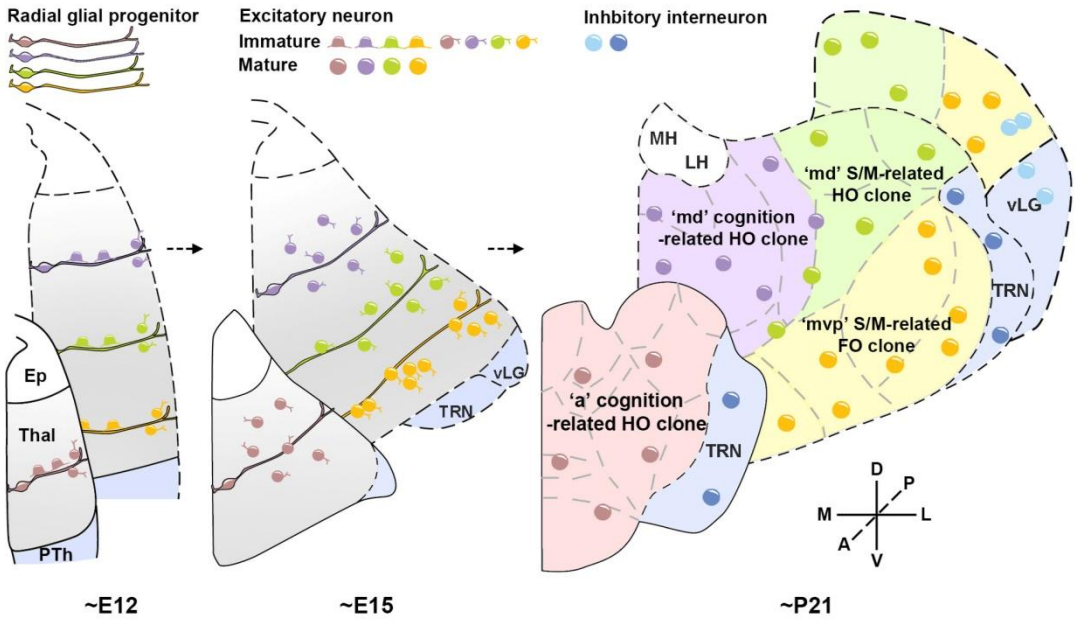

Figure 7.2: A diagram illustrating the ontogenetic origin and organization of thalamic nuclei and function. Individual thalamic RGPs and their progeny are similarly organized radially at E12 (left). As development proceeds, neurons in different thalamic regions exhibit distinct migration behaviors (middle), and eventually occupy thalamic nuclei associated with different functions (right).

Diverse migratory patterns of lineages have been suggested in the embryonic chick diencephalon [91,92]. In addition, it has been suggested that migrating cells follow both radial and non-radial glia pathways in the developing rat thalamus [124]. However, it is unclear how different migratory patterns may be related to distinct nuclear formation and functionality in the thalamus. In this study, we carried out a systematic clonal analysis of mouse thalamic progenitor cells using MADM, which provides fine resolution in progenitor behavior and lineage progression, as well as Cre-dependent retroviral labeling, in a temporal and spatial specific manner. Our clonal labeling and analysis is fundamentally different from the previous studies using the *Olig3-Cre* mouse line in conjunction with a reporter line that labels the entire progenitor population regardless of the timing of mitosis, or in utero electroporation that transiently transfects a large population of progenitors, resulting in the labeling of only

a subset of their progeny due to episomal plasmid dilution during progenitor cell division. The MADM or retroviral labeling allows the progeny to be labeled throughout the development starting soon after the TM treatment or retroviral infection. Our focus of E9-E12 coincides with the beginning phase of thalamic neurogenesis, thereby providing a comprehensive grasp of neuronal production and migration, and nuclear formation in the developing thalamus.

Interestingly, our unsupervised agglomerative hierarchical clustering analysis of the nuclear occupation of neurons in individual clones at the relatively mature stage (i.e. P21-24) not only reliably distinguished excitatory and inhibitory neuronal clones, but also identified three main excitatory neuron clonal subclusters that occupy largely non-overlapping sets of thalamic nuclei. These results suggest that the spatial configuration and nuclear occupation are the robust and reliable features of thalamic progenitors and their neuronal progeny (i.e. lineages) in the developing thalamus. Previous genetic fate mapping studies have shown that Neurogenin1/2 (NGN1/2-), OLIG2-, and DBX1-expressing progenitors in the caudal subdomains of the developing thalamus contribute to the cortex-projecting nuclei, the principal sensory nuclei, and the nuclei localized posteriodorsally, respectively [70,81]. Our finding of co-distribution of clonal clusters to certain thalamic nuclei at the single progenitor level is consistent with the previous observation at the population level. Interestingly, the nuclei harboring excitatory neuron progeny of OLIG2-expressing thalamic progenitors largely overlap with the nuclei occupied by the “mvp” cluster, indicating a lineal relationship between OLIG2-expressing thalamic progenitors and the “mvp” clones. It will be interesting to explore the lineal relationship between other progenitor subdomains and the remaining clonal clusters. Notably, additional subclusters may be revealed by further dissecting the hierarchical dendrogram. For example, the ‘md’ clonal cluster appears to have two subclusters largely corresponding to the clones

preferentially occupying the HO cognitive nuclei (e.g. MD, PVT, CM) and HO sensory/motor-related nuclei (e.g. PO, LP, dMG), respectively. On the other hand, the lineage-related organization is not absolute but preferential, as reflected in our quantitative analyses. While individual clonal clusters exhibit strong propensity in occupying distinct nuclei, clones in the same cluster show some variability. Thalamic RGPs are capable of producing glial cells as well, including both astrocytes and oligodendrocytes; however, there is no obvious correlation between the numbers of neurons and glial cells at the clonal level. In addition, while clonally related glia and neurons are located in close proximity, the nuclear occupation of clonally related glial cells did not exhibit any clear pattern, likely due to a higher degree of variability in clonal output of glial cells than that of neurons.

The differences in clonal behavior and neuronal organization are likely related to morphogen gradients and transcriptional regulations that affect thalamic progenitor specification and neuronal differentiation. Consistent with this, the distinct spatial configuration of clones can be observed at the embryonic stage. Previous studies have shown that SHH, FGF, and WNT act together to orchestrate the development and regionalization of the thalamus [68,78,81,83,125-127]. We found that neuronal clones in the medial ventral/posterior region with high levels of SHH activity are more radially organized, whereas neuronal clones in the anterior and mediodorsal regions with low levels of SHH activity are more tangentially organized. Moreover, enhancing SHH activity by SmoM2 expression suppresses tangential and promotes radial organization of clones in the anterior and dorsal regions, suggesting that SHH signaling influences the spatial organization of thalamic clones. Consistent with this change in clonal organization, the well-characterized marker genes such as *RORα* for the primary sensory nuclei exhibited elevated expression in the anterior and medial dorsal regions in the *SmoM2* thalamus. This change in nuclear identity and boundary prevents a

reliable systematic and quantitative analysis of nuclear occupation of neuronal clones in the mutant thalamus using the wild type ABA brain. Nonetheless, these results suggest that SHH signaling not only controls the gene expression and identity of thalamic progenitors, but also affects the spatial and functional organization of neuronal progeny arising from individual progenitors, as suggested previously [81,113]. Therefore, the precise localization of progenitors and the corresponding signaling environment likely regulate lineage progression and clone organization. Consistent with this, we observed a clear correlation between the spatial location of labeled RGPs at different embryonic stages and the regional localization of clones observed at P21-24. While a majority of thalamic RGPs exit the cell cycle and are depleted from the ventricular zone by E16, prior to the formation of most nuclear structures, this correlation suggests a link between embryonic progenitor cells and adult clones. It will be interesting to further explore the precise relationship between SHH and other signaling pathways and progenitor behavior and neuronal progeny migration responsible for distinct clonal organization and nuclear formation in the developing thalamus.

Besides the spatial regulation by a combination of signaling pathways, there are also important temporal regulations of neuronal generation and migration in the developing thalamus. Individual RGPs are capable of producing a cohort of neuronal progeny in a sequential manner either directly or indirectly via intermediate progenitors. The temporal dynamics of RGP and intermediate progenitor divisions of the corresponding clones likely determine the size and configuration of thalamic nuclei in which the clones reside, in conjunction with neuronal migration. Notably, besides the relative radial versus tangential dispersion difference, the average number of neurons in the ‘mvp’ clonal cluster occupying the FO sensory/motor-related nuclei appears to be higher than that in the ‘a’ clonal cluster occupying the HO cognitive

nuclei, which may contribute to the overall structural differences between these two general groups of nuclei. In addition, in stark contrast to that in the developing cortex, where neuronal migration occurs in a birth date-dependent inside-out fashion, neuronal migration in the developing thalamus follows a birth date-dependent outside-in pattern. Early born neurons migrate further and are located more laterally and dorsoposteriorly, whereas late born neurons are located closer to the midline. Therefore, while sharing close lineage relationships, neurons in the same clone likely also exhibit temporal differences in their maturation and other properties, which may contribute to neuronal diversity and nuclear distinction in the thalamus.

The progenitor origin of thalamic neurons is not only coupled to the structural organization, but also related to functional organization of the thalamus. The anterior and medial dorsal clones principally contribute to the nuclei of cognitive and sensory/motor-related HO functions, whereas the medial ventral posterior clones mostly contribute to the nuclei of sensory/motor-related FO functions. The thalamus is commonly demarcated into a large number of distinct nuclei with defined functions [1]. However, little is known about the general principles underlying the complex structural and functional organization of thalamic nuclei. Moreover, accumulating evidence suggests that, although useful, these nuclear divisions may not always be the relevant functional unit [4]. Our data showed that cognition-related HO nuclei in the anterior region share a similar progenitor origin, and sensory/motor-related FO nuclei in the medial ventral posterior region share a similar progenitor origin. In addition, sensory/motor-related HO nuclei share a close but largely distinguishable lineage relationship with cognition-related HO nuclei in the medial dorsal region. These results suggest that lineage relationships influence the functional organization of the thalamus.

Notably, this lineage-related functional organization manifests at the resolution beyond the conventional individual nuclear boundaries. For example, we found that neurons in the VM, RE, and RH exhibit two distinct progenitor/clonal origins. Neurons located in the anterior portion of these nuclei are largely derived from the 'a' clonal cluster, whereas neurons located in the posterior portion are predominantly originated from the 'mvp' clonal cluster. Interestingly, our further analysis of the previous axonal tracing experiments [6] showed that the anterior and posterior regions of VM, RE, and RH exhibit distinct thalamocortical axonal projection patterns. While the anterior regions predominantly innervate cognitive cortical areas such as the ACC and PLC, the posterior regions largely project to sensory/motor-related cortical areas. Taken together, these results demonstrate that clonal relationship predicts functionality of neurons both across different nuclei and within the same nucleus.

Importantly, we also observed a clonal segregation between the FO and HO sensory/motor-related nuclei across different modalities. While the 'mvp' clonal cluster predominantly contributes to the FO sensory/motor-related nuclei, the 'md' clonal cluster largely contributes to the HO sensory/motor-related nuclei. Consistent with this lineage segregation, we found that the gene expression profiles of the same order nuclei of different modalities are more similar than those of different order nuclei of the same modality at the neonatal stage. These results suggest that lineage relationships facilitate the establishment of order-specific circuit organization across different modalities in the thalamus. Previous studies have demonstrated that thalamic nuclei of the same order across different modalities exhibit similar properties in information processing [2,119,120], and are composed of neurons with extremely similar axonal arborization architectures. The distinct progenitor origin between neurons in the FO and HO nuclei likely contribute to their different morphologies, anatomical connections, and functional properties. In addition, we also observed a lineal

segregation of GABAergic interneurons in the TRN and LGN, which may have critical functional implications.

Limited intra-thalamic connectivity has been found to structurally or functionally organize the complex thalamic nuclei [1,4,66,128,129]. Our findings suggest that lineage-related development and organization provides a fundamental blueprint for the assembly and function of the thalamus. Consistent with this, it has previously been shown that the overall topography of thalamocortical axonal projections appears to be normal in the absence of any evoked synaptic transmission [130]. Moreover, our observation of a strong lineage segregation of the sensory/motor-related FO and HO nuclei across different modalities points to a model of the development of thalamic sensory/motor pathways in distinct phases; that is, the developmental origin promotes the establishment of a generic hierarchical framework which is further specified into different modalities, likely dependent on the distinctive inputs from the periphery and other brain regions [5,131,132].

7.2 Modality specification in the thalamus

Our study suggests that the hierarchical order of a thalamic nucleus is strongly influenced by its progenitor origin. Nuclei sharing a close lineage relationship tend to belong to the same order, but different functional modalities, which prompts us to ask: how is the modality specified? In other words, how are FO and HO nuclei of the same modality paired up during thalamus development?

7.2.1 Cortical influence on modality specification

The driver input determines the cell's receptive field property[8]. For example, the molecular and functional identity of layer IV pyramidal neurons is defined by the origin of their thalamocortical input [111]. Similarly, changes in the periphery sensory input have been shown to alter functional subdivisions of the corresponding thalamic

FO nucleus and the relevant corticofugal connectivity [133], indicating a degree of rewiring and plasticity of thalamic organization upon the manipulation of driver inputs. While this form of relatively late plasticity unlikely affects the spatial distribution of thalamic neurons, some properties of the principal thalamic subdivisions may change after neurogenesis and neuronal migration. Layer V cortical pyramidal cells provide driver inputs to HO thalamic nuclei, implying a potential role of layer V neurons in instructing the modality identity of HO nuclei. Future efforts combing mouse genetics with viral vector-based approaches to manipulate specific layer V neuronal population would offer new insight into thalamus modality specification.

7.2.2 Thalamic reticular influence on modality specification

In addition to peripheral and cortical layer V inputs, TRN inputs also arrive at the thalamus at an early developmental stage. Although TRN inputs are modulators and serve to modulate rather than determine the neuronal activity in the thalamus, the anatomical position of TRN in the thalamocortical circuit, the unique physiological properties of TRN neurons and the early onset of TRN innervation to thalamus collectively suggest its possible function in shaping thalamic nuclei specification, especially modality specification.

As discussed in Chapter 1.5.2, TRN is a sheath-like structure wrapping around the thalamus and provides inhibition to all other thalamic nuclei **(Figure 1.3)**. Single neuron tracing studies revealed extensive axonal arborizations of TRN cells[108,134-137]. Although the axonal arborization of most TRN cells is confined within a single nucleus, a small proportion of analyzed neurons were seen targeting both VP and PO, the FO and HO nuclei for somatosensation [137]. In line with this, dye-coupling studies of the somatosensory sector of the TRN identified two distinct types of gap junction-

coupled TRN neuron networks in rats [66]. While most neuronal clusters are elongated and spread narrowly across the thickness of the TRN with axons selectively inhibiting neurons within one nucleus, some coupled clusters have neurons distributed broadly across the thickness of the TRN, projecting to both FO and HO nuclei **(Figure 7.3)**. The two forms of spatially organized TRN neuronal clusters are associated with distinct axonal projection patterns, indicating two functionally distinct networks that correlate activity within or across thalamic nuclei. Gap junction-mediated electrical synapses allow synchronized activity of the coupled neurons [61,62], which might contribute to coordinated activities of their postsynaptic thalamic neurons. Thus we speculate that FO and HO nuclei within the same modality might receive afferents from clusters of electrically coupled TRN neurons, and therefore exhibit coordinated activities during development, which eventually drives them to form a pair in information processing. Supporting this possibility, TRN axons are observed in the thalamus as early as P0 (data not shown), even before the cortical axons reach the thalamus (P2-P10 in mice) [133], indicating their potential function in thalamus organization during development. Despite its early onset, all the current studies on TRN-thalamus connection focus on its contribution to sensory or cognitive perception in the adult animal. TRN's role in the developing thalamus remains unexplored.

Figure 7.3: Axonal projections and dye-coupling patterns of TRN neurons. (a) Drawing of an example of a coupled cluster and its injected TRN neuron sending axon terminations to the VP. The dashed line in the thalamus indicates the approximate location of the VP/PO border. **(b)** Drawing of a coupled cluster and its injected TRN neuron sending axon terminals to the VP/PO border area. **(c)** Drawing of a coupled cluster and its injected neuron sending axon terminations to the PO. **(d)** Drawing of a coupled cluster and its injected TRN neuron sending branched axon terminations to both the VP and PO. **(e)** Spread of clusters along the short axis of the TRN versus the axonal projection pattern. **(f)** Schematic diagram of distinct gap junction-coupling connectivity patterns. The blue circle indicates the connectivity pattern of spherical clusters, and the yellow ellipses indicate connectivity patterns of elongated or discoid clusters. Black circles and gray boxes indicate somata and axon terminals, respectively. Lines indicate axons or dendrites. Axons with dashed lines in the spherical cluster indicate uncertainty whether neurons in this cluster type are exclusively cells with branched axons or mixed populations with branched and non-branched axons. Adapted from Lee et al., (2014) [66].

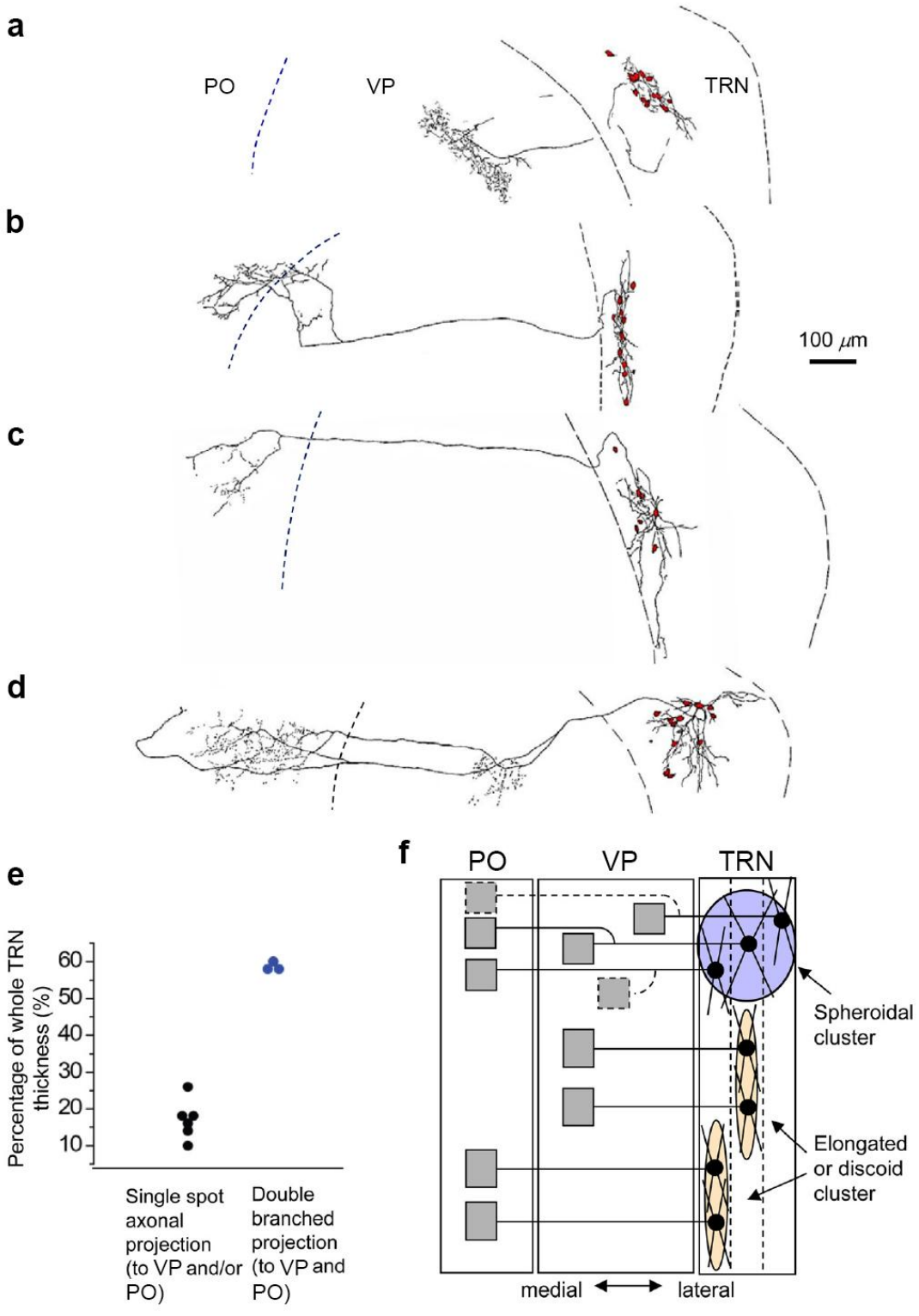
a
PO
VP
TRN
b
100 μm
c
d
e
Percentage of whole TRN thickness (%)
60
50
40
30
20
10
Single spot axonal projection (to VP and/or PO)
Double branched projection (to VP and PO)
f
PO
VP
TRN
Spheroidal cluster
Elongated or discoid cluster
medial
lateral

It should be noted that, although electrical synapses frequently interconnect interneurons in the TRN, current experiments suggesting synchronized TRN inputs to FO and HO nuclei are solely based on somatosensory thalamus. Whether this principle applies to other thalamic modalities requires further investigation. Generating a comprehensive TRN-thalamus connectivity map would greatly benefit future research on TRN function. It will also provide coordinates for precise labeling and manipulation of TRN regions related to specific thalamic nuclei.

7.3 Whole-mount clearing and reconstruction of long-range axonal projection

Each thalamic nucleus, especially the HO nucleus, makes functional synapses with multiple brain regions. Whether the diffused projection pattern reflects the many side branches of individual neurons or the mixing of neurons projecting to different regions remains poorly understood. Single neuron tracing studies with viral vectors revealed dynamic branching patterns of neurons distributed within the same nucleus [108,134-136]. In accordance with this observation, accumulating evidences suggest that nuclear divisions are not necessarily the relevant functional unit [6]. Our analysis of MADM-labeled neurons was based on their nuclear identity and did not take into account the neuronal diversity within individual nuclei. To gain a comprehensive understanding of the function of lineage related thalamic neurons, one approach is to perform whole-mount reconstruction of the complete morphology of labeled neurons. Imaging of the whole mammalian brain has recently become feasible thanks to the rapid progress on tissue clearing protocols [138,139]. The inevitable stretching of sections during the conventional serial sectioning and imaging processes renders it impossible to align multiple consecutive sections each containing a tiny piece of the bypass axon. In contrast, whole-mount reconstruction of intact tissues avoids the alignment

difficulties and makes it possible to trace the labeled neuron from the soma to its final axonal aborizations. MADM-based labeling generates samples ideal for whole-mount clearing and imaging. By adjusting the dose of TM, MADM allows sparse labeling in the desired brain region, which prevents high packing density of cells and fibers in most samples labeled by viral-based approaches. In addition, the original GFP and RFP signals can be further amplified by immunohistochemistry, which enables visualization of fine structures. We recently tried the iDISCO protocol on our MADM labeled samples [140,141], and were impressed by the transparency of the tissue and bright labeling of neurons projecting to remote brain regions. However, there are still technical concerns about the tissue clearing protocol. For example, noise caused by immunohistochemistry was observed throughout the brain and was especially prominent on the surface of the brain and inside the ventricles. Moreover, volume imaging generates very large data sets, which have become the bottleneck in the field of imaging cleared tissue and require specialized software programs and a powerful workstation to manage and analyze the acquired files [138,140]. Future research is needed towards lowering the noise and developing new tools to handle the data set.

Nonetheless, whole-mount clearing and reconstruction have already greatly expanded our knowledge of neuronal morphology and connectivity [138-140,142], and it will become an indispensible approach for neural circuit research in the future. In addition to thalamocortical neurons, this method can be applied to studying the influence of TRN on thalamus development as well, by tracing TRN neuron projection with single cell resolution.

7.4 Synaptic connectivity mapping in the mammalian brain

Once the entire morphologies of individual neurons are reconstructed, we would like to understand their function by examining their axonal targets. When measuring

the density of axonal projections, it is extremely challenging to distinguish between axons passing by a region and those making local synapses. Even if one can tell them apart based on morphology, the density of axonal projections does not fully represent the density of functional synapses. To overcome this limitation, genetic synaptic labeling methods have been developed to describe neuronal connectivity in the mammalian brain with synapse resolution and a quantified accuracy.

Mammalian GFP reconstitution across synaptic partners (mGRASP) can label synapses formed between two selectively labeled neuronal populations [143,144]. It is based on the functional complementation between two non-fluorescent fragments of GFP. Two split-GFP fragments are expressed in the pre- or post- synaptic terminals of two different neuronal populations. When two neurons expressing different fragments are tightly opposed through a synaptic cleft, two non-fluorescent fragments self assemble and form a fluorophore **(Figure 7.4)**. This method has been widely used in *C. elegans* and later in *Drosophila* [145-147], and it has recently been modified and applied to mark synapses in mice. Various types of adeno-associated virus (AAV) vectors expressing split-GFP dependent or independent of Cre have been generated to accommodate the needs of mapping local or long-range circuits [148]. However, the signal intensity of mGRASP-based labeling is relatively weak and can not be boosted by immunohistochemistry due to the lack of primary antibody specifically recognizing the reconstituted GFP [143,148]. When we introduced mGRASP vectors into mouse cortex by *in utero* electroporation, pre- and post-synaptic cells were successfully marked, but no obvious synapse labeling was observed. The lower expression level of split-GFP in neurons received electroporation than those infected by AAV might cause this. Future efforts are needed to improve the signal intensity of the reconstituted GFP and to develop novel antibodies for signal amplification.

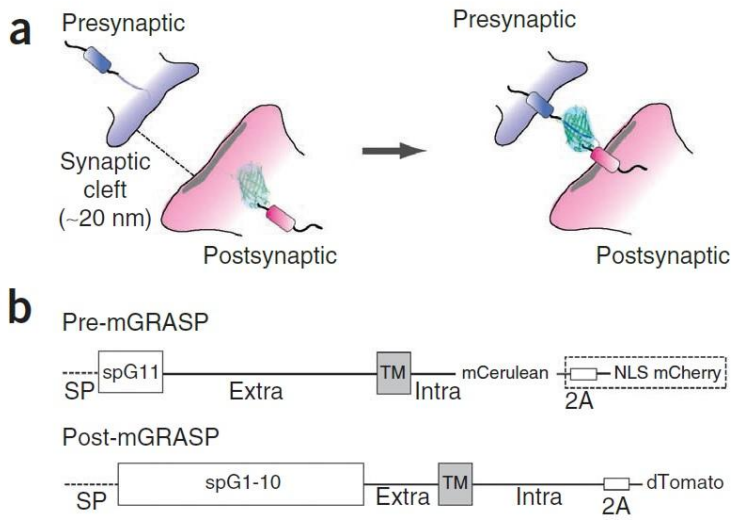

Figure 7.4: Synaptic mGRASP components. (a) Schematic illustration of mGRASP in the synapse. **(b)** Diagram of pre- and post-mGRASP composed of signal peptide (SP), split-GFP fragment GFP1-10 (spG1-10) or GFP11 (spG11), extracellular domain (extra), transmembrane domain (TM) and intracellular domain (intra) followed by fluorescent proteins (mCerulean, 2A-mCherry or 2A-dTomato). Adapted from Kim et al., (2011) [144].

The other available fluorescence-based synaptic detection approach is more robust and easier to incorporate, and utilizes AAV vectors expressing cytoplasmic tdTomato and presynaptic (synaptophysin-fused) GFP [7,149]. These viral vectors provide efficient synaptic labeling and allow amplification of the GFP signal by immunohistochemistry. The expression of these viral vectors are induced by Cre-mediated recombination, therefore can be restricted in the desired neuronal population by using cell subtype-type specific Cre lines. Compared to mGRASP where both pre- and post- synaptic fragments can be introduced to selective neuronal populations, this method labels presynaptic terminals without distinguishing the cell types of their postsynaptic targets. Nonetheless, with bright and robust synaptic labeling, this approach can be applied into tracing TRN innervation to the thalamus and also for

mapping the synaptic connectivity of clonally related thalamic neurons if delivered to the embryonic thalamus via *in utero* injection.

Despite their limitations, both synapse detection approaches provide detailed information about the number and distribution of synapses, contributing to the generation of a precise neuronal connectivity map in the mammalian brain. In addition, both approaches can be more powerful for quick and accurate connectivity mapping, if combined with optimized whole-mount clearing methods in the near future.

Chapter 8
Methods and Materials

8.1 Animals

MADM-11^{GT} (JAX Stock No. 013749) and *MADM-11*^{TG} (JAX Stock No. 013751) mice were produced as previously described [95]. *MADM11*, *Nestin-CreER*^{T2} [97], *R26-SmoM2-EYFP* [114], and *Olig3-Cre* [81] mice were kindly provided by Drs. Hippenmeyer, Kageyama, Joyner, and Nakagawa, respectively. Mice were bred and maintained according to guidelines established by the Institutional Animal Care and Use Committee of Memorial Sloan Kettering Cancer Center. For MADM labeling, *Nestin-CreER*$^{T2+/-}$*/MADM-11*$^{TG/TG}$ mice were crossed with *MADM-11*$^{GT/GT}$ mice and the time of pregnancy was determined by the presence of the vaginal plug (E0, around noon).

For clone induction, pregnant females were injected intraperitoneally with tamoxifen (T5648, Sigma) dissolved in corn oil (C8267, Sigma) at E9, E10, E11 and E12 at a dose of 5-25 μg/g body weight.

8.2 *in utero* intraventricular injection

In utero intraventricular injection of retrovirus was performed as previously described [85]. In brief, uterine horns of pregnant mice were exposed in a clean environment. Cre recombinase-dependent retrovirus expressing EGFP (~1.0 μL) mixed with fast green (2.5 mg/mL, Sigma) was injected into the third ventricle through a beveled calibrated glass micropipette (Drummond Scientific). After injection, the uterus was placed back in the abdominal cavity and the wound was surgically sutured. After surgery, the animal was placed in a recovery incubator under close monitoring until it fully recovered.

8.3 Serial sectioning and immunohistochemistry

Both male and female mice were perfused intracardially with 4% paraformaldehyde (PFA) in phosphate-buffered saline (PBS, pH 7.4). Brains were removed and post-fixed overnight at 4°C. Serial coronal sections of individual brains were prepared using a vibratome or cryostat (Leica Microsystems) and subjected to immunohistochemistry.

The following primary antibodies were used: chicken anti-GFP (1:1,000 dilution, GFP-1020, Aves Lab) [105], rabbit anti-RFP (1:1,000 dilution, 600-401-379, Rockland) [105], guinea pig anti-RFP (1:20,000 dilution, gift from J. Nicholas Betley, University of Pennsylvania), mouse anti-OLIG3 (1:200 dilution, MAB2456, R&D Systems) [70], rabbit anti-BLBP (1:200 dilution, ab32423, Abcam) [104], mouse anti-Ki-67 (1:500 dilution, 556003, BD Pharmingen) [104] mouse anti-TUJ1 (1:500 dilution, MMS-435P, Covance) [104], mouse anti-NESTIN (1:500 dilution, rat-401, Developmental Studies Hybridoma Bank) [104], mouse anti-NEUN (1:500 dilution, MAB377, Millipore) [150], rabbit anti-S100 (1:500 dilution, Z0311, Dako) [151], rabbit anti-OLIG2 (1:500 dilution, AB9610, Millipore) [152], and mouse anti-PARVALBUMIN (1:500 dilution, MAB1572, Millipore) [104]. Sections were mounted on glass slides, imaged using confocal microscopy (FV1000, Olympus or LSM700, Zeiss) and slide scanner (NanoZoomer 2.0-HT, Hamamatsu Photonics).

8.4 3D reconstruction and NND analysis

Sections were reconstructed using Neurolucida and StereoInvestigator (MBF Bioscience). Neurons, astrocytes, and oligodendrocytes were distinguished based on their morphology (e.g. nuclear size and neurite length) and marker expression. Each

section was analyzed sequentially in anterior to posterior order. The boundaries of the entire thalamus as well as the landmark nuclei including MH, LH, LGN, TRN, and parts of MGN and VM were traced in each section and aligned. Individually labeled neurons were represented as colored dots (~4 times the size of the cell body at P21-24 and ~2 times at E12). The anterior region of the thalamus was defined as the part before the appearance of the major sensory/motor nuclei (i.e. ABA sections 56-61) and the posterior region as the part following the separation of the thalamic hemispheres (i.e. ABA sections 78-92). The remaining part was defined as the medial region (i.e. ABA sections 62-77).

The distribution of the nearest neighbor distance (NND) reflects the spatial point pattern of the dataset, as previously described [103]. Specifically, given N cells in a dataset, for each cell i the distance to its closest neighbor was measured and denoted as di, the NND for cell i. The indicator function f (y, d) was then calculated as:

$$f(y,d) = \begin{cases} 1, & if\ d \le y, \\ 0, & otherwise. \end{cases}$$

Thus, the cumulative distribution function (CDF) of NND is:

$$G(y) = \sum_{i=1}^{N} f(y, d_i).$$

8.5 Thalamic nuclear registration

After 3D reconstruction, all serial sections of individual experimental thalami were aligned based on the midline. The cutting angle tiltation was corrected using a previously established method based on anatomical landmarks [6]. All corrected sections were then aligned based on the dorsal boundary of the thalamus. To register known

nuclei within our experimental thalami, the nuclei from the ABA were traced and linearly scaled to best fit the average experimental thalamus. The correspondence between individual experimental thalami and the ABA reference thalamus were further assessed by manual comparisons of the landmark structures (MH, LH, LGN, and TRN), and adjusted. The nuclear identities and corresponding numbers of labeled neurons of individual clones were then systematically inferred and manually confirmed. For clonal clustering, the fractions of individual clones located in different nuclei were calculated, standardized, and subjected to an unsupervised agglomerative hierarchical clustering analysis (Clustergram: Distance metric, Euclidean; Linkage, Average; MATLAB, MathWorks). The number of excitatory neuron clonal subclusters was validated by the Silhouette coefficient analysis (MATLAB, MathWorks). The criterion values (i.e. coefficients) in the Silhouette analysis peaked at three clusters within the range of number of clusters tested. For volume overlap estimation, the posterior domain of the thalamus (i.e. ABA sections 85-92) containing very few labeled neurons was not included. The volume of individual experimental thalami ($Vexperimental$) was compared to the volume of the scaled ABA reference thalamus ($Vreference$), and the volume overlap was estimated as

$$((Vexperimental \cap Vreference)) \,/\, Vexperimental$$

where '∩' is the logical AND operator (i.e. overlap).

Based on the literature [1], the following nuclei were considered as sensory/motor-related: SPF, VAL, VPL, VPM, dLG, vMG, PO, LP, dMG, PF, pRE, pRH, and pVM; and the following nuclei as cognition-related higher order: AD, AM, AV, CM, IAD, IAM, IMD, MD, LD, PT, PVT, aRE, aRH, and aVM. For quantification of the order versus modality segregation, only clones with more than

half of the neurons located in the well-characterized sensory/motor-related nuclei (i.e. VPM, VPL, PO, dLG, LP, dMG, vMG, VAL, and pVM) were included in the analysis. Specifically, VAL and pVM are motor-related nuclei; VPL, VPM, and PO are somatosensory-related nuclei; dLG and LP are visual related nuclei; vMG and dMG are auditory-related nuclei. Among them, VPL, VPM, dLG, vMG, VAL, and pVM are FO nuclei, and PO, LP, and dMG are HO nuclei.

Thalamocortical axonal projection labeling and analysis were done as previously described [6]. In brief, P14-18 C57BL/6J mice were anesthetized and stabilized in a custom stereotaxic apparatus. Recombinant adeno-associated viruses expressing either EGFP or tdTomato were injected into the thalamus using a beveled sharp glass micropipette. Coordinates for injections ranged from: 0.5 to −1.6 anterior to posterior, 0–1.6 lateral, and 2.8–4.2 deep from the pia (in mm from bregma). Animals were perfused transcardially with PBS followed by 4% PFA 14 days after the surgery. The brains were collected, post-fixed and sectioned coronally on a cryostat at 50 μm thickness. All sections were imaged on the Nanozoomer slide scanner (Hamamatsu) and Zeiss Axio Imager. A suite of custom algorithms using MATLAB (MathWorks) was developed to analyze and compare thalamic injections across animals. Each thalamus was manually traced and each injection site was manually marked, to generate the binary thalamus masks and injection masks. All thalamic masks were normalized, corrected for variability in cutting angle, and aligned together to obtain the averaged model thalamus. Then, each injection site was mapped onto the model thalamus. Finally, injection and target information for the injections were combined to localize the precise thalamic origin of the cortical projections.

8.6 Retrograde labeling and sequencing library preparation

To label thalamic neurons in VP and PO, and dLG and LP, ~20 nL Green and Red Retrobeads IX (Lumafluor, Inc) were stereotaxically injected to S1 and V1 of the anaesthetized P0 pups, respectively. Following the injection, pups were allowed to recover and returned to their mothers. At P4, brains were recovered and acute coronal slices (300 μm) were prepared using a vibratome (Leica Microsystems). Retrogradely labeled thalamic nuclei were visually identified and micro-dissected in oxygenated artificial cerebrospinal fluid (ACSF) containing 126 mM NaCl, 3 mM KCl, 1.25 mM KH_2PO4, 1.3 mM $MgSO_4$, 3.2 mM $CaCl_2$, 26 mM $NaHCO_3$, 10 mM glucose, and 2% fetal bovine serum, pH 7.4. RNA was extracted using an RNeasy Micro Kit (Qiagen).

The sequencing libraries were generated using CEL-Seq method, as previously described [122]. In brief, the samples from five regions of the same brain were barcoded and pooled for *in vitro* transcription reactions. The amplified RNA was fragmented and purified. The illumina 3' adaptor was added by ligation. RNA was then reversely transcribed into DNA, and the 3'-most fragments with both Illumina adaptors and a barcode were selected. The resulting DNA libraries were sequenced with paired-end reads, where the first read recovered the barcode, 8-bp sample barcode, and 10-bp random unique molecular identifier (UID), and the second read identified the mRNA transcripts.

8.7 RNA-seq data analysis

Reads were mapped to mm10 mouse reference genome with STAR [153]. Alignments with the same genome start position and the same UID sequences were identified as PCR induced duplicates and de-duplicated. HTSeq was used to count the number of alignments within each gene using default mode “union” [154]. To adjust the

library size, the size factor was estimated using "median ratio method" [155]. The UID counts of each sample were divided by the estimated size factor. To eliminate any bias from individual brains, another round of normalization was performed by subtracting the average UID counts across all samples from the same brain for each gene. To eliminate the effect caused by extremely lowly or highly expressed genes, genes with a maximum expression value below 50% or higher than 99% of all detected genes were removed. Then, based on the expression variance, the top 20% of the genes (2,367 genes) were used for further analysis.

The UID counts were normalized across the samples and plotted into a heatmap using the "heatmap.2" function from R package gplots. Dendrogram was generated by R function "hclust" by taking "1 - pearson correlations" as distances and using the "average" agglomeration method. Principle component analysis (PCA) was performed using the "prcomp" function from R package. Pair-wise pearson correlations between samples were calculated and plotted into a heatmap using the "heatmap.2" function from R package gplots.

8.8 RNA *in situ* hybridization

Cryostat sections (18 μm) of P4 brains were prepared and used for RNA *in situ* hybridization, as previously described [156]. In brief, the primer sequences for the *ROR*α probe were obtained from Allen Brain Database. T7 or SP6 promoter sequences were added to the 5' end of the reverse or forward primer sequences, respectively, which were then used for PCR amplification to generate the probe template. *In vitro* transcription of the resulted PCR product was performed to generate digoxigenin (DIG)-labeled antisense RNA probes. Hybridization was performed at 62 °C overnight, followed by post-hybridization washes. Sections were then incubated with alkaline phosphatase-coupled anti-DIG antibody (Roche, diluted 1:3000) at 4°C

overnight. For the visualization of the reaction product, sections were incubated in the dark at room temperature with freshly prepared NTMT buffer (100 mM NaCl, 100 mM Tris-HCl pH 9.5, 50 mM $MgCl_2$, 0.1% Tween20, 0.5 mg/mL Levamisol) containing NBT/BCIP (Roche). Once the color was fully developed, sections were washed, post-fixed with 4% PFA, dehydrated, and mounted with Permount (Fisher) for image acquisition using a slide scanner (NanoZoomer 2.0-HT, Hamamatsu Photonics).

8.9 Statistics

No statistical methods were used to predetermine sample sizes but our sample sizes are similar to those reported in previous publications [94,105]. Data collection and analysis were not randomized nor performed blind to the conditions of the experiments. No data points were excluded. Data are presented as median with interquartile range and whiskers as the minimum and maximum, or as mean±s.e.m., and statistical differences were determined using non-parametric Mann–Whitney test, unpaired t-test with Welch's correction (unequal variances), chi-square test, or linear regression analysis. Data distribution was not formally tested. Statistical significance was set at $p<0.05$. Exact p values are provided in the figure legends.

REFERENCES

1 Jones, E. G. *The Thalamus*. (Cambridge University Press, New York, 2007).

2 Sherman, S. M. Thalamus plays a central role in ongoing cortical functioning. *Nat Neurosci* **19**, 533-541, doi:10.1038/nn.4269 (2016).

3 Steriade, M. & Llinas, R. R. The functional states of the thalamus and the associated neuronal interplay. *Physiological reviews* **68**, 649-742 (1988).

4 Sherman, S. M. & Guillery, R. W. *Exploring the Thalamus and its Role in Cortical Function*. (MIT Press, Cambridge, MA, 2006).

5 O'Leary, D. D., Schlaggar, B. L. & Tuttle, R. Specification of neocortical areas and thalamocortical connections. *Annu Rev Neurosci* **17**, 419-439, doi:10.1146/annurev.ne.17.030194.002223 (1994).

6 Hunnicutt, B. J. *et al.* A comprehensive thalamocortical projection map at the mesoscopic level. *Nat Neurosci* **17**, 1276-1285, doi:10.1038/nn.3780 (2014).

7 Oh, S. W. *et al.* A mesoscale connectome of the mouse brain. *Nature* **508**, 207-214, doi:10.1038/nature13186 (2014).

8 Sherman, S. M. & Guillery, R. W. *Functional connections of cortical areas : a new view from the thalamus*. (MIT Press, 2013).

9 Sherman, S. M. & Guillery, R. W. On the actions that one nerve cell can have on another: distinguishing "drivers" from "modulators". *Proc Natl Acad Sci U S A* **95**, 7121-7126 (1998).

10 Sherman, S. M. & Guillery, R. W. *Functional Connetions of Cortical Areas*. (MIT Press, Cambridge, MA, 2013).

11 Guillery, R. W. & Sherman, S. M. Thalamic relay functions and their role in corticocortical communication: generalizations from the visual system. *Neuron* **33**, 163-175 (2002).

12 Bickford, M. E. Thalamic Circuit Diversity: Modulation of the Driver/Modulator Framework. *Front Neural Circuits* **9**, 86, doi:10.3389/fncir.2015.00086 (2015).

13 Rovo, Z., Ulbert, I. & Acsady, L. Drivers of the primate thalamus. *J Neurosci* **32**, 17894-17908, doi:10.1523/JNEUROSCI.2815-12.2012 (2012).

14 Reichova, I. & Sherman, S. M. Somatosensory corticothalamic projections: distinguishing drivers from modulators. *J Neurophysiol* **92**, 2185-2197, doi:10.1152/jn.00322.2004 (2004).

15 Bosch-Bouju, C., Hyland, B. I. & Parr-Brownlie, L. C. Motor thalamus integration of cortical, cerebellar and basal ganglia information: implications for normal and parkinsonian conditions. *Frontiers in computational neuroscience* **7**, 163, doi:10.3389/fncom.2013.00163 (2013).

16 Anderson, M. E. & Turner, R. S. Activity of neurons in cerebellar-receiving and pallidal-receiving areas of the thalamus of the behaving monkey. *Journal of neurophysiology* **66**, 879-893 (1991).

17 Smith, G. D. & Sherman, S. M. Detectability of excitatory versus inhibitory drive in an integrate-and-fire-or-burst thalamocortical relay neuron model. *The Journal of neuroscience : the official journal of the Society for Neuroscience* **22**, 10242-10250 (2002).

18 Nakamura, K. C., Sharott, A. & Magill, P. J. Temporal coupling with cortex distinguishes spontaneous neuronal activities in identified basal ganglia-recipient and cerebellar-recipient zones of the motor thalamus. *Cerebral cortex* **24**, 81-97, doi:10.1093/cercor/bhs287 (2014).

19 Luo, M. & Perkel, D. J. A GABAergic, strongly inhibitory projection to a thalamic nucleus in the zebra finch song system. *The Journal of neuroscience : the official journal of the Society for Neuroscience* **19**, 6700-6711 (1999).

20 Kuramoto, E. *et al.* Complementary distribution of glutamatergic cerebellar and GABAergic basal ganglia afferents to the rat motor thalamic nuclei. *The European journal of neuroscience* **33**, 95-109, doi:10.1111/j.1460-9568.2010.07481.x (2011).

21 Kultas-Ilinsky, K. & Ilinsky, I. A. Fine structure of the ventral lateral nucleus (VL) of the Macaca mulatta thalamus: cell types and synaptology. *The Journal of comparative neurology* **314**, 319-349, doi:10.1002/cne.903140209 (1991).

22 Mitchell, A. S. *et al.* Advances in understanding mechanisms of thalamic relays in cognition and behavior. *The Journal of neuroscience : the official journal of the Society for Neuroscience* **34**, 15340-15346, doi:10.1523/JNEUROSCI.3289-14.2014 (2014).

23 van Groen, T., Kadish, I. & Michael Wyss, J. Role of the anterodorsal and anteroventral nuclei of the thalamus in spatial memory in the rat. *Behavioural brain research* **132**, 19-28 (2002).

24 Aggleton, J. P. *et al.* Hippocampal-anterior thalamic pathways for memory: uncovering a network of direct and indirect actions. *The European journal of neuroscience* **31**, 2292-2307, doi:10.1111/j.1460-9568.2010.07251.x (2010).

25 Jankowski, M. M. *et al.* The anterior thalamus provides a subcortical circuit supporting memory and spatial navigation. *Frontiers in systems neuroscience* **7**, 45, doi:10.3389/fnsys.2013.00045 (2013).

26 Wright, N. F., Vann, S. D., Aggleton, J. P. & Nelson, A. J. A critical role for the anterior thalamus in directing attention to task-relevant stimuli. *The Journal of neuroscience : the official journal of the Society for Neuroscience* **35**, 5480-5488, doi:10.1523/JNEUROSCI.4945-14.2015 (2015).

27 Taube, J. S. The head direction signal: origins and sensory-motor integration. *Annual review of neuroscience* **30**, 181-207, doi:10.1146/annurev.neuro.29.051605.112854 (2007).

28 Clark, B. J. & Harvey, R. E. Do the anterior and lateral thalamic nuclei make distinct contributions to spatial representation and memory? *Neurobiology of learning and memory* **133**, 69-78, doi:10.1016/j.nlm.2016.06.002 (2016).

29 Mitchell, A. S. The mediodorsal thalamus as a higher order thalamic relay nucleus important for learning and decision-making. *Neuroscience and biobehavioral reviews* **54**, 76-88, doi:10.1016/j.neubiorev.2015.03.001 (2015).

30 Ray, J. P. & Price, J. L. The organization of the thalamocortical connections of the mediodorsal thalamic nucleus in the rat, related to the ventral forebrain-prefrontal cortex topography. *The Journal of comparative neurology* **323**, 167-197, doi:10.1002/cne.903230204 (1992).

31 Mitchell, A. S. & Chakraborty, S. What does the mediodorsal thalamus do? *Frontiers in systems neuroscience* **7**, 37, doi:10.3389/fnsys.2013.00037 (2013).

32 Isseroff, A., Rosvold, H. E., Galkin, T. W. & Goldman-Rakic, P. S. Spatial memory impairments following damage to the mediodorsal nucleus of the thalamus in rhesus monkeys. *Brain research* **232**, 97-113 (1982).

33 Hunt, P. R. & Aggleton, J. P. An examination of the spatial working memory deficit following neurotoxic medial dorsal thalamic lesions in rats. *Behavioural brain research* **97**, 129-141 (1998).

34 Mitchell, A. S. & Dalrymple-Alford, J. C. Dissociable memory effects after medial thalamus lesions in the rat. *The European journal of neuroscience* **22**, 973-985, doi:10.1111/j.1460-9568.2005.04199.x (2005).

35 Pergola, G. *et al.* Recall deficits in stroke patients with thalamic lesions covary with damage to the parvocellular mediodorsal nucleus of the thalamus. *Neuropsychologia* **50**, 2477-2491, doi:10.1016/j.neuropsychologia.2012.06.019 (2012).

36 Bolkan, S. S. *et al.* Thalamic projections sustain prefrontal activity during working memory maintenance. *Nature neuroscience* **20**, 987-996, doi:10.1038/nn.4568 (2017).

37 Lara-Vasquez, A., Espinosa, N., Duran, E., Stockle, M. & Fuentealba, P. Midline thalamic neurons are differentially engaged during hippocampus network oscillations. *Scientific reports* **6**, 29807, doi:10.1038/srep29807 (2016).

38 Delevich, K., Tucciarone, J., Huang, Z. J. & Li, B. The mediodorsal thalamus drives feedforward inhibition in the anterior cingulate cortex via parvalbumin interneurons. *The Journal of neuroscience : the official*

journal of the Society for Neuroscience **35**, 5743-5753, doi:10.1523/JNEUROSCI.4565-14.2015 (2015).

39 Penzo, M. A. *et al.* The paraventricular thalamus controls a central amygdala fear circuit. *Nature* **519**, 455-459, doi:10.1038/nature13978 (2015).

40 Halassa, M. M. & Acsady, L. Thalamic Inhibition: Diverse Sources, Diverse Scales. *Trends in neurosciences* **39**, 680-693, doi:10.1016/j.tins.2016.08.001 (2016).

41 Nakamura, H. Cerebellar projections to the ventral lateral geniculate nucleus and the thalamic reticular nucleus in the cat. *Journal of neuroscience research*, doi:10.1002/jnr.24105 (2017).

42 Bartho, P., Freund, T. F. & Acsady, L. Selective GABAergic innervation of thalamic nuclei from zona incerta. *The European journal of neuroscience* **16**, 999-1014 (2002).

43 Arcelli, P., Frassoni, C., Regondi, M. C., De Biasi, S. & Spreafico, R. GABAergic neurons in mammalian thalamus: a marker of thalamic complexity? *Brain research bulletin* **42**, 27-37 (1997).

44 Friedlander, M. J., Lin, C. S., Stanford, L. R. & Sherman, S. M. Morphology of functionally identified neurons in lateral geniculate nucleus of the cat. *Journal of neurophysiology* **46**, 80-129 (1981).

45 Sherman, S. M. Interneurons and triadic circuitry of the thalamus. *Trends Neurosci* **27**, 670-675, doi:10.1016/j.tins.2004.08.003 (2004).

46 Bloomfield, S. A., Hamos, J. E. & Sherman, S. M. Passive cable properties and morphological correlates of neurones in the lateral geniculate nucleus of the cat. *The Journal of physiology* **383**, 653-692 (1987).

47 Houser, C. R., Vaughn, J. E., Barber, R. P. & Roberts, E. GABA neurons are the major cell type of the nucleus reticularis thalami. *Brain research* **200**, 341-354 (1980).

48 Guillery, R. W., Feig, S. L. & Lozsadi, D. A. Paying attention to the thalamic reticular nucleus. *Trends Neurosci* **21**, 28-32 (1998).

49 Pinault, D. The thalamic reticular nucleus: structure, function and concept. *Brain Res Brain Res Rev* **46**, 1-31, doi:10.1016/j.brainresrev.2004.04.008 (2004).

50 Shosaku, A., Kayama, Y. & Sumitomo, I. Somatotopic organization in the rat thalamic reticular nucleus. *Brain Res* **311**, 57-63 (1984).

51 Crabtree, J. W. Organization in the somatosensory sector of the cat's thalamic reticular nucleus. *J Comp Neurol* **366**, 207-222, doi:10.1002/(SICI)1096-9861(19960304)366:2<207::AID-CNE2>3.0.CO;2-9 (1996).

52 Crabtree, J. W. The Somatotopic Organization Within the Rabbit's Thalamic Reticular Nucleus. *Eur J Neurosci* **4**, 1343-1351 (1992).

53 Crabtree, J. W. The Somatotopic Organization Within the Cat's Thalamic Reticular Nucleus. *Eur J Neurosci* **4**, 1352-1361 (1992).

54 Coleman, K. A. & Mitrofanis, J. Organization of the visual reticular thalamic nucleus of the rat. *Eur J Neurosci* **8**, 388-404 (1996).

55 Shosaku, A. & Sumitomo, I. Auditory neurons in the rat thalamic reticular nucleus. *Exp Brain Res* **49**, 432-442 (1983).

56 Villa, A. E. Physiological differentiation within the auditory part of the thalamic reticular nucleus of the cat. *Brain Res Brain Res Rev* **15**, 25-40 (1990).

57 Ilinsky, I. A., Ambardekar, A. V. & Kultas-Ilinsky, K. Organization of projections from the anterior pole of the nucleus reticularis thalami (NRT) to subdivisions of the motor thalamus: light and electron microscopic studies in the rhesus monkey. *J Comp Neurol* **409**, 369-384 (1999).

58 Gonzalo-Ruiz, A. & Lieberman, A. R. Topographic organization of projections from the thalamic reticular nucleus to the anterior thalamic nuclei in the rat. *Brain Res Bull* **37**, 17-35 (1995).

59 Halassa, M. M. *et al.* State-dependent architecture of thalamic reticular subnetworks. *Cell* **158**, 808-821, doi:10.1016/j.cell.2014.06.025 (2014).

60 Wimmer, R. D. *et al.* Thalamic control of sensory selection in divided attention. *Nature* **526**, 705-709, doi:10.1038/nature15398 (2015).

61 Long, M. A., Landisman, C. E. & Connors, B. W. Small clusters of electrically coupled neurons generate synchronous rhythms in the thalamic reticular nucleus. *J Neurosci* **24**, 341-349, doi:10.1523/JNEUROSCI.3358-03.2004 (2004).

62 Landisman, C. E. *et al.* Electrical synapses in the thalamic reticular nucleus. *J Neurosci* **22**, 1002-1009 (2002).

63 Haas, J. S., Greenwald, C. M. & Pereda, A. E. Activity-dependent plasticity of electrical synapses: increasing evidence for its presence and functional roles in the mammalian brain. *BMC cell biology* **17 Suppl 1**, 14, doi:10.1186/s12860-016-0090-z (2016).

64 Wang, Z., Neely, R. & Landisman, C. E. Activation of Group I and Group II Metabotropic Glutamate Receptors Causes LTD and LTP of Electrical Synapses in the Rat Thalamic Reticular Nucleus. *J Neurosci* **35**, 7616-7625, doi:10.1523/JNEUROSCI.3688-14.2015 (2015).

65 Landisman, C. E. & Connors, B. W. Long-term modulation of electrical synapses in the mammalian thalamus. *Science* **310**, 1809-1813, doi:10.1126/science.1114655 (2005).

66 Lee, S. C., Patrick, S. L., Richardson, K. A. & Connors, B. W. Two functionally distinct networks of gap junction-coupled inhibitory neurons in the thalamic reticular nucleus. *J Neurosci* **34**, 13170-13182, doi:10.1523/JNEUROSCI.0562-14.2014 (2014).

67 Lee, S. H., Govindaiah, G. & Cox, C. L. Heterogeneity of firing properties among rat thalamic reticular nucleus neurons. *The Journal of physiology* **582**, 195-208, doi:10.1113/jphysiol.2007.134254 (2007).

68 Nakagawa, Y. & Shimogori, T. Diversity of thalamic progenitor cells and postmitotic neurons. *Eur J Neurosci* **35**, 1554-1562, doi:10.1111/j.1460-9568.2012.08089.x (2012).

69 Rubenstein, J. L., Martinez, S., Shimamura, K. & Puelles, L. The embryonic vertebrate forebrain: the prosomeric model. *Science* **266**, 578-580 (1994).

70 Vue, T. Y. *et al.* Characterization of progenitor domains in the developing mouse thalamus. *J Comp Neurol* **505**, 73-91, doi:10.1002/cne.21467 (2007).

71 Inamura, N., Ono, K., Takebayashi, H., Zalc, B. & Ikenaka, K. Olig2 lineage cells generate GABAergic neurons in the prethalamic nuclei, including the zona incerta, ventral lateral geniculate nucleus and reticular thalamic nucleus. *Dev Neurosci* **33**, 118-129, doi:10.1159/000328974 (2011).

72 Jeong, Y. *et al.* Spatial and temporal requirements for sonic hedgehog in the regulation of thalamic interneuron identity. *Development* **138**, 531-541, doi:10.1242/dev.058917 (2011).

73 Delaunay, D. *et al.* Genetic tracing of subpopulation neurons in the prethalamus of mice (Mus musculus). *J Comp Neurol* **512**, 74-83, doi:10.1002/cne.21904 (2009).

74 Golding, B. *et al.* Retinal input directs the recruitment of inhibitory interneurons into thalamic visual circuits. *Neuron* **81**, 1057-1069, doi:10.1016/j.neuron.2014.01.032 (2014).

75 Letinic, K. & Rakic, P. Telencephalic origin of human thalamic GABAergic neurons. *Nat Neurosci* **4**, 931-936, doi:10.1038/nn0901-931 (2001).

76 Sidman, R. L. & Rakic, P. Neuronal migration, with special reference to developing human brain: a review. *Brain Res* **62**, 1-35 (1973).

77 Martinez-Ferre, A. & Martinez, S. Molecular regionalization of the diencephalon. *Front Neurosci* **6**, 73, doi:10.3389/fnins.2012.00073 (2012).

78 Scholpp, S. & Lumsden, A. Building a bridal chamber: development of the thalamus. *Trends Neurosci* **33**, 373-380, doi:10.1016/j.tins.2010.05.003 (2010).

79 Hagemann, A. I. & Scholpp, S. The Tale of the Three Brothers - Shh, Wnt, and Fgf during Development of the Thalamus. *Front Neurosci* **6**, 76, doi:10.3389/fnins.2012.00076 (2012).

80 Bluske, K. K. *et al.* beta-Catenin signaling specifies progenitor cell identity in parallel with Shh signaling in the developing mammalian thalamus. *Development* **139**, 2692-2702, doi:10.1242/dev.072314 (2012).

81 Vue, T. Y. *et al.* Sonic hedgehog signaling controls thalamic progenitor identity and nuclei specification in mice. *J Neurosci* **29**, 4484-4497, doi:10.1523/JNEUROSCI.0656-09.2009 (2009).

82 Bluske, K. K., Kawakami, Y., Koyano-Nakagawa, N. & Nakagawa, Y. Differential activity of Wnt/beta-catenin signaling in the embryonic mouse thalamus. *Dev Dyn* **238**, 3297-3309, doi:10.1002/dvdy.22167 (2009).

83 Kataoka, A. & Shimogori, T. Fgf8 controls regional identity in the developing thalamus. *Development* **135**, 2873-2881, doi:10.1242/dev.021618 (2008).

84 Rakic, P. Specification of cerebral cortical areas. *Science* **241**, 170-176 (1988).

85 Yu, Y. C., Bultje, R. S., Wang, X. & Shi, S. H. Specific synapses develop preferentially among sister excitatory neurons in the neocortex. *Nature* **458**, 501-504, doi:10.1038/nature07722 (2009).

86 Yu, Y. C. *et al.* Preferential electrical coupling regulates neocortical lineage-dependent microcircuit assembly. *Nature* **486**, 113-117, doi:10.1038/nature10958 (2012).

87 Li, Y. *et al.* Clonally related visual cortical neurons show similar stimulus feature selectivity. *Nature* **486**, 118-121, doi:10.1038/nature11110 (2012).

88 He, S., Li, Z., Ge, S., Yu, Y. C. & Shi, S. H. Inside-Out Radial Migration Facilitates Lineage-Dependent Neocortical Microcircuit Assembly. *Neuron* **86**, 1159-1166, doi:10.1016/j.neuron.2015.05.002 (2015).

89 McCormick, D. A., McGinley, M. J. & Salkoff, D. B. Brain state dependent activity in the cortex and thalamus. *Curr Opin Neurobiol* **31**, 133-140, doi:10.1016/j.conb.2014.10.003 (2015).

90 Lien, A. D. & Scanziani, M. Tuned thalamic excitation is amplified by visual cortical circuits. *Nat Neurosci* **16**, 1315-1323, doi:10.1038/nn.3488 (2013).

91 Golden, J. A. & Cepko, C. L. Clones in the chick diencephalon contain multiple cell types and siblings are widely dispersed. *Development* **122**, 65-78 (1996).

92 Golden, J. A., Zitz, J. C., McFadden, K. & Cepko, C. L. Cell migration in the developing chick diencephalon. *Development* **124**, 3525-3533 (1997).

93 Zong, H., Espinosa, J. S., Su, H. H., Muzumdar, M. D. & Luo, L. Mosaic analysis with double markers in mice. *Cell* **121**, 479-492, doi:10.1016/j.cell.2005.02.012 (2005).

94 Gao, P. *et al.* Deterministic progenitor behavior and unitary production of neurons in the neocortex. *Cell* **159**, 775-788, doi:10.1016/j.cell.2014.10.027 (2014).

95 Hippenmeyer, S. *et al.* Genetic mosaic dissection of Lis1 and Ndel1 in neuronal migration. *Neuron* **68**, 695-709, doi:10.1016/j.neuron.2010.09.027 (2010).

96 Ciceri, G. *et al.* Lineage-specific laminar organization of cortical GABAergic interneurons. *Nat Neurosci* **16**, 1199-1210, doi:10.1038/nn.3485 (2013).

97 Imayoshi, I., Ohtsuka, T., Metzger, D., Chambon, P. & Kageyama, R. Temporal regulation of Cre recombinase activity in neural stem cells. *Genesis* **44**, 233-238, doi:10.1002/dvg.20212 (2006).

98 Wang, L., Bluske, K. K., Dickel, L. K. & Nakagawa, Y. Basal progenitor cells in the embryonic mouse thalamus - their molecular characterization and the role of neurogenins and Pax6. *Neural development* **6**, 35, doi:10.1186/1749-8104-6-35 (2011).

99 Angevine, J. B., Jr. Time of neuron origin in the diencephalon of the mouse. An autoradiographic study. *J Comp Neurol* **139**, 129-187, doi:10.1002/cne.901390202 (1970).

100 Altman, J. & Bayer, S. A. Development of the rat thalamus: VI. The posterior lobule of the thalamic neuroepithelium and the time and site of origin and settling pattern of neurons of the lateral geniculate and lateral posterior nuclei. *J Comp Neurol* **284**, 581-601, doi:10.1002/cne.902840407 (1989).

101 Altman, J. & Bayer, S. A. Development of the rat thalamus: II. Time and site of origin and settling pattern of neurons derived from the anterior lobule of the thalamic neuroepithelium. *J Comp Neurol* **275**, 378-405, doi:10.1002/cne.902750305 (1988).

102 Clasca, F., Rubio-Garrido, P. & Jabaudon, D. Unveiling the diversity of thalamocortical neuron subtypes. *Eur J Neurosci* **35**, 1524-1532, doi:10.1111/j.1460-9568.2012.08033.x (2012).

103 Diggle, P. J. *Statistical Analysis of Spatial Point Patterns*. (Oxford University Press Inc., 2003).

104 Brown, K. N. *et al.* Clonal production and organization of inhibitory interneurons in the neocortex. *Science* **334**, 480-486 (2011).

105 Xu, H. T. *et al.* Distinct lineage-dependent structural and functional organization of the hippocampus. *Cell* **157**, 1552-1564, doi:10.1016/j.cell.2014.03.067 (2014).

106 Parri, H. R., Gould, T. M. & Crunelli, V. Sensory and cortical activation of distinct glial cell subtypes in the somatosensory thalamus of young rats. *Eur J Neurosci* **32**, 29-40, doi:10.1111/j.1460-9568.2010.07281.x (2010).

107 Rausell, E. & Jones, E. G. Histochemical and immunocytochemical compartments of the thalamic VPM nucleus in monkeys and their relationship to the representational map. *J Neurosci* **11**, 210-225 (1991).

108 Kuramoto, E. *et al.* Ventral medial nucleus neurons send thalamocortical afferents more widely and more preferentially to layer 1 than neurons of the ventral anterior-ventral lateral nuclear complex in the rat. *Cereb Cortex* **25**, 221-235, doi:10.1093/cercor/bht216 (2015).

109 Van der Werf, Y. D., Witter, M. P. & Groenewegen, H. J. The intralaminar and midline nuclei of the thalamus. Anatomical and

functional evidence for participation in processes of arousal and awareness. *Brain Res Brain Res Rev* **39**, 107-140 (2002).

110 Sherman, S. M. Thalamocortical interactions. *Curr Opin Neurobiol* **22**, 575-579, doi:10.1016/j.conb.2012.03.005 (2012).

111 Pouchelon, G. *et al.* Modality-specific thalamocortical inputs instruct the identity of postsynaptic L4 neurons. *Nature* **511**, 471-474, doi:10.1038/nature13390 (2014).

112 Sakai, S. T., Grofova, I. & Bruce, K. Nigrothalamic projections and nigrothalamocortical pathway to the medial agranular cortex in the rat: single- and double-labeling light and electron microscopic studies. *J Comp Neurol* **391**, 506-525 (1998).

113 Szabo, N. E., Zhao, T., Zhou, X. & Alvarez-Bolado, G. The role of Sonic hedgehog of neural origin in thalamic differentiation in the mouse. *J Neurosci* **29**, 2453-2466, doi:10.1523/JNEUROSCI.4524-08.2009 (2009).

114 Jeong, J., Mao, J., Tenzen, T., Kottmann, A. H. & McMahon, A. P. Hedgehog signaling in the neural crest cells regulates the patterning and growth of facial primordia. *Genes Dev* **18**, 937-951, doi:10.1101/gad.1190304 (2004).

115 Xie, J. *et al.* Activating Smoothened mutations in sporadic basal-cell carcinoma. *Nature* **391**, 90-92, doi:10.1038/34201 (1998).

116 Puelles, L. & Rubenstein, J. L. Expression patterns of homeobox and other putative regulatory genes in the embryonic mouse forebrain suggest a neuromeric organization. *Trends Neurosci* **16**, 472-479 (1993).

117 Shimamura, K., Hartigan, D. J., Martinez, S., Puelles, L. & Rubenstein, J. L. Longitudinal organization of the anterior neural plate and neural tube. *Development* **121**, 3923-3933 (1995).

118 Nakagawa, Y. & O'Leary, D. D. Dynamic patterned expression of orphan nuclear receptor genes RORalpha and RORbeta in developing mouse forebrain. *Dev Neurosci* **25**, 234-244, doi:72271 (2003).

119 Saalmann, Y. B. & Kastner, S. Cognitive and perceptual functions of the visual thalamus. *Neuron* **71**, 209-223, doi:10.1016/j.neuron.2011.06.027 (2011).

120 Roth, M. M. *et al.* Thalamic nuclei convey diverse contextual information to layer 1 of visual cortex. *Nat Neurosci*, doi:10.1038/nn.4197 (2015).

121 Chen, L., Guo, Q. & Li, J. Y. Transcription factor Gbx2 acts cell-nonautonomously to regulate the formation of lineage-restriction boundaries of the thalamus. *Development* **136**, 1317-1326, doi:10.1242/dev.030510 (2009).

122 Hashimshony, T., Wagner, F., Sher, N. & Yanai, I. CEL-Seq: single-cell RNA-Seq by multiplexed linear amplification. *Cell reports* **2**, 666-673, doi:10.1016/j.celrep.2012.08.003 (2012).

123 Frangeul, L. *et al.* A cross-modal genetic framework for the development and plasticity of sensory pathways. *Nature* **538**, 96-98, doi:10.1038/nature19770 (2016).

124 Frassoni, C., Amadeo, A., Ortino, B., Jaranowska, A. & Spreafico, R. Organization of radial and non-radial glia in the developing rat thalamus. *J Comp Neurol* **428**, 527-542 (2000).

125 Nakagawa, Y. & O'Leary, D. D. Combinatorial expression patterns of LIM-homeodomain and other regulatory genes parcellate developing thalamus. *J Neurosci* **21**, 2711-2725 (2001).

126 Suzuki-Hirano, A. *et al.* Dynamic spatiotemporal gene expression in embryonic mouse thalamus. *J Comp Neurol* **519**, 528-543, doi:10.1002/cne.22531 (2011).

127 Chatterjee, M. & Li, J. Y. Patterning and compartment formation in the diencephalon. *Front Neurosci* **6**, 66, doi:10.3389/fnins.2012.00066 (2012).

128 Crabtree, J. W., Collingridge, G. L. & Isaac, J. T. A new intrathalamic pathway linking modality-related nuclei in the dorsal thalamus. *Nat Neurosci* **1**, 389-394, doi:10.1038/1603 (1998).

129 Shu, Y. & McCormick, D. A. Inhibitory interactions between ferret thalamic reticular neurons. *J Neurophysiol* **87**, 2571-2576, doi:10.1152/jn.00850.2001 (2002).

130 Molnar, Z. *et al.* Normal development of embryonic thalamocortical connectivity in the absence of evoked synaptic activity. *J Neurosci* **22**, 10313-10323 (2002).

131 Stellwagen, D. & Shatz, C. J. An instructive role for retinal waves in the development of retinogeniculate connectivity. *Neuron* **33**, 357-367 (2002).

132 Hahm, J. O., Cramer, K. S. & Sur, M. Pattern formation by retinal afferents in the ferret lateral geniculate nucleus: developmental segregation and the role of N-methyl-D-aspartate receptors. *J Comp Neurol* **411**, 327-345 (1999).

133 Grant, E., Hoerder-Suabedissen, A. & Molnar, Z. The Regulation of Corticofugal Fiber Targeting by Retinal Inputs. *Cereb Cortex* **26**, 1336-1348, doi:10.1093/cercor/bhv315 (2016).

134 Nakamura, H., Hioki, H., Furuta, T. & Kaneko, T. Different cortical projections from three subdivisions of the rat lateral posterior thalamic nucleus: a single-neuron tracing study with viral vectors. *Eur J Neurosci* **41**, 1294-1310, doi:10.1111/ejn.12882 (2015).

135 Unzai, T., Kuramoto, E., Kaneko, T. & Fujiyama, F. Quantitative Analyses of the Projection of Individual Neurons from the Midline Thalamic Nuclei to the Striosome and Matrix Compartments of the Rat Striatum. *Cereb Cortex* **27**, 1164-1181, doi:10.1093/cercor/bhv295 (2017).

136 Kuramoto, E. *et al.* Individual mediodorsal thalamic neurons project to multiple areas of the rat prefrontal cortex: A single neuron-tracing study using virus vectors. *J Comp Neurol* **525**, 166-185, doi:10.1002/cne.24054 (2017).

137 Pinault, D., Bourassa, J. & Deschenes, M. The axonal arborization of single thalamic reticular neurons in the somatosensory thalamus of the rat. *Eur J Neurosci* **7**, 31-40 (1995).

138 Vigouroux, R. J., Belle, M. & Chedotal, A. Neuroscience in the third dimension: shedding new light on the brain with tissue clearing. *Mol Brain* **10**, 33, doi:10.1186/s13041-017-0314-y (2017).

139 Richardson, D. S. & Lichtman, J. W. Clarifying Tissue Clearing. *Cell* **162**, 246-257, doi:10.1016/j.cell.2015.06.067 (2015).

140 Renier, N. *et al.* Mapping of Brain Activity by Automated Volume Analysis of Immediate Early Genes. *Cell* **165**, 1789-1802, doi:10.1016/j.cell.2016.05.007 (2016).

141 Renier, N. *et al.* iDISCO: a simple, rapid method to immunolabel large tissue samples for volume imaging. *Cell* **159**, 896-910, doi:10.1016/j.cell.2014.10.010 (2014).

142 Belle, M. *et al.* Tridimensional Visualization and Analysis of Early Human Development. *Cell* **169**, 161-173 e112, doi:10.1016/j.cell.2017.03.008 (2017).

143 Yamagata, M. & Sanes, J. R. Transgenic strategy for identifying synaptic connections in mice by fluorescence complementation (GRASP). *Front Mol Neurosci* **5**, 18, doi:10.3389/fnmol.2012.00018 (2012).

144 Kim, J. *et al.* mGRASP enables mapping mammalian synaptic connectivity with light microscopy. *Nat Methods* **9**, 96-102, doi:10.1038/nmeth.1784 (2011).

145 Gong, Z. *et al.* Two pairs of neurons in the central brain control Drosophila innate light preference. *Science* **330**, 499-502, doi:10.1126/science.1195993 (2010).

146 Gordon, M. D. & Scott, K. Motor control in a Drosophila taste circuit. *Neuron* **61**, 373-384, doi:10.1016/j.neuron.2008.12.033 (2009).

147 Feinberg, E. H. *et al.* GFP Reconstitution Across Synaptic Partners (GRASP) defines cell contacts and synapses in living nervous systems. *Neuron* **57**, 353-363, doi:10.1016/j.neuron.2007.11.030 (2008).

148 Feng, L., Kwon, O., Lee, B., Oh, W. C. & Kim, J. Using mammalian GFP reconstitution across synaptic partners (mGRASP) to map synaptic

connectivity in the mouse brain. *Nat Protoc* **9**, 2425-2437, doi:10.1038/nprot.2014.166 (2014).

149 Li, L. *et al.* Visualizing the distribution of synapses from individual neurons in the mouse brain. *PLoS One* **5**, e11503, doi:10.1371/journal.pone.0011503 (2010).

150 Ha, G. E. *et al.* The Ca2+-activated chloride channel anoctamin-2 mediates spike-frequency adaptation and regulates sensory transmission in thalamocortical neurons. *Nature communications* **7**, 13791, doi:10.1038/ncomms13791 (2016).

151 Bombeiro, A. L. *et al.* MHC-I and PirB Upregulation in the Central and Peripheral Nervous System following Sciatic Nerve Injury. *PLoS One* **11**, e0161463, doi:10.1371/journal.pone.0161463 (2016).

152 Tan, X. *et al.* Vascular Influence on Ventral Telencephalic Progenitors and Neocortical Interneuron Production. *Dev Cell* **36**, 624-638, doi:10.1016/j.devcel.2016.02.023 (2016).

153 Dobin, A. *et al.* STAR: ultrafast universal RNA-seq aligner. *Bioinformatics* **29**, 15-21, doi:10.1093/bioinformatics/bts635 (2013).

154 Anders, S., Pyl, P. T. & Huber, W. HTSeq--a Python framework to work with high-throughput sequencing data. *Bioinformatics* **31**, 166-169, doi:10.1093/bioinformatics/btu638 (2015).

155 Anders, S. & Huber, W. Differential expression analysis for sequence count data. *Genome biology* **11**, R106, doi:10.1186/gb-2010-11-10-r106 (2010).

156 Blaess, S. *et al.* Temporal-spatial changes in Sonic Hedgehog expression and signaling reveal different potentials of ventral mesencephalic progenitors to populate distinct ventral midbrain nuclei. *Neural development* **6**, 29, doi:10.1186/1749-8104-6-29 (2011).